UNIVERSITY OF NOVA GORICA

GRADUATE SCHOOL

TOWARDS EFFICIENT REMOVAL OF CONTAMINANTS IN WATER FROM HOUSEHOLD APPLIANCES BY TiO_2-PHOTOCATALYSIS: DESIGN, OPTIMIZATION AND PERFORMANCE STUDIES OF THE PHOTOREACTOR WITH IMMOBILIZED CATALYSTS

Marko Kete

DISSERTATION

Mentors: Prof. Dr. Urška Lavrenčič Štangar

Dr. Monica Celotto

Nova Gorica, 2015

UNIVERZA V NOVI GORICI

FAKULTETA ZA PODIPLOMSKI ŠTUDIJ

K UČINKOVITEMU ODSTRANJEVANJU ONESNAŽEVAL PRISOTNIH V ODPADNI VODI IZ GOSPODINJSKIH APARATOV Z UPORABO TiO_2-FOTOKATALIZE: IZDELAVA, OPTIMIZACIJA IN ŠTUDIJA UČINKOVITOSTI FOTOREAKTORJA Z IMOBILIZIRANIM KATALIZATORJEM

Marko Kete

DISERTACIJA

Mentorici: Prof. Dr. Urška Lavrenčič Štangar

Dr. Monica Celotto

Nova Gorica, 2015

Zahvala

Navkljub svojemu egoizmu noben človek ne more ostati osamljen: sila Ljubezni, ki se ji ne more upirati, ga vleče in zaradi nje gravitira k drugemu ter SAMO v povezavi z drugim (»vsem«) dobiva svoj Smisel in svojo Resnico.

Vladimir Sergejevič Solovjov

Hvala vsem ki ste me vtkali v svoje Življenje!

Acknowledgements

Doctoral study of M. Kete was partly co-financed by the European Union through the European Social Fund. Co-financing is carried out within the framework of the Operational Program for Human Resources Development for 2007-2013, 1. development priority: Promoting entrepreneurship and adaptability; priority 1.3: Scholarship Scheme.

Summary

Increasing demand of clean water resources due to industrialization, population growth, long-term droughts caused by too low amounts of rainfall in combination with high evaporation or too large demand of freshwater from the population, has become more or less an issue worldwide including both industrial and developing countries. Domestic in-house specific water demand in industrialized countries approximates 100-150 L/p/d (liters per capita per day), of which 60-75% is transformed into grey water, which is less polluted fraction of waste waters released from households. Part of total household water consumption (7 – 24%) is used for clothes washing. Even if this waste water contains surfactants, textile dyes and other contaminants, represents a source of water, which could be reused in households after appropriate treatment.

Photocatalytic properties of titanium(IV) oxide (TiO_2) in anatase form can be used for various purposes, including photocatalytic purification of waste water. This advanced oxidation process (AOP) is still confronted by different technological issues like: (I) its slow degradation of organic pollutants, especially in higher concentrations, and (II) its implementation in terms of use of photocatalyst in photocatalytic reactor (suspended or immobilized).

Photocatalytic ozonation (PH-OZ) process using TiO_2 photocatalyst conducted in acidic water environment often leads to synergistic effect in terms of decomposition and mineralization of water organic contaminants, which makes the process suitable for grey waste water treatment or pretreatment of drinking water. The synergism is among other factors (pH, O_3 dose, T…) greatly influenced by photocatalyst physicochemical properties and pollutant type. In the present work, five different commercial TiO_2 photocatalysts (P25, PC500, PC100, PC10 and JRC-TiO-6) were tested in $O_2/TiO_2/UV$, O_3/TiO_2 and $O_3/TiO_2/UV$ systems. It is shown that surface area of TiO_2 primary particles is very important for surface reactions of dichloroacetic acid – DCAA degradation and all mineralization reactions, which is on the other hand not true for thiacloprid. In the last case it seems that degree of nanoparticles agglomeration negatively influences the degradation, which implies that reactions of thiacloprid degradation are occurring primarily in solution bulk, around agglomerates. Another phenomena that was detected is that synergistic effect in PH-OZ process is, in contrast to pollutants which do adsorb to TiO_2 (DCAA), much more expressed in the case of pollutants which do not adsorb or their adsorption is low (thiacloprid). This implies that PH-OZ process is taking place predominantly on surface of TiO_2 agglomerate exposed to solution bulk. On the other hand are surface oxidations of DCAA and mineralization reactions much faster in comparison to thiacloprid degradation reactions in solution bulk. All this suggests, that high surface area of photocatalyst is crucial for fast surface reactions, like mineralization, while good dispersivity and charge separation are important characteristics when it comes to photocatalytic degradation of non-adsorbed organic pollutants. It is demonstrated that photocatalysts PC500 with its high surface area and P25 with good dispersivity and probably better charge separation are good combination for PH-OZ process implementation.

The PH-OZ process can be conducted in different reactor configurations. For such an application suspended or fixed photocatalytic reactors can be used. Those with fixed phase seem to be preferred due to some advantages, one of them is the avoidance of photocatalyst filtration. To avoid leaching and exfoliation of the fixed phase, an immobilization procedure leading to a good adhesion of a catalyst to a substrate is crucial. Further in this work, we present physical and photocatalytic characterization results of five commercially available TiO_2 photocatalysts (P25, P90, PC500, KRONOClean 7000 and VPC-10) and one pigment (Hombitan LO-CR-S-M), which were successfully immobilized on glass slides by a ″sol suspension″ procedure. Different mechanical tests and characterization methods were used to evaluate the stability and morphology of the layers. Evaluation of photocatalytic activity was done by tests under UVA and UV-Vis irradiation, using a method based on the detection of the fluorescent oxidation product of terephthalic acid (TPA), i.e., hydroxylterephthalic acid (HTPA). Aeroxide® P90 incorporated into the silica-titania binder was the most photocatalytically active layer and, unlike the others, showed significant increase of photocatalytic activity through the entire range of tested UVA irradiation intensities (2.3 mW/cm^2 - 6.1 mW/cm^2). The high mechanical stability of some photocatalytic layers allows using them in photocatalytic reactors for water purification.

Compact reactor designed for treatment of less polluted waste water was developed on the basis of scientific literature and experience. With (I) utilization of custom made Al_2O_3 porous reticulated monolith foams, which serve as TiO_2 carriers, offering high photocatalytically active surface and (II) placement of irradiation source (lamps) inside the reactor, significant reduction in dimensions was achieved (12 cm x 20 cm) in comparison to prototype reactor. Despite size reduction, the overall photocatalytic cleaning capacity increased. The constructed compact reactor also represents the flexible concept and can be easily adapted to requirements, concerning its dimensions and cleaning capacity.

With degradation of LAS+PBIS and RB 19 as representatives of surfactants and textile dyes respectively, commonly found in household gray waste water and phenol as trace contaminant, an evaluation of PH-OZ and photocatalytic processes in prototype and compact reactor has been performed. Experiments conducted in prototype reactor in presence of immobilized P25+PC500, P25 or P90 photocatalysts were performed to check dark adsorption, differences in degradation kinetics among pollutants according to AOPs used and influence of pH to RB 19 degradation. These results were then used to explain and evaluate the photocatalytic efficiency of compact reactor, where three different photocatalysts and one mixture (P25, P90, PC500 and P25+PC500) were immobilized on foamed Al_2O_3 monolith. From this research of LAS+PBIS, phenol and RB 19 degradation in two reactors it can be concluded, that RB 19 and phenol are easily degradable in particular due to small and simpler molecule (phenol) and low stability in presence of ozone (RB 19). On the other hand LAS and PBIS are more resistant, so that PH-OZ process is actually not much more efficient in comparison to photocatalysis. The series of experiments in compact reactor was conducted at neutral-acidic pH, since it was shown in prototype reactor, that alkaline pH negatively influences both PH-OZ and photocatalysis. The increase in photocatalyst geometrical surface to volume of treated solution was increased by 37 times in comparison to prototype reactor, but this did not reflect proportionally in PH-OZ or photocatalysis mineralization efficiency. Synergistic effect was generally much more expressed in mineralization reactions, but was in case of LAS+PBIS mineralization still minimal. Actually was P25, when used in combination with O_2, even more efficient. Nevertheless TOC half lives in compact reactor are despite higher concentrations of pollutants relatively much shorter (13 – 43 min) in comparison to prototype, which looks promising in case of using the similar reactor in reality. The present work was concluded by performing the experiment with simulated waste water, which was prepared by using all four model pollutants (RB19, phenol, LAS and PBIS) present in tap water. The experiment showed that PH-OZ process is due to its higher cleaning capacity more suitable for treating waste waters with higher loading of organic pollutants and therefore represents more realistic application. The mineralization process half-life has been, despite the higher concentration of organic carbon only 20% longer in comparison to PH-OZ degradation of LAS and PBIS in the same reactor.

Key words: photocatalysis, ozonation, water treatment, photocatalytic reactor, surfactants

Povzetek

Dejavniki kot so: povečevanje potrebe in pomanjkanje neonesnaženih virov vode zaradi hitrega industrijskega razvoja, rasti prebivalstva, daljših sušnih obdobij, kot posledica majhne količine padavin in večjega izhlapevanja ali prevelike porabe pitne vode, so postali problem po vsem svetu, vključno z industrializiranimi državami in državami v razvoju. Poraba vode v gospodinjstvih se v industrializiranih državah giblje med 100 in 150 L/p/d (litrov na prebivalca na dan) in od te je je 60-75% v obliki sive vode, ki predstavlja lažje onesnaženo frakcijo, zavržene. Del celokupne porabe vode v gospodinjstvih (7 – 24%) se porabi za pranje oblačil. Kljub temu, da ta odpadna voda vsebuje površinsko aktivne snovi, tekstilna barvila in druga onesnaževala, je lažje onesnažena (ti. siva voda) in zato predstavlja vir vode, ki se po primernem postopku čiščenja lahko ponovno uporabi v gospodinjstvu.

Fotokatalitske lastnosti titanovega(IV) oksida (TiO_2) v kristalinični obliki anatasa omogočajo, da se TiO_2 lahko uporablja v različne namene, vključno za fotokatalitsko čiščenje odpadne vode. Ta napredna oksidacijska metoda (NOM) se še vedno sooča z različnimi tehnološkimi ovirami, kot so: (i) počasna razgradnja organskih onesnaževal, zlasti če so le te v višjih koncentracijah in (II), njena implementacija v smislu uporabe TiO_2 fotokatalizatorja v fotokatalitskih reaktorjih (npr.: v obliki suspenzije ali imobiliziran na nosilni substrat).

Proces fotokatalitske ozonacije (FO-OZ), pri katerem uporabljamo TiO_2, v kislem vodnem okolju pogosto vodi do učinka sinergije v smislu hitrejše razgradnje in mineralizacije organskih onesnaževal prisotnih v vodi, zaradi česar je ta tehnologija primerna za čiščenje lažje onesnažene odpadne vode (ti. sive vode) ali za predhodno obdelavo pitne vode. Učinek sinergije je poleg nekaterih faktorjev (pH, doze O_3, T,…) zelo odvisen tudi od fizikalno-kemijskih lastnosti TiO_2 fotokatalizatorja in kemijskih značilnosti organskega onesnaževala. V prvem delu disertacije je bilo testiranih pet različnih komercialnih TiO_2 fotokatalizatorjev (P25, PC500, PC100, PC10 in JRC-TiO-6) in sicer v procesu fotokatalize (O_2/TiO_2/UV) in FO-OZ (O_3/TiO_2/UV). Rezultati eksperimentov so pokazali, da je površina primarnih delcev TiO_2 zelo pomembna v primeru reakcij razgradnje diklorocetne kisline – DCAA in reakcij mineralizacije, ki potekajo na sami površini fotokatalizatorja, kar pa ne drži v primeru tiakloprida. V tem primeru rezultati kažejo, da stopnja aglomeracije TiO_2 nanodelcev negativno vpliva na njegovo razgradnjo, iz česar sledi, da reakcije razgradnje potekajo pretežno v raztopini izven aglomeratov. Iz rezultatov je razvidno tudi, da je sinergijski učinek za razliko od molekul, ki se močno adsorbirajo na površino TiO_2 (DCAA), veliko bolj izražen v primeru molekul, ki se ne adsorbirajo, oziroma se v manjši meri adsorbirajo na fotokatalizator (tiakloprid). To pomeni, da sam proces FO-OZ poteka pretežno na površini TiO_2 aglomerata, ki je izpostavljena vodnemu okolju. Po drugi strani je hitrost reakcije razgradnje DCAA na površini fotokatalizatorja višja v primerjavi z reakcijo razgradnje tiakloprida v vodnem mediju. Vse to kaže, da je velika površina fotokatalizatorja ključnega pomena v primeru hitrih površinskih reakcij, kot je npr. mineralizacija, medtem ko so dobra disperzivnost in separacija nabojev pomembni lastnosti, ko gre za fotokatalitsko razgradnjo organskih onesnaževal, ki se ne adsorbirajo na površino fotokatalizatorja. Rezultati so pokazali, da sta fotokatalizatorja PC500 z veliko površino in P25 z dobro disperzivnostjo in verjetno boljšo separacijo nabojev, dobra kombinacija za uporabo v sistemu fotokatalitske ozonacije.

Omenjeni proces se lahko uporablja v reaktorskih sistemih s suspendiranim ali imobiliziranim TiO_2 fotokatalizatorjem. Reaktorji z imobiliziranim TiO_2 so zaradi nekaterih prednosti bolj zaželeni, med njimi je ena od pomembnejših ta, da ni potrebe po filtraciji v vodi suspendiranih delcev fotokatalizatorja. Učinkovita imobilizacija fotokatalizatorja je tako ključna, saj z njo lahko dosežemo potrebno adhezijo, mehansko obstojnost TiO_2 plasti in posledično preprečimo luščenje. V disertaciji so predstavljene fizikalne in fotokatalitske lastnosti plasti, pripravljene iz petih komercialnih fotokatalizatorjev (P25, P90, PC500, KRONOClean 7000, VPC-10) in enega pigmenta (Hombitan LO-CR-S-M), ki so bile uspešno imobilizirane na objektna stekla s postopkom oplaščenja iz t.im. ˝sol-suspenzije˝. Z različnimi metodami sta bili ovrednoteni mehanska stabilnost in morfologija plasti. Fotokatalitska aktivnost je bila določena z metodo, ki temelji na detekciji fluorescence oksidacijskega produkta tereftalne kisline (TFK), tj. hidroksitereftalne kisline (HTFK), in sicer z uporabo UVA in vidne svetlobe. Plast, izdelana iz Aeroxide® P90, se je pokazala kot najbolj fotokatalitsko aktivna in je v nasprotju z ostalimi pokazala znatno povišanje fotokatalitske aktivnosti preko celotnega razpona intenzitete

obsevanja (2.3 mW/cm^2 - 6.1 mW/cm^2). Visoka mehanska stabilnost nekaterih plasti omogoča njihovo uporabo v reaktorjih z namenom čiščenja vode.

Kompaktni reaktor, ki je bil dizajniran za čiščenje manj onesnažene vode, je bil razvit na podlagi znanstvene literature in izkušenj. Z imobilizacijo TiO_2 na specifično oblikovane penjene monolite iz Al_2O_3, ki posedujejo veliko geometrijsko površino, in postavitvijo UV sijalk v središče reaktorja je bilo v primerjavi s prototipnim reaktorjem doseženo bistveno zmanjšanje zunanjih dimenzij reaktorja (12 cm x 20 cm). Kljub zmanjšanju dimenzij se je čistilna kapaciteta reaktorja povečala. Predstavljen in izdelan kompaktni reaktor predstavlja fleksibilen koncept, kateremu se lahko glede na potrebe čistilne zmogljivosti spreminja dolžino, v manjši meri pa tudi premer.

S testi razgradnje v sivi odpadni vodi običajno prisotnih surfaktantov (LAS in PBIS) ter tekstilnega barvila (Reactive blue 19 – RB 19) in fenola kot pogosto prisotnega polutanta je bila v prototipnem in kompaktnem reaktorju opravljena ocena učinkovitosti procesov FO-OZ in fotokatalize. Eksperimenti v prototipnem reaktorju v prisotnosti fotokatalizatorjev P25+PC500, P25 in P90 so bili izvedeni z namenom določitve temne adsorpcije na površino fotokatalizatorja, razlik v kinetiki razgradnje glede na uporabljeno NOM in vpliv pH vodne raztopine na razgradnjo RB 19. Dobljeni rezultati so nato sluzili za primerjavo in razlago fotokatalitske učinkovitosti kompaktnega reaktorja, v katerem so bili uporabljeni trije fotokatalizatorji (P25, P90, PC500) in mešanica (P25+PC500), imobilizirani na Al_2O_3 monolit. Iz testov razgradnje omenjenih polutantov (LAS+PBIS, fenol in RB 19) se lahko zaključi, da sta RB 19 in fenol lažje razgradljiva zaradi preprostejše oblike molekule (fenol) in majhne kemijske stabilnosti v prisotnosti ozona (RB 19). Po drugi strani sta LAS in PBIS bolj inertna, tako da je proces FO-OZ le v manjši meri učinkovitejši v primerjavi s fotokatalizo. Serija eksperimentov je bila v kompaktnem reaktorju izvedena v nevtralno-kislih pogojih, saj so testi v prototipnem reaktorju pokazali, da bazični pH negativno vpliva na obe uporabljeni oksidacijski metodi, FO-OZ in fotokatalizo. Kljub večji geometrijski površini katalizatorja, ki je v primerjavi s prototipnim reaktorjem 37x večja, se v primeru razgradnje in mineralizacije le ta ne odraža v sorazmernem deležu. Pojav sinergije je bil veliko bolj izražen v procesu mineralizacije, vendar v primeru mineralizacije surfaktantov minimalen in v primeru P25 je bil proces fotokatalize celo bolj učinkovit od FO-OZ. Kljub že omenjenemu in višjim koncentracijam celokupnega organskega ogljika, so razpolovni časi v primerjavi s tistimi v prototipnem reaktorju relatvno kratki (13 – 43 min), kar potencialno obeta uporabo podobnega reaktorja v praksi. Pričujoče delo je zaključeno s predstavitvijo rezultatov eksperimentov razgradnje simulirane odpadne vode v kompaktnem reaktorju, ki je bila pripravljena z raztapljanjem omenjenih štirih modelnih onesnaževal (RB19, fenol, LAS in PBIS) v vodovodni vodi. Rezultati kažejo, da je proces FO-OZ zaradi njegove večje učinkovitosti bolj primeren za čiščenje sive odpadne vode in zato bolj primeren za dejansko uporabo. Razpolovni čas mineralizacije je bil v tem primeru kljub višji koncentraciji organskega ogljika le za ca. 20% daljši v primerjavi s FO-OZ razgradnjo LAS in PBIS v istem reaktorju.

Ključne besede: fotokataliza, ozonacija, čiščenje vode, fotokatalitski reaktor, surfaktanti

Table of contents

List of tables

List of figures

1 Introduction with theoretical background

Increasing demand and shortage of clean water resources due to the rapid development of industrialization, population growth, long-term droughts caused by too low amounts of rainfall in combination with high evaporation (e.g., Australia) or too large demands of freshwater from the population (e.g., Japan), have become an issue worldwide including both industrial and developing countries. It is estimated that around 4 billion people worldwide experience to have no or little access to clean and sanitized water supply, and millions of people die of severe waterborne diseases annually (Malato et al. 2009). These statistical figures are expected to grow in the short future with increasing water contamination due to overwhelming discharge of micropollutants and contaminants into the natural water cycle (Richardson 2008; Suarez et al. 2008; Wintgens et al. 2008). In view to suppress the worsening of clean water shortage, development of advanced water treatment technologies with low cost and high efficiency is desirable. One of several options is the possible reuse of onsite rural waste-water or the treated municipal waste water from treatment plants for agricultural and industrial activities (Bradley et al. 2002) which constitute one of the largest possible water resources. Smaller, but not negligible water resources represent waste waters from household appliances, amounting 7 – 24% (10.5 L – 46.2 L) of total daily household water consumption (Liu et al. 2005; Willis et al. 2011).

Currently available water treatment technologies (adsorption, coagulation) merely concentrate the pollutants present by transferring them to other phases and in this way they are not completely "eliminated" (Padmanabhan et al. 2006). Other conventional water treatment methods (sedimentation, filtration, chemical and membrane technologies) involve high operating costs and could generate toxic secondary pollutants (Gaya and Abdullah 2008). Chlorination has been the most commonly and widely used disinfection process but by-products generated from this process are mutagenic and carcinogenic to human (Coleman et al. 2005; Yang and Cheng 2007; Lu et al. 2009). These have led to the rapid R&D in the field of "Advanced Oxidation Processes (AOPs)" as the innovative water treatment technologies for mineralization and disinfection (Esplugas et al. 2002; Pera-Titus et al. 2004). The rationale of these AOPs is based on the in-situ generation of highly reactive species (i.e. H_2O_2, $OH^{\bullet}$, $O_2^{\bullet-}$, O_3) for mineralization of refractory organic compounds, water pathogens and disinfection by-products (Esplugas et al. 2002; Pera-Titus et al. 2004). Among the semiconductor catalysts, titanium dioxide (TiO_2) has received the greatest interest in R&D of photocatalysis technology. TiO_2 in anatase crystalline structure is the most active photocatalyst under the photon energy of 300 nm < λ < 390 nm and remains stable after the repeated catalytic cycles (Malato et al. 2009). The other properties of TiO_2 catalyst, such as chemical and thermal stability or resistance to chemical breakdown and strong mechanical properties have promoted its wide application in photocatalytic water treatment.

So far, the application of TiO_2-photocatalysis belonging to AOPs for water treatment is still experiencing a series of technical challenges. The post-separation of the TiO_2 catalyst nanoparticles after water treatment remains the major obstacle towards an industrial process and immobilization is one possible solution despite its lower efficiency.

1.1 Research goals

1.1.1 Objectives

The main goal of this thesis is to develop and to implement photocatalysis process in conjunction with treatment of household effluents towards an efficient technology for removing water contaminants. For establishing such a system, a high-efficiency photocatalytic reactor was planned and constructed. To achieve the desired performance, the system should enable to use synergistic effect of TiO_2 photocatalysis coupled with ozonation and the most appropriate substrate for photocatalyst immobilization to maintain high surface of catalyst versus reactor volume ratio. The geometry of final reactor is based on results of photocatalytic degradation in prototype reactor.

1.1.2 Expected results

Expected result of the PhD research project is an efficient reactor system enabling photocatalytic oxidation and photocatalytic ozonation, which will roughly consist of UV irradiation source, light

substrate with firmly immobilized photocatalyst, ozone purge system and a solid frame. At best, system could be then used for drinking water disinfection and micro pollutants removal as well as for waste water treatment with lower concentrations of hazardous substances in outflows from households.

1.2 Waste water

There are various definitions of waste water, one of them, provided by WHO, is:

Waste water is "liquid waste discharged from homes, commercial premises and similar sources to individual disposal systems or to municipal sewer pipes, and which contains mainly human excreta and used water. When produced mainly by household and commercial activities, it is called domestic or municipal waste water or domestic sewage. In this context, domestic sewage does not contain industrial effluents at levels that could pose threats to the functioning of the sewerage system, treatment plant, public health or the environment (European Commission 2007)."

From general and broader point of view the waste water is water, which is affected in quality by any anthropogenic influence. There is a wide range of waste waters and an equally wide range of technologies and techniques for mitigating the impacts of waste waters on the receiving environment.

1.2.1 Waste water types

Broadly speaking we distinguish among different types of waste water (Vymazal 2009):

- Municipal waste waters: (I) sanitary sewage – spent water from residences and institutions, (II) sewage treatment plant discharge, (II) pharmaceuticals and personal care products and (IV) greywater (also known as sullage water: water from household functions such as washing dishes, laundry or bath water without any input from toilets) (Eriksson et al. 2002).

- Industrial: (I) petrochemical and chemical industries, (II) pulp and paper, textile and tannery industries, (III) abattoir and meet processing effluents, (III) food processing, (IV) winery and distillery and (V) other industrial effluents (lignite pyrolysis waste water, metals, heavy metals,…).

- Agricultural: (I) pig farms effluents, (II) fish farm effluents and (III) dairy effluents.

- Landfill leachate: rain water which flows through municipal solid waste landfills.

- Surface run-off (also known as stormwater runoff): (I) airport runoff, (II) greenhouse and nursery runoff, (III) agricultural runoff and (IV) urban and highway runoff.

1.2.2 Waste waters from households – Grey waste water

Domestic in-house specific water demand in industrialized countries approximates 100-150 L/p/d (liters per capita per day), of which 60-75% (Christova-Boal et al. 1996; Friedler 2004) is transformed into greywater, while most of the rest is consumed for toilet flushing and released as blackwater. Grey waste water is defined as waste water without any input from toilets, which means that it corresponds to waste water produced in bathtubs, showers, hand basins, laundry machines and kitchen sinks, in households, office buildings, schools, etc. (Christova-Boal et al. 1996). The pH of grey waste waters is in the range from 6.5 to 8.7 while the total organic carbon (TOC) concentrations can be from 1 up to several hundred mg/L, and faecal coliforms of about 10^4–10^6 CFU/100 mL (Friedler et al. 2005; Matos et al. 2011).

A part of greywater resource is represented by waste waters from household appliances, such as washing machine, which amounts 7 – 24% of total household water consumption (China - 150 L/p/d, Japan 190 L/p/d and America 308 L/p/d; year 2002). The amount of water, calculated according to the proportion used for clothes washing is 10.5 L/p/d in case of China, 46.2 L/p/d for

America and 45.6 L in Japan (Liu et al. 2005; Willis et al. 2011) or in case of Australian Gold Coast City, 30 L/p/d (19%) of total 158 L/p/d is used for clothes washing (Liu et al. 2005; Willis et al. 2011).

1.2.2.1 Model pollutant compounds

Linear alkylbenzene sulfonates (LAS) are currently the most used anionic surfactants (more than 25% of all surfactants used) in the formulation of household and laundry detergents, hand dishwashing liquids, shampoos, and other personal care products. Commercial LAS are available as a mixture of homologues, with a different length of the alkyl chain (C10 to C14) (Camacho-Munoz et al. 2014), where a sulfonated benzene ring can be attached at various isomer positions (usually between 2 and 7) (Fountoulakis et al. 2009). Due to their widespread use, LAS are ubiquitous water contaminants. The concentrations of LAS in raw waste water have been reported to range from 1 to 21 mg/L (Fountoulakis et al. 2009; Camacho-Munoz et al. 2014). It is known that they are highly biodegradable under aerobic conditions and are completely eliminated by the activated sludge process. It was reported (Camacho-Munoz et al. 2014), that average concentration of LAS homologues in urban waste water (3 – 5 mg/L) was even higher than those measured in industrial waste water (0.2 – 0.5 mg/L), despite the use of LAS in the studied industrialized area (laundries, surfactants production, etc.).

2-Phenyl-5-benzimidazolesulfonic acid (PBIS) is a commonly used, water soluble sunscreen UVB agent and can be therefore found in grey waste waters also (Hernandez-Leal et al. 2011). According to some data (Etchepare and Hoek 2015), its maximum detected concentration was 15.3 µg/L. PBIS drinking water standard/toxicity threshold value is evaluated to be 40 mg/kg of body weight per day (Etchepare and Hoek 2015).

Dyes can be also found in grey waste water effluents (Eriksson et al. 2002) and it was reported that the presence of dyes and other colored compounds was the key determining factor in getting the wider social acceptance of greywater recycling and reuse schemes (Radcliffe 2006). Textile dyes are classified into many types based on the type of textile fiber fixation, such as acid, alkaline, direct, dispersed, and reactive methods. Use of reactive dyes by the textile industry has grown steadily because they react well with fibers and their color is stable. Generally, they are photolytically/chemically stable and either not biodegradable under aerobic conditions or they degrade slowly via conventional biological processes, producing vividly colored treated effluents (Guimaraes et al. 2012). They are highly soluble in water and as effluents contain environmentally problematic and toxic compounds (He et al. 2008; Liu et al. 2010 and references therein). Among them, reactive blue 19 (RB 19) is easily available and commonly used in the textile industries (Guimaraes et al. 2012). The mutagenic properties of RB 19 due to the presence of electrophilic vinyl sulfone groups (Guimaraes et al. 2012), dictate importance to remove it from water.

Phenol is one of the most common organic water pollutants, because it is toxic even at low concentrations, and also its presence in natural waters can lead further to the formation of substituted compounds during disinfection and oxidation processes. Consequently it has been chosen frequently as a model pollutant in particular with respect to waste water treatments (Busca et al. 2008). Currently, phenol is produced in a quantities of about 6 million ton/yr worldwide, with a significantly increasing trend (Busca et al. 2008). Phenol as pure substance is used as a disinfectant (cream and shaving soaps), in veterinary medicine as an internal antiseptic and gastric anesthetic, as a reagent in chemical analysis and as a primary petrochemical intermediate. Its largest use (35%) is to produce phenolic resins. Phenol may be converted into xylenols, alkylphenols, chlorophenols, aniline, and other secondary intermediates in the production of surfactants, fertilizers, explosives, paints and paint removers, textiles, rubber, plastic plasticizers, antioxidants, curing agents and so on. Phenol is also a building block for the synthesis of pharmaceuticals, such as, e.g., aspirin (Busca et al. 2008). Phenols are present in waste water of various industries (refineries, coking operations, coal processing, petrochemicals, pharmaceutical, plastics, wood products, paint, and pulp and paper). Internally, phenol at low concentrations can affect the liver, kidneys, lungs, and vascular system. The Environmental Protection Agency has therefore set a water purification standard of less than 1 ppb of phenol in surface waters (Busca et al. 2008).

Neonicotinoid pesticides are due to their wide use for effective crop protection against insect pests a pollution source for both ground and surface waters and can be therefore in low concentrations (approx. 0.1 μgL^{-1}) found also in drinking water (Seccia et al. 2005; Banic et al. 2011). Thiacloprid belongs to the second generation of neonicotinoid insecticides (Jeschke et al. 2001) and is well known as pesticide, which acts on the insect nervous system as an antagonist of the nicotinic acetylcholine receptors (Krohn 2001; Cernigoj et al. 2007a; Banic et al. 2011). Studies of environmental behavior have shown that in acidic or neutral aqueous media the thiacloprid can be still detected after 6 months and in alkaline conditions (pH 10) only 10% of thiacloprid was degraded (Cernigoj et al. 2007a; Banic et al. 2011). The calculated half-life in soil under field conditions was calculated to be 9 – 27 days in northern Europe and 10 – 16 days in southern Europe (Krohn 2001).

Dichloroacetic acid (DCAA) is one of the many haloacetic acids (HAAs) formed during water disinfection using chlorine, chloramines, chlorine dioxide, and ozone, but they are generally formed at highest levels with chlorination (Duirk and Valentine 2006; Richardson et al. 2007). Sources of DCAA contamination include: (I) water chlorination, (II) through use as a veterinary and human pharmaceutical, and (III) from its use as a disinfectant and surfactant (Hanson et al. 2003 and references therein). Haloacetic acids (HAAs), such as DCAA, are strong acids with low Henry's law constants in their ionized form so they are expected to partition into aquatic systems (Hanson et al. 2003). Concentrations of DCAA in treated drinkingwater typically range from 5 to 20 µg/L, although concentrations greater than 100 µg/L have been measured (Richardson et al. 2007; Fitzsimmons et al. 2009 and references therein). An average is still under guideline upper limit, which is for DCAA set at 0.05 mg/L (Richardson et al. 2007). The HAAs represent a recognized health risk to humans and their effects on mammals have been extensively investigated (Fitzsimmons et al. 2009 and references therein). DCAA belongs to group which clearly exhibit the features of most IARC declared human carcinogens, i.e., they are mutagenic, trans-species carcinogens (Richardson et al. 2007), but at higher concentrations or long-term exposure.

1.2.3 Reuse of grey waste water

Two important reasons like (I) water shortage, caused by too low amounts of rainfall in combination with high evaporation (e.g., Australia) and (II) too large demands of freshwater from the population (e.g., Japan) are the driving force of an increasing interest in the reuse of grey waste water, including both industrial and developing countries (Eriksson et al. 2002). The explanation is that this fraction of waste water is less polluted than municipal waste water in the absence of faeces, urine and toilet paper.

For example, in the period 2004–2005 compared with 2001–2002, Australian households experienced a ten-fold increase in the use of reused water. In the future, there is a high probability that the supply of recycled water in many Australian communities with dual water supply systems will be increased because of the increasing water shortage and rapidly spreading urbanization (Mainali et al. 2011). However, in many countries including Australia, Slovenia and Italy, potable quality water is still typically used for laundry activities.

The decrease of water consumption was achieved by development of more water efficient household appliances. In addition, the current persisting and increasing water stress impels the society to learn from global experiences and to improve this efficiency even further. To recycle water and reuse is believed to be more sustainable option and in fact, a positive trend for using the recycled water was observed (Mainali et al. 2011).

The risk of spreading of diseases, due to exposure to micro-organisms in the water, will be a crucial point (Eriksson et al. 2002) and the treated water aesthetics as well as assuring the durability of appliances (Mainali et al. 2011). General public demands for reused water in households is higher water quality in comparison with garden watering and toilet flushing applications. Higher quality recycled water requires a higher level of treatment, which is usually more expensive and more energy intensive.

1.2.3.1 Removal of model pollutant compounds by AOPs

Advanced oxidation processes (AOPs) are one part of water treatment approaches, which diversify in many different (Gultekin and Ince 2007; Oppenlander 2007). Ozonation, photocatalysis and photocatalytic ozonation as a part of AOPs have due to their high oxidation ability a great potential in terms of water treatment. Photocatalytic ozonation is even considered to be one of the most effective in terms of decomposition of organic species (Agustina et al. 2005; Beltran et al. 2005; Dominguez et al. 2005; Gimeno et al. 2007; Beltran et al. 2010; Cernigoj et al. 2010; Jing et al. 2011; Oyama et al. 2011; Yildirim et al. 2011; Rodriguez et al. 2012; Zsilak et al. 2014) and water disinfection (Nasuhoglu et al. 2012; Horn et al. 2014).

It was demonstrated that LAS can be only partially removed by ozonation alone (Beltran et al. 2000), ultrasound (Manousaki et al. 2004) and ozonation in presence of additives (Rivera-Utrilla et al. 2008), while it is under aerobic conditions in much longer process completely eliminated by the activated sludge process (Camacho-Munoz et al. 2014). On the other hand, the UV-filter 2-phenyl-5-benzimidazolesulfonic acid (PBIS) was not removed during biological treatment (Hernandez-Leal et al. 2011) but it showed that it is susceptible for ozonation.

RB 19 dye is chemically and photolytically stable and was slowly degraded by application of H_2O_2 at appropriate dosages with UV light. On the other hand, Fenton process rapidly decolorized the solution, but maximum TOC removal was limited to 94.5% (Guimaraes et al. 2012). Additionally can be blue dye removed by ozonation (Panda and Mathews 2014), and completely mineralized by photocatalysis (Liu et al. 2010; Marques et al. 2010; Hadjltaief et al. 2014). Generally, decolorization of solution is achieved rapidly while the mineralization step is much slower process.

There are numerous phenol removal technologies studied and used (Busca et al. 2008) and photocatalysis is a technique that can be performed without the addition of costly reactants or much energy supply. This makes, in perspective, this technology a very interesting and was shown (Vione et al. 2005) among many others, that photocatalysis can efficiently degrade phenol. This pollutant can also be completely degraded but not completely mineralized in direct ozonation (Sano et al. 2007; Turhan and Uzman 2008; Chen et al. 2014), while the application of photocatalytic ozonation shortened the time for complete removal of phenol and additionally greatly enhanced its mineralization rate (Chen et al. 2014), which is a target achievement when speaking about removal of pollutants from waste water and water streams.

Thiacloprid can be efficiently removed by different AOPs like heterogeneous photo-Fenton (Banic et al. 2011), photocatalysis (Cernigoj et al. 2007a; Banic et al. 2011), photocatalysis with presence of H_2O_2 (Banic et al. 2011), photocatalytic ozonation (Cernigoj et al. 2007) and is during removal processes degraded to many possible intermediates. It is relatively stable to direct ozone attack at acidic pH (Cernigoj et al. 2007a).

Dichloroacetic acid (DCAA) represents highly stable polar molecules. It is a model of aliphatic organic acid with simple molecule with 2 C atoms, which charge depends on the pH of water media and is rather stable against ozone oxidation (Kopf et al. 2000; Zhai et al. 2010). More efficient it can be degraded and thus removed by catalytic ozonation using ZnO as catalyst (Zhai et al. 2010) and by photocatalysis (Enriquez et al. 2007; Czili and Horvath 2009).

1.3 Advanced oxidation processes – AOPs

Advanced Oxidation Processes (AOPs) were developed for water and air cleaning, polluted by persistent organic pollutants and basically imitate natural oxidation processes. The main goal of these processes is to degrade and if required mineralize organic pollutants to CO_2, water and mineral acids (Oppenlander 2007):

$$C_nH_mX_n \xrightarrow{h\nu, O_2} nCO_2 + (m-z)/2H_2O + zHX \qquad \textbf{Equation 1}$$

The essence is formation of reactive and short-lived oxygen containing intermediates such as hydroxyl radicals ($^{\bullet}OH$), which occur in the majority of AOPs. The hydroxyl radical is an elecrophilic, powerful oxidant and a short lived, highly reactive, and non-selective reagent (Andreozzi et al. 1999; Oppenlander 2007). When it reacts with organic molecules it can produce

(I) water via the reaction with organic hydrogen, (II) organic radical cations by electron abstraction and (III) it reacts with double bond in aromatic structures by addition reaction (Legrini et al. 1993).

Production of $^{\bullet}OH$ radicals is an expensive process and therefore it is obvious that AOPs should not replace, whenever possible, the more economic treatment technologies (eg. biological degradation) (Andreozzi et al. 1999), especially in case of COD values higher than 5 g/L.

1.3.1 AOPs for water treatment

1.3.1.1 Fenton/photoassisted Fenton process – homogeneous catalysis/photocatalysis

The most important process of homogeneous photocatalysis in the aqueous phase (pH range 2.5 to 5) is Fenton or photo-Fenton reaction. In the first case (Fenton) hydroxyl radicals are formed by using salts of Fe^{2+} and H_2O_2 as oxidant (Equation 2), while in case of photo-Fenton this process exploits photoreduction of Fe^{3+} ions and its complexes, so that the Fe^{2+} ions are not consumed during photocatalytic reactions. Dominant, $[Fe(OH)]^{2+}$ complex absorbs the UV irradiation (<400 nm) (Equation 3), which means that it is possible to effectively exploit the UV portion of the solar spectrum. Concentrations of iron may be in case of photo-Fenton lower than for conventional Fenton reaction. At completion of both processes iron must be precipitated and removed. Quantum yield of Fe^{2+} photoproduction is relatively low, but it can be increased by introduction of ferrioxalate complex ($[Fe(C_2O_4)_3]^{3+}$) (Equation 4) (Andreozzi et al. 1999; Oppenlander 2007).

Fenton: $Fe^{2+} + H_2O_2 \rightarrow Fe^{3+} + OH^- + {}^{\bullet}OH$ **Equation 2**

Photo-Fenton: $[Fe(OH)]^{2+} + h\nu \rightarrow Fe^{2+} + {}^{\bullet}OH$ **Equation 3**

Photo-Fenton (Ferrioxalate complex) overall reaction:
$2Fe^{3+} + {C_2O_4}^{2-} + h\nu \rightarrow 2Fe^{2+} + 2CO_2$
Equation 4

The main disadvantages of the Fenton or photo-Fenton process are: (I) the use of H_2O_2, (II) low pH during the reaction, (III) removal of iron salts and (IV) possible residue of H_2O_2 in treated water after the process completion.

1.3.1.2 Photoinduced oxidation

In this type of oxidation process, auxiliary oxidant containing oxygen absorbs electromagnetic irradiation, which leads to molecule excitation. Consequently, the oxidant molecules are cleaved and primary reactive oxygen species are generated, which are in most cases hydroxyl radicals ($^{\bullet}OH$) or oxygen atoms in the ground or excited state (Andreozzi et al. 1999; Oppenlander 2007). Most often hydrogen peroxide (H_2O_2) and ozone (O_3) are used as auxiliary oxidants.

Homolytic cleavage (Equation 5) of H_2O_2 happens when peroxide absorbs a photon of an appropriate energy (≤ 280 nm), resulting in two hydroxyl radicals.

$H_2O_2 \xrightarrow{h\nu} {H_2O_2}^{*} \rightarrow 2\ {}^{\bullet}OH$ **Equation 5**

The degree of photolysis in an aqueous medium depends on the pH and increases with alkalinity of medium, which is probably due to a larger absorption coefficient of the peroxide anion compared with the neutral molecule of H_2O_2 (Andreozzi et al. 1999). It has been used to remove water pollutants in low concentrations (chlorine, nitrates, sulfides,…) and as disinfectant (Neyens and Baeyens 2003). At high concentrations of persistent chemical pollutants this process is less important due to slow oxidation reaction.

Ozone is widely and successfully used for various forms of oxidative water treatment. For use in the treatment of water, ozone is usually produced using an ozonator, which is fed by oxygen or dry air. Molecule of ozone is in the ground state a diradical and powerful oxidant. Ozone primarily reacts with the reactants attacking its electrophilic terminal oxygen atom. The most common reactions of ozone in aqueous medium are electron transfer reactions, the transfer of an oxygen

atom and reactions in which the addition of ozone to the double bond in organic molecules occurs (Hoigne 1998).

By absorption of UV radiation below 320 nm it is efficiently decomposed. The primary product is atomic oxygen, which further reacts with water forming H_2O_2 (Cernigoj et al. 2007a):

$$O_3 + h\nu\ (< 320\ nm) \rightarrow\ O(^1D) +\ O_2 \qquad \textbf{Equation 6}$$

$$O(^1D) + H_2O \rightarrow\ H_2O_2 \qquad \textbf{Equation 7}$$

Often irradiation with UV light is avoided by the addition of hydrogen peroxide and such a system is called Peroxone (Oppenlander 2007). The process of this kind is expensive, but more effective than ozonation alone. Good property of ozone is its high absorption of UV radiation in comparison to the H_2O_2, but the main disadvantages are high production cost and consuming energy source (UV-B/C lamp). In addition, ozone is toxic gas with aggressive odor, which has to be decomposed before the release into the atmosphere (Cernigoj 2007).

1.3.1.3 Heterogeneous photocatalysis

In contrast to the homogeneous photocatalysis, in the case of heterogeneous photocatalysis two phases are present. Typically semiconductor presents the solid phase (TiO_2, ZnO, CdS, etc.), which is insoluble in liquid phase. The process is driven by photons of sufficient energy, which excites the semiconductor and simultaneously produces exiton, or in other words a pair of excited electron and positive hole. In water or air these separated charges generate primary oxidants like superoxide anion and hydroxyl radical, respectively. Among many others, TiO_2 photocatalysis belongs to the group of heterogeneous photocatalytic processes.

1.4 TiO_2 photocatalysis

A ‘‘photocatalytic reaction’’ can be defined as a chemical reaction induced by photoabsorption of a solid material, or ‘‘photocatalyst,’’ which remains unchanged during the reaction. So the explanation that may be consistent with most definitions is that solid acts catalytically (without change) under electromagnetic irradiation. ‘‘Photocatalysis’’ is the conceptual name for the photocatalytic reactions (Ohtani 2008).

Photocatalysis is often introduced with the aid of a schematic representation of the electronic structures of semiconducting materials, a band model; an electron in an electron-filled valence band (VB) is excited by photoirradiation to a vacant conduction band (CB), which is separated by a forbidden band, a band gap, from the VB, leaving a positive hole in the VB. These electrons and positive holes drive reduction and oxidation, respectively, of compounds adsorbed on the surface of a photocatalyst. In the definition given above, however, no limitation based on the electronic structure of a photocatalyst is included. For example, isolated chemical species, not having the above-mentioned band structure, can be a photocatalyst, and even when a bulk material is used, the photoabsorption and resultant photocatalytic reaction may proceed at a localized site when, for example, photocatalysts are photoirradiated at a wavelength near the band gap. Therefore, the interpretation using a band model is not always adequate for understanding photocatalysis. In this sense, the term ‘‘heterogeneous photocatalytic reaction (photocatalysis)’’ seems better than ‘‘semiconductor photocatalytic reaction’’ based on the electronic band structure (Ohtani 2008).

1.4.1 TiO_2 crystal structure

There are three most frequent polymorphic modifications of titanium(IV) oxide: anatase, rutile and brookite. Under high pressure columbite and some other phases of TiO_2 can be produced. Of these, anatase and rutile crystallize in tetragonal crystal system, brookite in the orthorhombic, while less important columbite in monoclinic modification. The highest photocatalytic activity of all TiO_2 crystal structures has been found for anatase crystalline form. All three frequent modifications can be found in nature, but they can also be synthesized. It has been reported that rutile is the most stable phase for particles above 35 nm and anatase for nanoparticles below 11 nm. Brookite has been found to be the most stable for nanoparticles in the 11 – 35 nm range (Fujishima et al. 2008), but this depends on the synthesis conditions.

1.4.2 Fundamentals of TiO_2 photocatalysis

Titanium dioxide has been widely used as a photocatalyst for generating charge carriers thereby inducing a series of reductive and oxidative reactions on its surface. Photoinduced reactions are activated by absorption of a photon with sufficient energy (λ ≤ 400 nm), meaning that its energy is equal or higher than the band-gap energy (E_g) of the catalyst, usually 3.2 eV for anatase or 3.0 eV for rutile. The absorption leads to a charge separation due to the promotion of an electron (e^-) from the valence band of the semiconductor catalyst to the conduction band thus generating a hole (h^+) in the valence band. The phenomena of the electron-hole pair formation when the TiO_2 particle is irradiated with adequate $h\boldsymbol{\nu}$ is presented in **Figure 1**. In order to have a photocatalyzed reaction, the e^--h^+ recombination, subsequent to the initial charge separation, must be prevented as much as possible (Gerven et al. 2007). The series of chain oxidative-reductive reactions (Equations 8 - 17) that occur at the photon activated surface was postulated as follows (Gaya and Abdullah 2008; Czili and Horvath 2009):

Photoexcitation: $TiO_2 + h\nu \rightarrow e^-_{CB\ (TiO_2)} + h^+_{VB\ (TiO_2)}$ **Equation 8**

Charge-carrier trapping of e^-: $e^-_{CB} \rightarrow e^-_{TR}$ **Equation 9**

Charge-carrier trapping of h^+: $h^+_{VB} \rightarrow h^+_{TR}$ **Equation 10**

Electron-hole recombination: $e^-_{TR} + h^+_{VB}(h^+_{TR}) \rightarrow e^-_{VB} + heat$ **Equation 11**

Photoexcited e^- scavenging: $(O_2)_{ads} + e^- \rightarrow O_2^{\bullet -}$ **Equation 12**

Oxidation of hydroxyls: $Ti - OH + h^+(TiO_2) \rightarrow Ti - OH^\bullet$ **Equation 13**

Photodegradation by $^\bullet$OH: $R - H + {}^\bullet OH \rightarrow R^\bullet + H_2O$ **Equation 14**

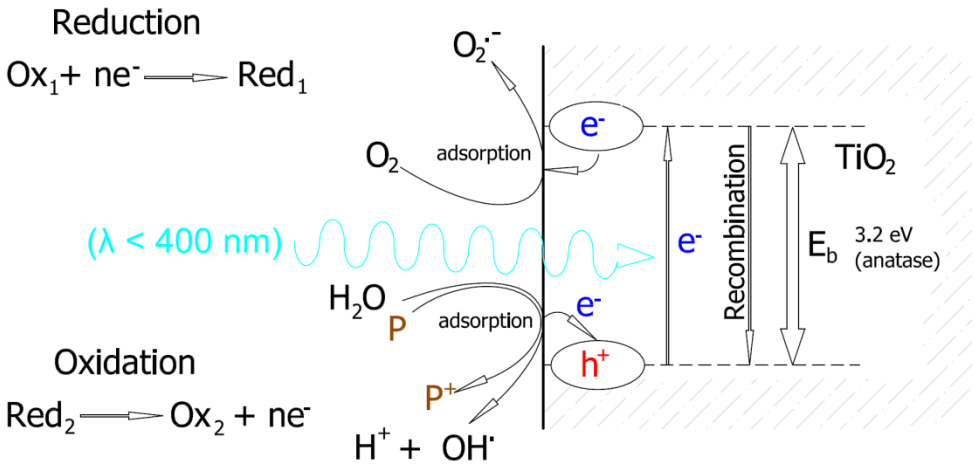

Figure 1. Photo-induced formation process of electron-hole pair in a semiconductor TiO_2 particle with the presence of water pollutant (P).

Direct photoholes:
$R^\cdot + h^+ \rightarrow R^{+\cdot} \rightarrow Intermediate(s)/final\ degradation\ products$ **Equation 15**

Protonation of superoxides: $O_2^{\bullet -} + H^+ \rightarrow HOO^\bullet$ **Equation 16**

Co-scavenging of e^-: $HOO^\bullet + e^- \rightarrow HO_2^-$ **Equation 17**

Formation of H_2O_2: $HO_2^- + H^+ \rightarrow H_2O_2$ **Equation 18**

The e^-_{TR} and h^+_{TR} in Equation 11 represent the surface trapped conduction-band electron and valence-band hole, respectively. The h^+_{TR} are powerful oxidants, while e^-_{TR} are good reducing agents, depending on the type of catalysts and oxidation conditions. These trapped carriers mainly exist near the particle surface and do not recombine immediately after photoexcitation. In the absence of electron scavengers, the photoexcited electron recombines with the valence band hole in nanoseconds with simultaneous release of heat energy (Equation 11). The recombination is unwanted process and to prevent it, the presence of electron scavengers (O_2, O_3, etc.), is vital for successful functioning of photocatalysis. Equation 12 illustrates how the presence of dissolved oxygen (DO) prevents the recombination of electron-hole pair and allows the formation of superoxide radicals ($O_2^{\bullet-}$). By protonation of $O_2^{\bullet-}$ radical the hydroperoxyl radical ($HO_2^{\bullet}$) can be further produced and subsequently H_2O_2 as shown in Equations 16 and 17, respectively. The $HO_2^{\bullet}$ radical formed was also reported to have scavenging property and thus, the co-existence of these radical species can doubly prolong the recombination time of the h^+_{TR} in the entire photocatalysis reaction. Without the presence of water molecules, the highly reactive hydroxyl radicals ($^{\bullet}OH$) could not be formed (Gaya and Abdullah 2008) and impede the photodegradation of liquid phase organics. Although the h^+_{TR} has been widely regarded for its ability to oxidize organic species directly, this possibility is remained inconclusive (Gaya and Abdullah 2008; Chong et al. 2010).

Many mechanistic studies on TiO_2 photodegradation of different organic compounds have been extensively investigated. Aromatic compounds can be hydroxylated by the reactive $^{\bullet}OH$ radical that leads to successive oxidation/addition and eventually ring opening. The resulting intermediates, mostly aldehydes and carboxylic acids will be further carboxylated to produce carbon dioxide and water. The understanding of the reaction steps that involves photodegradation of organics on the photon activated surface of TiO_2, is essential in the formulation of kinetic expression. If the irradiation time is extended for heterogeneous photocatalysis, the liquid phase organic compounds are degraded to its corresponding intermediates and further mineralized to carbon dioxide and water (Equation 19) (Chong et al. 2010).

$$organic\ contaminants \xrightarrow{TiO_2/h\nu} intermediate(s) \rightarrow CO_2 + H_2O \qquad \textbf{Equation 19}$$

The overall photocatalytic reaction (Equation 19) can be divided into five independent steps (**Figure 2**) (Fogler 1999; Herrmann 1999):

1. Transfer of the reactants in the fluid phase to the surface.

2. Adsorption of the organic contaminant(s) onto the photon activated TiO_2 surface (i.e. surface activation by photon energy occurs simultaneously in this step).

3. Photocatalytic reaction in the adsorbed phase (e.g. A/B).

4. Desorption of the product(s) (e.g. B) from the photocatalyst surface.

5. Removal of the product(s) from the interface region(s) to the bulk fluid (e.g. B).

The overall rate of reaction is equal to the slowest step. When the mass transfer steps (1 and 5) are very fast compared with the reaction steps (2, 3 and 4), the organic concentrations in the immediate vicinity of the active sites are indistinguishable from those in the bulk liquid phase, the mass transfer steps are not rate limiting and do not affect the overall rate of photocatalytic reaction. It was also reported, that adsorption of pollutant molecules or surface contact with the catalyst during the photocatalytic degradation is very important (Vinodgopal and Kamat 1992) and if the mass transfer steps are rate limiting, a change in the aeration or liquid flow conditions may alter the overall photocatalytic reaction rate (Chong et al. 2010).

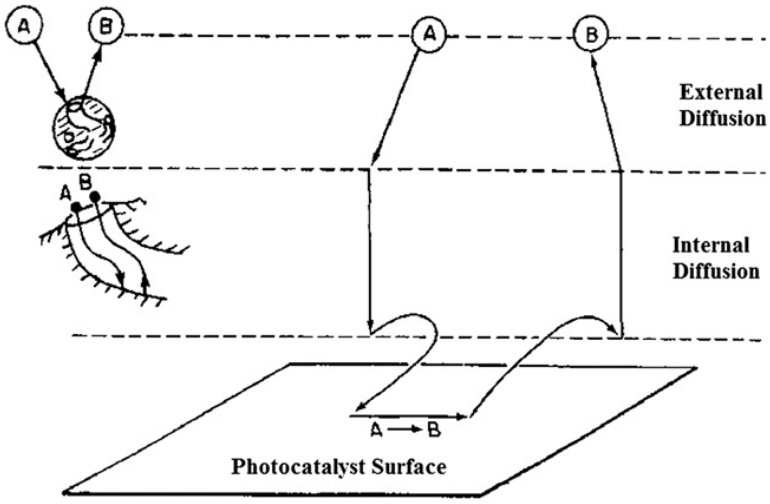

Figure 2. Steps in heterogeneous catalytic reaction (Fogler 1999).

1.4.3 TiO_2 photocatalysis in water

There are two ways of using TiO_2 photocatalyst for photocatalytic degradation process in solution:

(1) particles of photocatalyst suspended in aqueous media or

(2) immobilized on suitable support material.

1.4.3.1 Suspended TiO_2 photocatalyst

Although suspended photocatalyst systems always give higher degradation rates, there is one obvious problem arising from it. Basically, the particle size of catalyst powders synthesized by the industry is in the range of 10–200 nm. Therefore, the reactor must be equipped with a liquid–solid separator, additional process step of post-separation (Yang and Li 2007) like: catalyst recovery hybridization with conventional sedimentation (Fernandez-Ibanez et al. 2003), cross-flow filtration (Doll and Frimmel 2005), various membrane filtrations (Zhao et al. 2002; Zhang et al. 2008) or induced coagulation coupled with microfiltration (MF) hybridization, which it was reported that it can recover the remaining 3 % of the catalyst particles for reuse (Malato et al. 2009). All this increases the costs of the whole process and complicates it. The second problem arising from a suspension system is that the fine solid particles from the effluent may cause turbidity in the downstream. Taking into account the above problems and also from the economic point of view, immobilization of photocatalyst seems to offer a plausible solution.

1.4.3.2 Immobilized TiO_2 photocatalyst

Nano-dimension TiO_2 catalyst allows having a large surface area-to-volume ratio and can further promote the efficient charge separation and trapping at the physical surface (Nagaveni et al. 2004a; Nagaveni et al. 2004b). It was reported that light opaqueness of this nanoscale TiO_2 catalyst has an enhanced oxidation capability in comparison to the bulk catalysts (Siddiquey et al. 2008). Although the nanoscale TiO_2 catalysts show considerable improvement in terms of their physical and chemical properties, their particle size and morphology remains the main problem in a large scale water treatment process (Byrne et al. 1998).

To simplify the potential system for water treatment, various materials have been explored as a TiO_2 support for the photodegradation of contaminants in polluted water. Immobilization of photocatalyst can be carried out on a transparent substrate: glass, fused silica, glass fibers and others or on an opaque substrate like: activated carbon, ceramics, metals and others (Shan et al. 2010 and references therein).

1.4.4 Modification and doping of TiO_2 photocatalyst

As it was already mentioned, initiation of photocatalytic reactions is directly related to photon absorption; in case of TiO_2 photocatalysis light with $\lambda \leq 400$ nm is required for catalysts activation. In order to utilize the vast abundance of outdoor solar and indoor irradiation, both with much higher proportion of irradiation with longer wavelengths $\lambda \geq 400$ nm, different modifications of the photocatalyst were made. To extend the photoresponse of TiO_2 catalyst in visible part of solar spectrum, various material engineering solutions have been devised, including composite photocatalysts with carbon nanotubes, dyed sensitizers, noble metals or metal ions incorporation, transition metals and non-metals doping (Malato et al. 2009; Pelaez et al. 2012). The main purpose for utilizing these material engineering strategies is to balance both the half-reaction rates of the photocatalytic reaction by adding electron acceptor, or modifying the catalyst structure and composition. Different mechanisms to enhance the photoactivity of the catalyst are presented in **Figure 3**.

In case of dye sensitized coupling, the excited dye molecules under solar (visible) irradiation can inject additional electrons to conduction band of semiconductor to initiate the catalytic reactions and thus enhance the formation of electron-hole pairs (**Figure 3**a). Dyes such as Methylene Blue, Azure A/B/C, Fluorescein, Rhodamin B and Malachite green have been most frequently used and widely functionalized under solar irradiation (Malato et al. 2009).

Transitional metal ion doping (Figure 3b), rare earth metal ion doping and non-metals doping have also been investigated for enhancing photocatalytic activity of TiO_2. Doping with metal/non-metal ions could extend the photo-response of TiO_2 into visible spectrum, since it introduces bulk and surface defects which can influence on trapping and transferring electrons/holes. Because photocatalytic reaction can only occur at the photocatalysts surface, carrier transport is as important as carrier trapping. Consequently, ions should be doped near the surface of TiO_2 particles for a better charge transfer. It was found that Fe, Rh, Mo, V, Ru, Re, and Os metal ions can increase photocatalytic activity. Fe and Cu ions can trap not only electrons but also holes, and additionally also introduce energy levels which are near to conduction/valence band edge of TiO_2. For that reason, doping of either Fe or Cu ions is recommended for enhancement of photocatalytic activity. Likewise, enhanced photocatalytic activities were observed at certain doping content of different rare earth metal ions (e.g. La, Ce, Er, Pr, Gd, Nd and Sm) and non-metal dopants (e.g. N, C, F, S and etc.) (Malato et al. 2009). On the other hand it was also observed that introduction of dopant can sometimes decrease photocatalytic activity due to anomalies in crystal structure and poorly crystallized or even amorphous lattice regions of photocatalyst, which serve as recombination sites.

Metal ion implantation has been reported as an effective method to modify semiconductor electronic structures to improve visible light response. Transition metal ions or oxides, such as Cr, Fe, Ni and V were found to shift smoothly to visible light regions up to 600 nm, depending on the kind of metal implanted. Metal ion implanted TiO_2 is believed to be the most effective photocatalyst for solar energy utilization and is in general called as the ‘‘second generation photocatalyst’’ (Malato et al. 2009).

Optimal deposited amount of noble metals (e.g. Ag, Ni, Cu, Pt, Rh, and Pd) with Fermi level lower than TiO_2 is used to enhance charge separation on the TiO_2 surface (**Figure 3**c). These metals enhance electron transfer and prolong the surface charge separation and thus reduce recombination of e^--h^+ pairs. Although noble metals coupling could be efficient, their cost-effectiveness for an industrial application is usually replaced by more economical transition metals or non-metals doping (Malato et al. 2009).

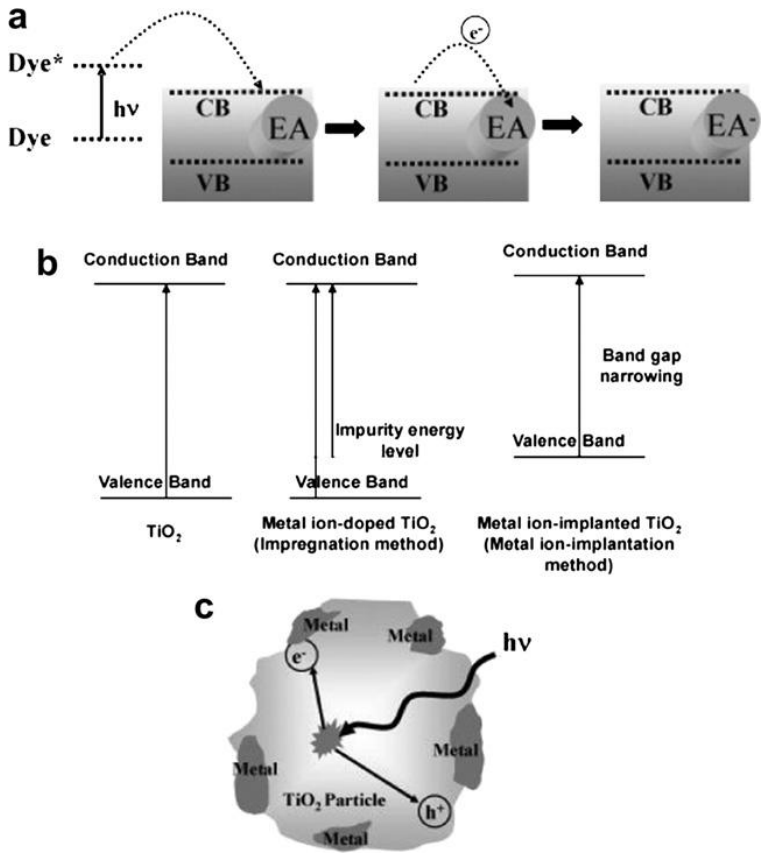

Figure 3. (a) Steps of excitation with a sensitizer in the presence of an adsorbed organic electron acceptor (EA); (b) Scheme of TiO_2 band structures, chemically ion-doped TiO_2 and physically ion-implanted TiO_2; (c) Electron capture by a metal in contact with a semiconductor surface (Malato et al. 2009).

Semiconductor coupling is another way to produce photocatalysts which can use visible part of electromagnetic irradiation for production of excitons (e^--h^+ pairs). Composite semiconductors are produced when a large band gap semiconductor is coupled with a small band gap semiconductor with a more negative conduction band level. Very important facts are that the small band gap semiconductor should be able to be excited by visible light and the electron transfer from the small band gap semiconductor to the large band gap semiconductor should be fast and efficient. CdS and WO_3 were most often used to couple with TIO_2 (Malato et al. 2009).

1.4.5 Technologies for deposition of photocatalytic films

Immobilization procedure of photocatalytic nanoparticles is an important step, because it has to provide stable, mechanical resistant layer. This means that at least the following conditions should be satisfied: (I) good adhesion, which enables layer durability without photocatalyst leaching and exfoliation; (II) no deactivation of the photocatalyst by the attachment process (Imoberdorf et al. 2010; Shan et al. 2010; Plesch et al. 2012); and (III) good interparticle bonding (Kete et al. 2014). There are many different methods for the immobilization of TiO_2 photocatalyst and a promising strategy for producing a highly active photocatalytic coating is the attachment of stable photocatalyst particles onto a support without any reduction in activity. Numerous techniques were reported for preparing supported titania, for instance, thermal bonding (Qiu and Zheng 2007), sol–gel (Mallak et al. 2007; Novotna et al. 2008; Kesmez et al. 2009; Lopez et al. 2013; Sampaio et al. 2013), liquid phase deposition (Mallak et al. 2007), powder modified titania sol (Chen and Dionysiou 2006; Chen and Dionysiou 2008; Miranda-Garcia et al. 2010; Miranda-Garcia et al. 2011; Šuligoj et al. 2010), sol-spray (Neti et al. 2010; Dostanic et al. 2013), inkjet printing (Cerna et al. 2013), using organic polymers (Nawi and Zain 2012), thermal bonding with additional UV laser treatment (Kim et al. 2010), physical vapor deposition (Armelao et al. 2007), chemical vapor deposition, electro-deposition (Shan et al. 2010) and an all-titania wash coating method (Peng et al. 2008).

1.4.5.1 Hybrid immobilization procedure (sol-suspension procedure)

Hybrid immobilization procedure includes first preparation of a sol–gel solution, which is then enriched with TiO_2 powder, resulting in a so-called sol-suspension. The preparation of highly photocatalytically active sol-suspensions relies on photoactive TiO_2 powder (can be a commercial one, such as Degussa P25, Millennium PC500, or anion doped TiO_2 for extending absorption into visible part of solar spectrum, such as N-doped VPC-10, C-doped KRONOClean 7000), which is suspended in a binder solution composed of colloidal and hydrolyzed SiO_2 and additionally also hydrolyzed TiO_2 (Šuligoj et al. 2010). The characteristic of sol-suspensions and their deposition is that all the procedures include thermal treatment only up to 200°C, i.e. low-temperature treatments. The final product consists of up to several μm thick coating of highly active photocatalyst deposited onto various surfaces. This immobilization procedure has some important advantages, such as good repeatability of prepared films and sol-suspension composition, which allows different approaches of immobilization: by dip coating, with brush or air-brush that are easily obtainable in an environmental laboratory or elsewhere.

1.4.5.2 Substrates for immobilization

As mentioned above, there are many different material types and possibilities to immobilize the photocatalyst. In our case the aim is to predominantly use porous monolith (Al_2O_3), beside glass slides as the most extensively used substrate. This decision is justified by two reasons: (i) substrates are light and mechanically stable and (ii) hybrid immobilization procedure is an appropriate method to immobilize highly photocatalytically active commercial TiO_2 to these supports. Prepared immobilized catalysts on different supports were used in a prototype and compact photocatalytic reactor.

1.4.6 Photocatalytic reactors

As it was already mentioned, photocatalysts can be used as suspended in water or immobilized on different supports. Likewise, the reactor systems for water treatment are generally classified into two main configurations (Herrmann 1999): (1) reactors with suspended photocatalyst particles (Ray and Beenackers 1997; Salaices et al. 2001; Benotti et al. 2009; Ray 2009) and (2) reactors with photocatalyst immobilized onto continuous inert carrier or substrate (Raupp et al. 2001; Ochuma et al. 2007; Plesch et al. 2009; Miranda-Garcia et al. 2011; Wang et al. 2014). Main features that differentiate between these two configurations are that the first one requires an additional separation of the dispersed particles, so special filtration unit for the TiO_2 recovery, while the latter permits a continuous operation. In both configurations there are various types/designs of reactors used in the photocatalytic water treatment on laboratory and industrial scale.

The most important factors in configuring a photocatalytic reactor are the total irradiated surface area of catalyst per unit volume and light distribution within the reactor. Slurry–type photocatalytic reactor usually exhibits a high total surface area of photocatalyst per unit volume, while the fixed–bed configuration is often associated with mass transfer limitation over the immobilized layer of photocatalysts (Imoberdorf et al. 2010), which can be improved by using appropriate photocatalyst carrier. In photocatalytic reactor direct photon utilization is preferred, what means that the photocatalysts are directly activated by light photons without assistance of various parabolic light deflectors/mirrors to transfer the photons. To achieve uniformity in photon flux distribution within the reactor, a correct position of light source is essential to ensure maximal and symmetrical light transmission and distribution (Imoberdorf et al. 2010).

1.4.6.1 Reactors with suspended particles of TiO_2 photocatalyst

1.4.6.1.1 Slurry annular reactor (SAR)

Two concentric tubes, the inner being transparent to radiation, make up the SAR unit. The TiO_2 suspension flows through an annular channel created by the two tubes. The lamp is placed inside the inner transparent tube. This geometry has the advantage of providing a symmetric irradiation field (Sopajaree et al. 1999; Andreozzi et al. 2000).

1.4.6.1.2 Open upflow reactor (OUR)

The OUR has immersed lamps placed perpendicularly to the dominant direction of the water flow (Alberici and Jardim 1994). This configuration with a non–symmetric irradiation field entails a more complex reactor model and requires a larger reactor volume than that of the SAR to achieve the same performance.

1.4.6.1.3 Hybrid photocatalytic–membrane reactor system

The hybrid photocatalytic–membrane reactor system is generally known as the "photocatalytic membrane reactors" (PMRs) (Benotti et al. 2009). This is owing to the nature of the hybrid system where the membrane filtration unit could be configured into different positioning with the photocatalytic reactor. With these PMRs, one of the main operational issues is the transmembrane pressure, which determines both the filtration rate and operating costs. It was known that the PMR treatment costs increase if the photocatalysts with small particle and colloidal size are used. With both the microfiltration (MF) and ultrafiltration (UF) membrane filtration, the fine photocatalyst particles can cause membrane fouling and subsequently reduce membrane permeate flux.

Among all the hybrid PMR systems, the pilot Photo–CatTM system (**Figure 4**) (manufactured by Purifics Inc., Ontario, London) has shown the potential application. In the Photo–CatTM system, the water stream passes through a pre–filter bag and a cartridge filter before being mixed with a nanoparticle TiO_2 slurry stream. The mixed stream then passes through the reactor within the 3 mm annulus of the 32 UV lamps aligned in series, which can be individually controlled for the varying water quality. The overall hydraulic residence time passes between 1 and 32 s, depending on the number of UV lights being turned on. A cross–flow ceramic membrane TiO_2 recovery unit is hybridized downstream of the reactor to remove the TiO_2 from the flow stream, while allowing the treated water to exit. The retentive TiO_2 stream is recycled and remixed with the fresh TiO_2 slurry stream that enters the reactor system (Benotti et al. 2009).

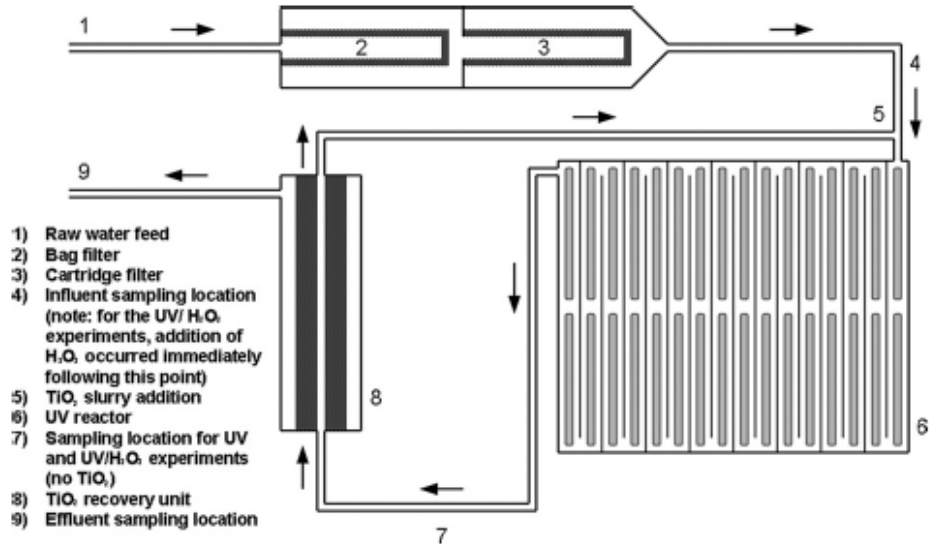

Figure 4. General scheme of photocatalytic membrane reactor pilot system (Benotti et al. 2009).

1.4.6.1.4 Swirl flow reactor (SFR)

Two circular glass plates constitute the SFR reactor. The TiO_2 water suspension is injected tangentially in the outer reactor section creating a swirl and promoting high mixing of the TiO_2 suspension. The TiO_2 suspension leaves the unit from the center of a top plate (Ray and Beenackers 1997; Chen and Ray 1998; Chen and Ray 1999). This unit provides well–mixed slurry with potentially non–uniform irradiation, which results in an associated complex reactor model.

1.4.6.1.5 Taylor vortex reactor (TVR)

The TVR consists of two coaxial cylinders and free–flowing particle slurry circulating in the annular channel. Light bulbs are mounted in the inner cylinder. A vortex–induced fluid instability is generated via inner cylinder rotation. The catalyst is irradiated periodically as vortices move catalyst particles closer to the irradiated reactor section. Optimum operating conditions of 300–rpm inner cylinder rotation and a catalyst loading of 10 gL^{-1} provide an efficiency that is three times larger than that of a conventional slurry reactor (Sczechowski et al. 1995). A disadvantage of the TVR configuration is the complexity of its moving parts.

1.4.6.1.6 Turbulent slurry reactor (TSR)

The TSR is a finned, turbulent slurry system with a ceramic membrane for the separation and the recycling of the catalyst. The membrane is periodically cleaned with an air back–flow. According to their developers, the TSR's main advantages are its compact design and its expected high efficiency (Say 1990; Butters and Powell 1995).

1.4.6.1.7 Photo–CREC–water–II

Photo-CREC-water II is an annular vessel with a lamp placed in the center of the reactor. In the upper section, there is a slurry distribution system ensuring intense mixing of the slurry suspension at the reactor entry. The unit is equipped with quartz windows and accessory collimator tubes. This configuration allows the measurement of photon absorption and the quantification of back and forward reflection, and it is of particular value to establish energy and quantum efficiencies in photocatalytic reactor units (Salaices et al. 2001; Ray 2009).

1.4.6.1.8 Photo–CREC–water–III

Photo–CREC–water III is an annular vessel with external illumination. This unit is designed to simulate a solar-irradiated reactor. The reactor is irradiated externally by a set of eight UV lamps permitting the simulation of solar irradiation. This unit shares a number of features with Photo–CREC–water II (Salaices et al. 2001; Ray 2009).

1.4.6.2 Reactors with immobilized TiO_2 photocatalyst

Photocatalytic reactors in which the TiO_2 is immobilized on the surface of an inert support may be divided in four principal types (Imoberdorf et al. 2010):

•membrane, monoliths, or equivalent forms of catalytic wall reactors,

•optical fiber reactors,

•fluidized bed reactors, and

•packed bed reactors.

1.4.6.2.1 Membrane, monoliths, or equivalent forms of catalytic wall reactors

Membrane Reactors:

In the “photocatalytic membrane reactors” (PMRs) with immobilized photocatalyst the membrane module functionalizes as the support for the photocatalyst particles and barrier against the different organic molecules in the reaction water. The photocatalytic reaction takes place on the surface of the membrane or within its pores and it was reported that photooxidation efficiency of the contaminants is higher when an immobilized PM was used, rather than in the case of PMRs with suspended catalyst particles (Molinari et al. 2004). But immobilizing the photocatalyst particles might cause severe destruction to the membrane structure owing to their close contact with both UV light and hydroxyl radicals. In view of this, the hybridization configuration of the membrane process using photocatalysts in suspension appears to be the more promising arrangement.

Monolith Reactors:

Ceramic foams of various compositions like Al_2O_3 (**Figure 5**), SiC, cordierite or others (e. aluminum) (Wang et al. 2014), produced by the polymer sponge or replica method possess beside high stability many beneficial properties. This is an open, three-dimensional network structure with an interconnecting porosity (5 – 20 PPI – pores per inch) in the range of 75–95 vol%, high inner geometric surface area, low density, good permeability and a low pressure drop (Plesch et al. 2012).

Figure 5. Commercial alumina–mullite Vukopor foam (left) and laboratory made alumina EMPA ceramic foam (right) with the pore dimensions of 15 pores per inch (ppi) (Plesch et al. 2012).

In addition, the photocatalytic TiO_2/Al_2O_3 composite membranes exhibit high water permeability, reliable organic retention, and anti-biofouling properties. Consequently, these photocatalytic TiO_2 films and membranes (**Figure 6**), when further optimized, can be applied in the development of promising air, water and waste water treatment and reuse systems (Raupp et al. 2001; Ochuma et al. 2007; Plesch et al. 2009; Wang et al. 2014).

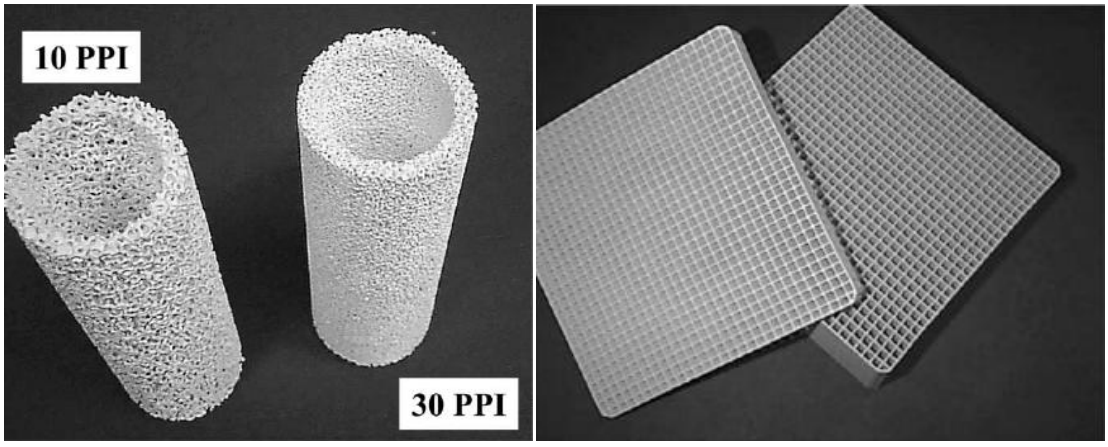

Figure 6. Photograph of two alumina reticulated foam monoliths fabricated for an annular photocatalytic reactor (left) and titania-coated and an uncoated cordierite monolith (right) (Raupp et al. 2001).

The best specific photocatalytic activity was obtained with foams of a greatest pore size of 10 to 15 PPI. This can be explained by the fact, that with an increasing pore size a better flow of solution through the porous foam structure is reached and similarly a better access of UV light to

the active TiO_2 surface is realized (Plesch et al. 2009). In some cases reactors with TiO_2-coated reticulates were even more efficient compared with the reactions carried out using TiO_2 in suspension, if the concentration was not optimized (Ochuma et al. 2007). Consequently, the performance of these coated foam monoliths shows great promise for the use of immobilized TiO_2 for large-scale application of photocatalytic treatment of contaminated water and for improving the overall process economics (Ochuma et al. 2007; Plesch et al. 2009).

Multiple Tube Reactor (MTR):

The MTR (**Figure 7**) is designed with a cylindrical vessel (5–6 cm of diameter) containing 54 hollow quartz glass tubes (diameter 0.6 cm) externally coated with photocatalyst. The MTR resembles a shell and tube heat exchanger with the water to be treated flowing in the shell side of the MTR. The irradiation is distributed in hollow tubes via an aluminum reflector (Ray and Beenackers 1998a; Mukherjee and Ray 1999). The MTR provides a large activated photocatalyst area per unit reactor volume.

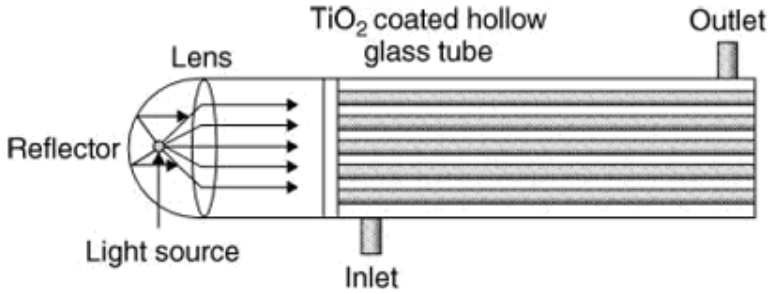

Figure 7. Schematic representation of a multiple tube reactor (Ray and Beenackers 1998b).

1.4.6.2.2 Optical fiber reactors - OFR

The optical fiber reactor (**Figure 8**) is designed with fiber optic cables bringing irradiation to the supported TiO_2. This system can allow the irradiation of a remotely located photocatalyst with minimum scattering and uniform irradiation. The cost of optic fibers and the energy losses during beam focusing and photon transfer are two disadvantages that can lessen the appeal of the OFR design. A typical OFR includes Degussa P25 immobilized on quartz optical fibers and a Xe arc UV–radiation lamp (310–375 nm) (Hofstadler et al. 1994; Peill and Hoffmann 1998).

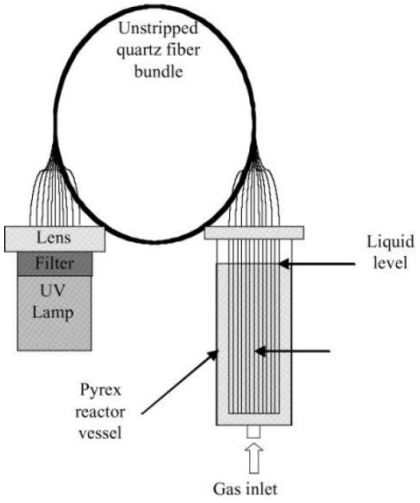

Figure 8. Schematic representation of the optical-fiber bundled array photocatalytic reactor system (Peill and Hoffmann 1998).

1.4.6.2.3 Fluidized bed photocatalytic reactors (FBPRs)

In the case of FBPRs photocatalyst is immobilized on different inert supports of small 3D size (quartz sand, glass beads) which are used in photocatalytic reactor. Upward flow of polluted water suspends the immobilized catalyst, which more or less floats in the stream (**Figure 9**).

The advantages offered by FBPRs are: efficient contact between the catalyst and the pollutants, they provide good mixing of reactant and catalyst, high catalyst loading, low mass transfer resistances, the low pressure drop, and the high TiO_2 surface exposure to UV-radiation. Besides, FBPRs with an annular-type configuration could enable a more efficient use of the radiation emitted by UV lamps (Nelson et al. 2007). One serious concern with fluidization processes, however, is elutriation of particles, which causes loss of catalyst and downstream line blockage. Thus, catalyst elutriation is an important design factor, in addition to the reaction rate during fluidized bed operation.

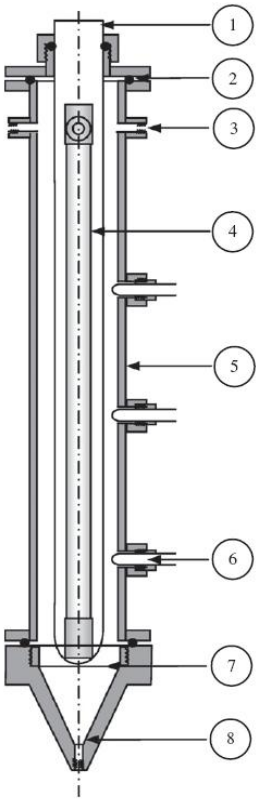

Figure 9. Fluidized bed photocatalytic reactor: (1) quartz sleeve (Φ = 3. 0 cm), (2) o-rings, (3) water outlet (×4), (4) UV lamp, (5) acrylic tube (Φ = 5. 0 cm), (6) quartz sleeves (Φ = 1. 5 cm), (7) narrow grid, and (8) water inlet (Nelson et al. 2007).

1.4.6.2.4 Packed bed reactor (PBR)

The PBR is an annular packed unit irradiated by a central lamp (Figure 10). Several variations of the PBR are reported:

•TiO_2 coated glass mesh (Robertson and Henderson 1990),

•TiO_2 coated glass wool (Al-Ekabi et al. 1989),

•TiO_2 coated glass beads (Al-Ekabi et al. 1989; Roupp et al. 1997).

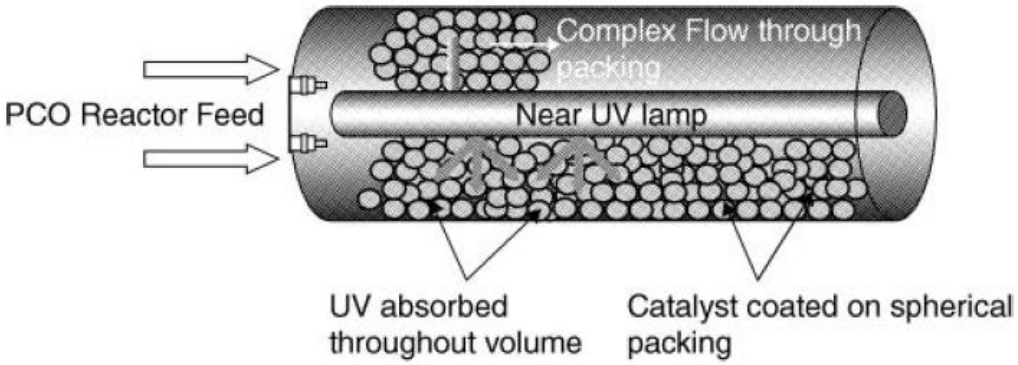

Figure 10. Annular packed-bed reactor (Roupp et al. 1997).

A possible drawback of the PBR results from the uneven or partial photocatalyst irradiation. Uneven flow distribution may also limit the amount of water contacting the irradiated TiO_2 and thus negatively influencing the overall PBR unit's performance. On the other hand packed-bed photocatalytic reactors offer mainly five important advantages: (1) no separation processes to remove the catalyst from the treated stream are needed, such as the ones required for slurry reactors; (2) it is possible to significantly increase the photocatalytic surface by using the proper filling; (3) thin films of TiO_2 can be immobilized on UV-transparent substrates and used as the reactor filling, which benefit the radiation distribution inside of the reactor; (4) the fluid dynamics of the reactor is improved with respect to those reactors without filling, enhancing the mixing of reactants, which tend to reduce the undesirable diffusive resistances; and finally, (5) the packed bed reactors have less catalysts attrition problems, such as the ones present in fluidized bed reactors (Imoberdorf et al. 2010).

1.4.7 Factors in the photo-reactor that affect its performance

1.4.7.1 Properties of photocatalyst

The differences in the photocatalytic activity are likely to be related to surface and structural semiconductor properties such as crystal composition, surface area, particle size distribution, porosity, band gap and surface hydroxyl density. These properties could affect the adsorption behavior of a pollutant or intermediate molecule and the life time and recombination rate of electron-hole pairs. Particle size and agglomeration are of primary importance in heterogeneous catalysis, because it they are directly related to the efficiency of a catalyst through the definition of its specific surface area (Gaya and Abdullah 2008; Ahmed et al. 2011). Numerous forms of TiO_2 have been synthesized by different methods to arrive at a photocatalyst exhibiting desirable physical properties, activity and stability for photocatalytic application.

A number of commercially available catalysts have been tested for the photocatalytic degradation of various organic compounds in an aqueous environment. **Table 1** in Section 2.3.1 (p. 27) presents the specification and characteristics of some commercial TiO_2 samples from different producers: Evonik Degussa (P25), Millennium (PC 500, PC100, PC10) and Sakai Chemical Industry Co., Ltd. (JRC-TiO-6). There are many publications (Ohtani et al. 1992; Enriquez et al. 2007; Gumy et al. 2008; Hathway and Jenks 2008; Song et al. 2010; Paola et al. 2014) pointing out different characteristics of tested TiO_2 photocatalysts that influence the photocatalytic degradation of different organic compounds. Since there are many different combinations of TiO_2 photocatalysis/oxidant processes, it is obvious that role and importance of certain semiconductor property could change, depending on process applied.

1.4.7.2 Concentration of photocatalyst

1.4.7.2.1 Slurry reactors

In slurry reactors photocatalytic degradation rate initially increases with photocatalyst loading and decreases at high values because of light scattering and screening effects. The tendency towards

agglomeration of nanoparticles also increases at high concentration of photocatalyst, resulting in a reduction in irradiated catalyst surface area which reflects in lower photocatalytic degradation rate of contaminant. Optimum catalyst concentration varies and is dependent on type of photocatalyst and reactor geometry. The range used covers concentrations between 0,5 – 12 g/L and most often the optimal concentration is somewhere between 0.8 and 3 g/L (Minero and Vione 2006; Cernigoj et al. 2007b; Chong et al. 2010).

1.4.7.2.2 Reactors with immobilized photocatalyst

In reactors with immobilized photocatalyst the appropriate deposit thickness of photocatalyst is needed to achieve optimal light utilization. Some authors (Krysa et al. 2005; Doucet et al. 2006) studied the light properties of Evonik Degussa P25 and TiO_2 prepared with hydrolysis deposited on a flat plate or glass by ultraviolet spectrophotometry at 355 or 365 nm, respectively. They studied oxalic acid degradation rate (Krysa et al. 2005) or reflected (R), absorbed (A), and transmitted (T) light fractions, which are plotted in **Figure 11** (Doucet et al. 2006). The experiments showed that a maximum of absorbed light fraction and a maximum of reflected light fraction were reached for a surface load of about 1 mg/cm^2. Krysa et al. showed that there was no increase of oxalic acid degradation rate when the surface load was above 0.4 mg/cm^2 and corresponding thickness of the photocatalytic layer above 1.0 µm. They report that a layer thickness between 1 and 1.5 µm is enough to absorb more than 90% of UVA (355 nm) radiation (Krysa et al. 2005). According to this, it would not be necessary to use a larger amount of catalyst, but a thicker layer may provide more specific surface area for pollutants adsorption and storing in the vicinity of the photocatalytically active area.

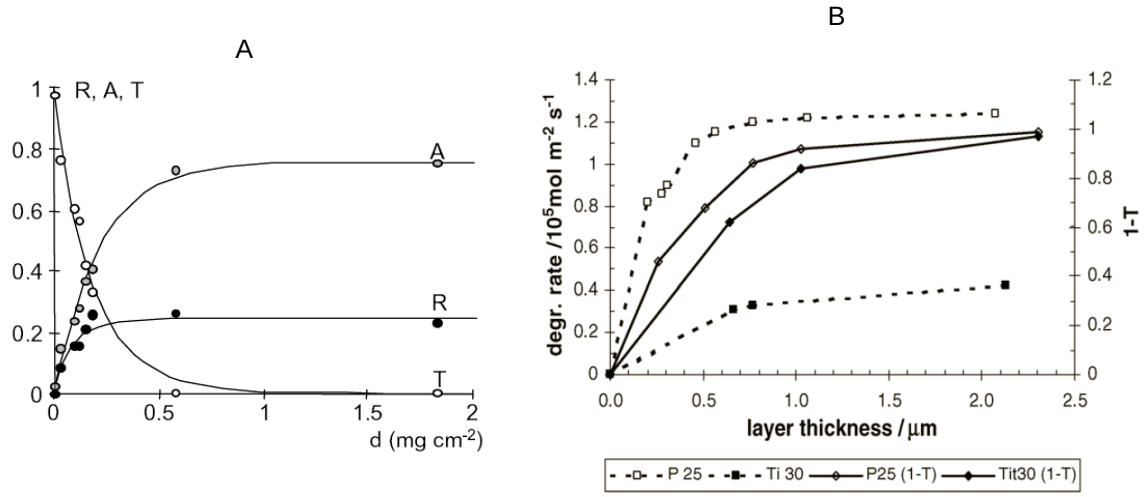

Figure 11. (A) Deposit light balance at 365 nm, catalyst deposited on a flat plate (Doucet et al. 2006) and (B) photodegradation rate of oxalic acid on two photocatalytic layers (λ_{max} = 355 nm) and amount of light absorbed at 355 nm (1−T) as a function of hypothetical layer thickness (Krysa et al. 2005).

1.4.7.3 pH of treated waste water

Electrostatic interaction between photocatalyst surface, solvent molecules, pollutant molecules and charged radicals which are formed during photocatalytic oxidation, strongly depends on the solution pH, which has also an influence on protonation and deprotonation of the organic pollutants. While some compounds are uncharged at common pH conditions, other compounds exhibit a wide variation in charge and physico–chemical properties. Therefore the pH of the solution can play a key role in the adsorption to photocatalysts surface and oxidation of pollutants. Under acidic or alkaline conditions, the ionization state of the surface of the photocatalyst can also be protonated or deprotonated, respectively (Yang et al. 2007):

$$pH < P_{ZC}: \quad \equiv Ti - OH + H^+ \leftrightarrow \equiv Ti - OH_2^+ \qquad \textbf{Equation 20}$$

$$pH > P_{ZC}: \quad \equiv Ti - OH + OH^- \leftrightarrow \equiv Ti - O^- + H_2O \qquad \textbf{Equation 21}$$

where $\equiv Ti - OH_2^+$, $\equiv Ti - OH$ and $\equiv Ti - O^-$ are positive, neutral and negative hydrous TiO_2 surface functional groups, respectively. In very simple terms, interactions with cationic electron donors and electron acceptors will be favored for heterogeneous chemisorption at high pH under conditions in which $pH > pH_{zpc}$, while anionic electron donors and acceptors will be favored at low pH under conditions in which $pH < pH_{zpc}$ (Lu et al. 1996).

Additionally pH influences also reactions in water bulk. For example, if ozone is introduced and combined with photocatalysis as electron scavenger and oxidant at low pH, it will react selectively with organic molecules in solution bulk and perform as efficient electron scavenger. On the other hand it will be efficiently decomposed by hydroxide anions in alkaline environment generating different reactive species and hydroxyl radicals, but its role as electron scavenger will be significantly reduced. Final observation at alkaline pH was diminished synergy of combined process – $TiO_2/UV/O_3$ (Cernigoj et al. 2007a; Lucas et al. 2009; Yildirim et al. 2011; Shin et al. 2013).

1.4.7.4 Dissolved oxygen

The role of dissolved oxygen in TiO_2 water photocatalysis reaction is to assure sufficient electron scavengers to trap the excited conduction–band electron from recombination (Equation 12). The oxygen doesn't affect the adsorption of pollutant molecule on the TiO_2 catalyst surface, because the reduction reaction occurs at a different location from where oxidation occurs (Malato et al. 2009). Other roles for oxygen may involve the formation of other ROS and the stabilization of radical intermediates, mineralization and direct photocatalytic reactions (Equation 16, 22, 23) (Pichat et al. 2000; Wang et al. 2002; Czili and Horvath 2009). The difference between using air or oxygen during water photocatalysis is usually not very drastic as the mass transfer of oxygen to the close vicinity of the surface is the rate determining step (Habibi et al. 2005).

$$2O_2^{-\bullet} + 2H_2O \rightarrow H_2O_2 + O_2 + 2OH^- \qquad \textbf{Equation 22}$$

$$Cl_2CH - COO^- + O_{2\,(ads)}^{-\bullet} \rightarrow ClC^{\bullet}H - COO^- + Cl^- + O_2 \qquad \textbf{Equation 23}$$

1.4.7.5 Other oxidants/electron acceptors

Recombination of (electron-hole) e^--h^+ pairs in photocatalysis means waste of energy and is therefore one of the main weaknesses in the application of TiO_2 photocatalysis. In the absence of suitable electron acceptors or donors, the recombination step is predominant and thus it decreases the quantum yield. To mitigate of e^--h^+ recombination is crucial step to ensure higher efficiency of photocatalysis. Addition of external oxidant/electron acceptors to TiO_2 photocatalytic process increases the rate of photocatalytic degradation by (1) prevention of e^--h^+ recombination by accepting the conduction band electron; (2) increasing the hydroxyl radical concentration and oxidation rate of intermediate compound; and (3) generating more radical species and other oxidizing species to accelerate the degradation of intermediate compounds. Since $^{\bullet}OH$ appears to play an important role in photocatalytic degradation, different electron acceptors such as H_2O_2, O_3, $KBrO_3$, and $K_2S_2O_8$ were investigated (Ahmed et al. 2011).

1.4.7.5.1 Ozone

Photocatalytic ozonation (PH-OZ) process is the result of coupling of photocatalysis and ozonation processes and is considered to be one of the most effective in terms of decomposition of organic species (Agustina et al. 2005; Beltran et al. 2005; Dominguez et al. 2005; Gimeno et al. 2007; Beltran et al. 2010; Cernigoj et al. 2010b; Jing et al. 2011; Oyama et al. 2011; Yildirim et al. 2011; Rodriguez et al. 2012; Zsilak et al. 2014) and disinfection (Nasuhoglu et al. 2012; Horn et al. 2014). This enhanced ability to degrade and disinfect organic material originates from the synergy of coupled photocatalysis and ozonation (Beltran et al. 2008; Cernigoj et al. 2010b; Jing et al. 2011; Rivas et al. 2012; Tomova et al. 2012; Shin et al. 2013; Zsilak et al. 2014), which normally occur in neutral and acidic pH (Cernigoj et al. 2007a). The whole process normally takes place in polluted water, where the photocatalyst, commonly TiO_2, and ozone (dissolved/gas) are introduced, while the whole system is being irradiated with light of appropriate photon energy to activate the photocatalyst. The main resulting advantages of mentioned process are higher quantities of different radical species with high oxidation potential (Beltran et al. 2009; Rodriguez

et al. 2012) and consequently variety of oxidation reactions possible due to the ozone presence. Ozone can react in three ways (Mehrjouei et al. 2014):

(I) by direct attack of organic pollutant present in the bulk:

$$Organic\ pollutant + O_3 \rightarrow Products + Intermediates + Other\ oxidative\ species \quad \textbf{Equation 24}$$

or (II) adsorbed onto catalyst surface, it can decompose in the solution via chain reactions to form hydroxyl radicals and continue the oxidation process indirectly:

$$TiO_2 - OH_2^+ + O_{3(ads)} \rightarrow TiO_2 - O^{\bullet}H^+ + HO_3^{\bullet} \quad \textbf{Equation 25}$$

$$TiO_2 - O^{\bullet}H^+ + H_2O \rightarrow TiO_2 - OH_2^+ + {}^{\bullet}OH \quad \textbf{Equation 26}$$

and (III) ozone molecules can also adsorb on the surface of illuminated photocatalysts and participate in the surface redox reactions as a trap for the electron–hole pairs generated in the photo excitation process:

$$Ti(IV) + e_{cb}^-(TiO_2) + O_3 \rightarrow Ti(IV) - O_3^{-\bullet} \quad \textbf{Equation 27}$$

$$Ti(IV) - O_3^{-\bullet} + \mathrm{H}^+ \rightarrow Ti(IV) - HO_3^{\bullet} \quad \textbf{Equation 28}$$

$$Ti(IV) - HO_3^{\bullet} \rightarrow Ti(IV) - OH^{\bullet} + O_2 \quad \textbf{Equation 29}$$

In the latter case, other oxidative species, such as hydroxyl radicals ($OH^{\bullet}$), ozonide radicals ($O_3^{\bullet-}$), hydrogen trioxyradicals ($HO_3^{\bullet}$), hydroperoxyl radicals ($HO_2^{\bullet}$) and hydrogen peroxide (H_2O_2), will be synergistically formed on the catalyst surface to follow the oxidation process.

The effectiveness of PH-OZ is highly dependent on conditions which take place in polluted water: temperature (Beltran et al. 2002; Shin et al. 2013), pH (Cernigoj et al. 2007a; Lucas et al. 2009; Yildirim et al. 2011; Shin et al. 2013), ozone concentration or dose (Beltran et al. 2002; Jing et al. 2011; Yildirim et al. 2011; Shin et al. 2013), type of pollutant molecule (Kopf et al. 2000; Gumy et al. 2008; Lucas et al. 2009), initial concentration of pollutant (Yildirim et al. 2011), irradiation type (UV-C, UV-A) (Ohtani et al. 1992) and intensity and last but not least, physicochemical characteristics of photocatalyst (TiO_2), eg. crystal form/composition, particle size, surface density of hydroxyl groups (Ohtani et al. 1992; Song et al. 2010) and in case of suspended photocatalyst, its suspended amount (Beltran et al. 2002; Yildirim et al. 2011; Shin et al. 2013).

1.4.7.6 Type of pollutant and concentration

Photocatalytic reaction is also highly dependent on pollutant type and its concentration. It is known that high concentration of target compound (Herrmann 1999; Gaya and Abdullah 2008) can decrease the photocatalytic efficiency since it is in higher quantity adsorbed on photocatalyst and/or diminishes transparency of treated water for the certain light radiation which is necessary for the excitation of a catalyst. In case of adsorption, more pollutant molecules are adsorbed on the TiO_2 surface, which consequently means the increased need for oxidative species produced by photocatalyst. When the limit of radical production is reached, degradation rate does not increase but is stabilized. The pollutant molecules and degradation products strongly adsorb and cover the entire TiO_2 surface, which leads to reduction in the degradation rate and in worst case to photocatalyst deactivation – photocatalyst poisoning (Gaya and Abdullah 2008; Chong et al. 2010).

From the molecule point of view, its chemical stability and polarity define degradation mechanism, while its absorption spectrum can influence the photocatalyst performance. For example, organic molecules which can adhere effectively to the surface of the photocatalyst will be more susceptible to direct oxidation (Gaya and Abdullah 2008) and more resistant molecules often require additional biological pretreatment or additional use of oxidants (eg. O_3) in combination with photocatalysis to increase the rate of degradation. Additionally, if the molecule absorbs in the

region of electromagnetic irradiation which is also important for excitation of photocatalyst, this can decrease the number of incident photons which are relevant for photocatalyst excitation.

1.4.7.7 Interfering substances

The inorganic anions, which naturally occur in water, such as Cl^-, NO_3^-, SO_4^{2-}, CO_3^{2-} and HCO_3^-, can act as holes (h^+) and hydroxyl radicals scavengers or, depending on the solution pH, compete with the target pollutant for the active sites. Result of scavenging reactions are inorganic anion radicals (eg. $CO_3^{\bullet-}$, $NO_3^{\bullet}$, etc.) which have lower oxidation potential in comparison to h^+ and $^{\bullet}OH$ (Andreozzi et al. 1999):

$$HCO_3^- + {}^{\bullet}OH \rightarrow CO_3^{-\bullet} + H_2O \qquad \textbf{Equation 30}$$

$$CO_3^{2-} + {}^{\bullet}OH \rightarrow CO_3^{-\bullet} + OH^- \qquad \textbf{Equation 31}$$

Therefore, a decrease of the photodegradation efficiency in the presence of inorganic ions is usually observed. Adsorption of water components like calcium, magnesium, iron, zinc, copper, bicarbonate, phosphate, nitrate, sulphate, chloride, and dissolved organic matters onto the surface of TiO_2, can affect the photocatalytic degradation rate of organic pollutants (Ahmed et al. 2011). As it was already mentioned in previous chapter, the concentration and pollutant type, as well as organic and inorganic solids contribute to the water turbidity and can therefore influence the formation of $^{\bullet}OH$ radicals as well, because of its shading effect (Ahmed et al. 2011).

1.4.7.8 Intensity and wavelength of irradiation

The wavelength of irradiation and consequently its source must be chosen with respect to photocatalyst used. Irradiation should contain photons of an appropriate energy to overcome band gap threshold, for instance in case of TiO_2 this energy is ≥3.02 eV (Herrmann 1999), meaning that photons of ≤400 nm should be used. The photocatalytic conversion of pollutants is directly related to irradiation intensity or flux and its distribution within the reactor. With increasing the flux, number of excitons (e^- - h^+) and consequently number of reactive species increase. It is considered that the rate is proportional to radiation flux to the certain intensity (25 $mWcm^{-2}$), above which the relationship changes to square root (Herrmann 1999). But this cannot be claimed in general, because the proportional relationship range can differ among photocatalysts (Kete et al. 2014) and reactor systems. At high intensities, the reaction rate is independent of light intensity. This is likely, because at low intensity reactions involving e^- - h^+ formation are predominant and recombination is insignificant. Formation of e^- - h^+ pairs within the photocatalyst is smaller than the oxidizable organic substrate concentration and hence a linear rate law is expected at low fluxes, whereas the photocatalytic degradation efficiency was shown to be limited to the electron-hole recombination at high photon flux (Ahmed et al. 2011). Anyhow, it is very important that light intensity and lamp positions are optimized for a given reactor system to ensure effective photocatalytic process.

1.4.7.9 Temperature

Water treatment processes are usually carried out at a temperature from 10 to 80°C, since the polluted water can be already cooled down in drain pipe system or be potentially treated immediately after formation, for instance in washing machine. This temperature range is considered not to have drastic influence on photocatalytic phenomena (Herrmann 1999), but rather on oxygen and if used, ozone concentration. Low concentration of these excellent electron scavengers can thus directly influence photocatalytic process and decrease its efficiency.

1.4.7.10 Reactor optimization

It is necessary to optimize the reactor in the view of all mentioned parameters, as can the optimal operating conditions be very different from case to case. These differences may arise from: (I) the use of different catalyst and loading, (II) use of additional oxidants/electron acceptors, (III) different reactor system, geometry and purpose, (IV) irradiation sources, (V) use of different photocatalyst supports, (VI) the type and degree of contamination and others.

The operation parameters of photoreactor would affect the system indifferently, so multi–variable optimization approach is actually required to optimize a photoreactor system as parameter interaction might exist. This has led to the application of effective design of experiments, statistical analysis and response surface analysis for photocatalytic studies. Using this approach, different permutations of experimental design are involved and the operational parameters and spans are defined (Chong et al. 2010).

2 Part A: Photocatalytic ozonation - Study of reaction parameters and mechanism

2.1 Introduction

The efficiency and potential use of photocatalytic ozonation process (PH-OZ) for water treatment, but on the other hand its complexity were the main motivation aspects for present research. The main attention was given to the influence on PH-OZ process regarding pollutant molecule polarity and its interaction with photocatalysts having different physicochemical characteristics. The main question/task of the work presented herein was how to perform PH-OZ process to maximize the efficiency and consequently shorten the time needed for organics mineralization. The study deals with mechanistic aspects of photocatalytic ozonation degradation of two organic probes, thiacloprid and dichloroacetic acid – DCAA (**Figure 12**) in presence of different commercial TiO_2 powders. Thiacloprid is representative of neutral organic molecules and is well known neonicotinoid pesticide (Krohn 2001; Cernigoj et al. 2007a; Banic et al. 2011), while DCAA represents highly stable polar molecules. Thiacloprid belongs to the second generation of neonicotinoid insecticides and is during different photocatalytic processes degraded to many possible intermediates. It is relatively stable to direct ozone attack at acidic pH (Cernigoj et al. 2007a). On the other hand DCAA, a model of aliphatic organic acid, is simple molecule with 2 C atoms, which charge depends on the pH of water media and does not react with ozone. Different types of AOPs (photocatalysis, catalytic ozonation, photocatalytic ozonation) were used to study/compare degradation of two different molecules simultaneously present in water and on the basis of the results some proposals are given how to optimize the process of photocatalytic ozonation.

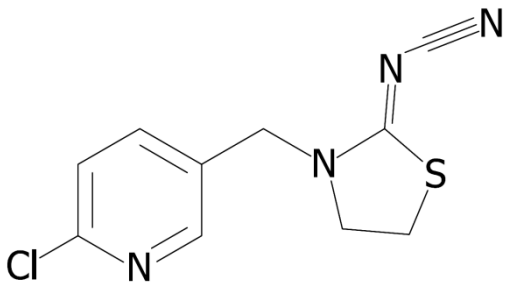

Thiacloprid

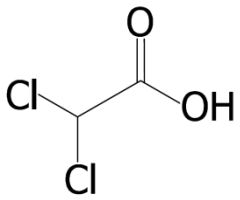

Dichloroacetic acid – DCAA

Figure 12. Molecule structures of thiacloprid and DCAA.

2.2 Experimental details

2.2.1 Chemicals

Pure thiacloprid was already available and obtained by extraction from commercial technical product Calypso SC 480 (Bayer) (Obana et al. 2003; Cernigoj et al. 2007a), other chemicals were used as purchased: perchloric acid ($HClO_4$, 70%) from AppliChem, dichloroacetic acid (DCAA, 99%) from Alfa Aesar, sodium fluoride (NaF, ≥99%) from Sigma-Aldrich, acetonitrile (HPLC grade) from J.T. Baker and ammonium acetate ($C_2H_7NO_2$, ≥96%) from Merck. All aqueous solutions were prepared using highly pure water from the NANOpure system (Barnstead) and acidified using perchloric acid. Commercial TiO_2 nanopowders were obtained from: Evonik Degussa (Aeroxide® P25), Cristal Global (Millennium/CristalACTiV™ PC10, PC100, PC500) and Sakai Chemical Industry Co., Ltd. (JRC-TiO-6 – TiO_2 in rutile phase, later denoted as RUTILE). To conduct the experiments, argon (5.0), pure oxygen (5.1) or ozone generator fed with pure oxygen (5.1) were used.

2.2.2 Photoreactor and ozonator

The experiments of photocatalytic (PC) / photo-ozonation / catalytic ozonation / photocatalytic ozonation (PH-OZ) degradation of DCAA and thiacloprid simultaneously present in solution, were done in a circulation batch slurry reactor. This reactor system consists of irradiation chamber

(Cernigoj et al. 2007b), quartz reactor cell (ca. 100 mL) placed in the center of irradiation chamber, sampling vessel and peristaltic pump. All the parts were connected by Teflon tubes and neoprene tube for peristaltic pump. The total volume of reactor system was 300 mL. High flow rate (1 L/min) and magnetic stirrer in sample vessel enable extremely turbulent mixing. The source of UVA irradiation was one UVA lamp (CLEO 20W, 438 mm × 26 mm, Philips; broad maximum at 355 nm). Irradiation flux inside the reactor cell was determined by ferrioxalate actinometry (Murov S.L. 1993) and considered as low, 5.23×10^{-5} einstein/min (1.7 $mWcm^{-2}$). During the experiment, the system was constantly purged with oxygen (O_2/TiO_2/UV) or ozone (O_3/TiO_2/UV and O_3/UV and O_3/TiO_2/dark). Sampling vessel with integrated cooling system enable constant temperature (T = 18±1 °C) of circulating water solution. The pH was monitored by pH probe (HI 1131B pH probe connected to Hanna 8417) placed in the sampling vessel.

Ozone or oxygen was bubbled into the bottom of the sampling vessel through the glass frit near the suction to reactor cell which provides good mixing and stable supply of gas. Ozone was generated by Pacific Ozone Technology equipment (model LAB21) fed with pure oxygen (5.1). Concentration of dissolved ozone and temperature in water solution of organic probes (DCAA, thiacloprid) were monitored during experiments in sample vessel by on-line Multi-sensor Measuring Instrument MS 08 with ozone sensor tip, AMT Analysenmesstechnik GmbH, Germany. Input of ozone was constant and before starting the experiment the circulating solution was saturated, so that the concentration of dissolved ozone was $\gamma(O_3)$ = 4 mg/L in all experiments.

2.2.3 Analytical procedures

To determine DCAA and thiacloprid concentration, HPLC analyses were made on HP 1100 Series chromatograph coupled with DAD detector. For thiacloprid existing method (Cernigoj et al. 2007a) was used, while to detect DCAA slightly modified method from Enriquez et al. (Enriquez et al. 2007) was used. The DCAA separations were done using Aminex HPX-87H ion exclusion column using 5 mM H_2SO_4 in water as the eluent, with the run duration of 24 min. The eluent flow rate was 0.4 mL/min and injection volume 10 µL. DCAA was detected at 210 nm.

The total organic carbon (TOC) was determined by using Analitik Jena AG MULTI N/C 3100 apparatus. The TOC analysis method included purging with oxygen (150 s), sample volume for analysis was 500 µL and washing volume 2 mL. Samples were incinerated at temperature of 850 °C and detector maximum peak integration time was 300 s. Prior to the analysis samples were acidified by 2M HCl (125 µL) to remove inorganic CO_2. All samples containing TiO_2 were centrifuged to separate TiO_2 nanoparticles from solution before analysis.

2.2.4 Characterization of photocatalysts

2.2.4.1 BET surface area

The specific surface areas of photocatalysts were determined according to Brunauer–Emmett–Teller (BET) theory (Brunauer et al. 1938), using nitrogen sorption isotherms obtained at 77.3 K (Tristar II 3020 Surface Area Analyzer, Micromeritics). Before procedure of BET surface area analysis, nanopowders were cleaned and dried by flushing with nitrogen (5.0) for 4 to 6 h at 130 °C.

2.2.4.2 Dynamic light scattering (DLS) – agglomerate size

The sizes of nanoparticle agglomerates were measured by dynamic light scattering (DLS) technique, using a particle size analyzer 90Plus (Brookhaven Instruments Corporation). The suspensions used for measurements were prepared by dispersing a small amount of nanopowder in highly pure acidified water (c ≈ 45±10 mg/L, pH = 3.0). Suspensions were sonicated for 10 min in an ultrasonic bath and left for 1h to stabilize and after that measured for 3 min.

2.2.4.3 SEM analysis

To determine primary particle size of TiO_2 samples, the JSM 7001 TTLS (JEOL) scanning electron microscope operating on 30 keV was used. Image was compiled by using secondary electrons.

2.2.4.4 Surface OH groups

The procedure to determine the amount of surface OH groups was the same as already reported (Ohtani et al. 1992; Kete et al. 2014), using nanopowders as received. Each sample of TiO_2 (P25, PC500, PC100, JRC-TIO-6 – 2g or PC10 – 4g) was suspended in NaF alkaline water solution (0.1M, 100 mL, pH=10.6) by stirring for 20h. Higher amount of PC10 was used to increase measurement accuracy due to low BET of this photocatalyst. After that the suspension was centrifuged to remove TiO_2 nanoparticles and the concentration of fluoride in the supernatant was measured. The amphoteric nature of surface hydroxyls allows their exchange by fluoride anion, what is perceived as a reduction of fluoride concentration. To measure concentration differences of F^- ions, a fluoride selective ion electrode Orion 9409BN in combination with a 9001 single junction reference electrode (Thermo Scientific) was used. Each sample was used in three parallels, where each parallel was measured twice, and then an average of OH concentration was calculated. During measurements with electrodes the temperature of solution was kept constant, T = 19.7±0.2 °C.

2.2.5 Degradation experiments of DCAA and thiacloprid

Degradation experiments of two simultaneous organic probes (DCAA and thiacloprid) were performed in a circulation batch slurry reactor with overall volume of 300 mL. Experiments were conducted in acidic conditions, where solution of DCAA and thiacloprid was prepared as follows: (I) tihiacloprid solution (126 mg/L) was prepared in acidified water (pH = 3.0) and denoted as Solution 1, (II) separately, 412 µL of DCAA was dissolved in 1 L of thiacloprid water solution (126 mg/L) and denoted as Solution 2. Prior the experiment, Solution 2 (60 mL) was used to test dark adsorption, so 0.3 or 0.9 g of TiO_2 photocatalyst was added and in dark homogenized in ultrasound bath for one hour, after that 1.5 mL sample was taken for HPLC analysis. Then 240 mL of Solution 1 was poured into reactor during operation of peristaltic pump and cooled (T = 18±1 °C). Solution in reactor was then purged with ozone for 7 min and immediately the rest of Solution 2 with TiO_2 (58.5 mL) from dark adsorption was added. Final concentrations were 1 or 3 g/L for TiO_2 and 126 mg/L ($5x10^{-4}$ M) for thiacloprid and 129 mg/L ($1x10^{-3}$ M) for DCAA. After 30 s of circulating and mixing the experiment started and UVA lamp was turned on or in case of dark experiment, the lamp was off. Samples for HPLC (1.5 mL) and TOC (25 mL) analysis were taken at specified time intervals, purged with argon (5.0) and centrifuged.

2.3 Results and discussion

2.3.1 Physicochemical properties

In the **Table 1** properties of commercial TiO_2 powders used in catalytic degradation experiments are presented. According to literature (Ohtani et al. 1992; Song et al. 2010; Paola et al. 2014), three main properties of photocatalyst are playing important role in the process of photocatalytic ozonation and these are: (I) crystalline structure, (II) BET surface area and (III) density of surface OH groups. All mentioned factors are interconnected, because first two influences the third, surface OH groups, which act as active sites for O_3 decomposition (Ohtani et al. 1992).

Table 1. Physicochemical properties of five commercial TiO_2 powders.

Photocatalyst	Crystalline structure [a]	Average primary particle size [nm][d]	Agglomerate size [nm]	BET of commercial TiO_2 powder [m^2/g]	Surface OH density [µmol/m^2]	IEP
PC10	A (≥ 98 %)	65 - 75	444 ± 3	10.0	1.41 ± 0.35	5.7[b]
PC100	A (≥ 95 %)	15 - 25	421 ± 2	81.6	4.38 ± 0.30	5.9[c]
PC500	A (≥ 99 %)	5 - 11	520 ± 4	286	1.71 ± 0.21	6.2[b]
P25	A (70 – 80 %), R (30 – 20 %)	20 - 32	293 ± 4	52.4	1.73 ± 0.51	7.0[b]
JRC-TiO-6	R (≥ 99 %)	50 - 75	210 ± 10	87.5	1.75 ± 0.35	/

[a] Obtained from producers datasheets
[b] IEP – isoelectric point data obtained from (Gumy et al. 2008)
[c] IEP – isoelectric point data obtained from (Ryu and Choi 2008)
[d] Data obtained from SEM analysis

Song et al. (Song et al. 2010) report, that rutile has higher surface hydroxyl density in comparison to anatase which leads to faster phenol catalytic ozonation degradation, while Ohtani et al. (Ohtani et al. 1992) presents just linear correlation to BET surface area. Additionally Paola et al. (Paola et al. 2014) show that crystallinity of TiO_2 plays an important role and higher amorphous phase content in TiO_2 may also lead to higher OH surface density which does not reflect in a better photocatalytic activity. According to **Table 1**, the surface OH density is the same for all used TiO_2 samples irrespective to sample crystalline structure, which results in linear dependence of surface OH concentration to BET surface of TiO_2 sample (**Figure 13**). Higher amount of surface OH groups is directly correlated with increasing BET. The exception is PC100 with more than twice higher surface hydroxyl density in comparison to others, which is due to a lower crystallinity (Paola et al. 2014) (**Table 1**).

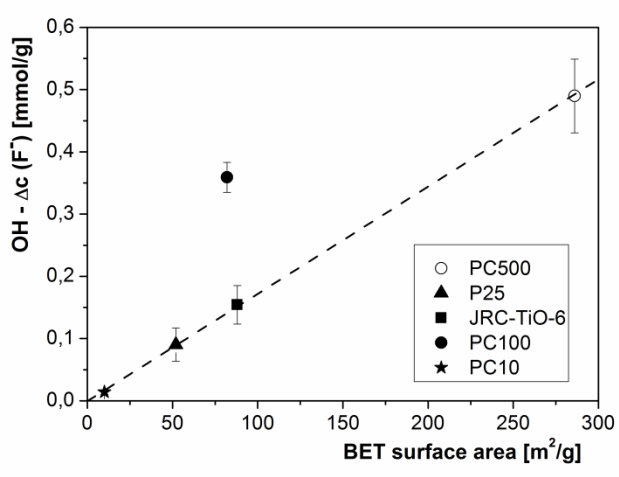

Figure 13. Concentration of hydroxyls in dependence of photocatalysts BET surface area. The concentration of F^- adsorbed corresponds to OH concentration.

DLS analysis was performed under the similar experimental conditions (aqueous suspension with pH 3.0) used in catalytic experiments to evaluate the correlation between TiO_2 agglomeration effect and catalytic activity of TiO_2 samples. The results show (**Table 1**), that TiO_2 samples with smaller particles (PC500, PC100) tend to form larger agglomerates in comparison to those with bigger primary particles (PC10, JRC-TiO2-6, and P25).

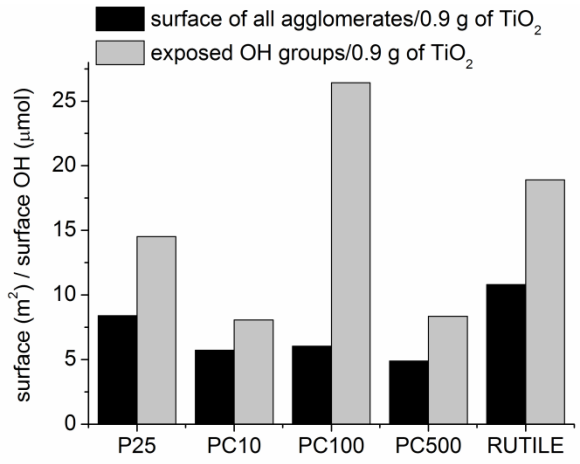

Figure 14. Theoretical exposed surface/surface OH groups of all agglomerates per 0.9 g of TiO_2.

The sizes of agglomerates were used also to evaluate theoretical surface and total amount of surface OH groups exposed to water bulk for each TiO_2 sample (**Figure 14**). These numbers were calculated per 0.9 g of TiO_2 on the basis of agglomerate size, anatase/rutile density and ratio and with assumption that nanoparticles form spherical agglomerates:

$$S_{TOT} = \frac{\left[\frac{(w_R * 0.9g)}{\rho(TiO_{2\ Rutile})} + \frac{(w_A * 0.9g)}{\rho(TiO_{2\ Anatase})}\right]_{volume\ of\ 0.9\ g\ \ TiO_2}}{\left[\frac{3}{4}\pi r^3\right]_{volume\ of\ one\ agglomerate}} * \left[4\pi r^2\right]_{agglomerate\ surface\ area}$$

$$N_{surf\ OH} = S_{TOT} * \rho_{surf\ OH}$$

The result revealed, that catalysts with smaller agglomerates offer higher exposed surface area in comparison to others, which is also true for exposed amount of surface OH, with the exception of PC100 which has much higher OH surface density.

2.3.2 Results of DCAA and thiacloprid degradation

As mentioned in Experimental part, experiments were conducted at acidic pH (3.0). Similarly as in case of other studies (Beltran et al. 2002), this was because the degradation of organic pollutants in water using ozone leads to carboxylic acids resulting in low pH and to limit production of hydroxyl radicals from non catalytic ozone decomposition (Glaze et al. 1987; Lucas et al. 2009). While increasing ozone concentration normally reflects in higher degradation rates, this is not true for TiO_2 catalyst and it must be optimized (Beltran et al. 2002; Shin et al. 2013). In present case the flow of ozone, highly turbulent system and temperature were kept constant during all experiments and maximum degradation rates were achieved by suspending 3g of TiO_2 per 1L of reaction solution. These constant conditions allow to compare degradation ability of different photocatalysts and the impact of their physicochemical characteristics on degradation kinetics of two different types of organic molecules, simultaneously present in the water solution.

2.3.2.1 Dark adsorption and TOC modeling

Adsorption of thiacloprid and DCAA to different TiO_2 photocatalysts was checked to see, if it has any influence to their degradation kinetics in later AOP processes (**Figure 15**). The results show, that DCAA is generally in greater proportion adsorbed to TiO_2 in comparison to thiacloprid. As it was mentioned by others (Czili and Horvath 2009), DCAA adsorbs to photocatalysts with higher BET, which is true also in our case with the exception of PC100. This catalyst has much higher surface OH density which could be unfavorable to DCAA adsorption. On the other hand, thiacloprid adsorption is low, but it is in case of PC10 and PC100 still adsorbed in greater proportion in comparison to DCAA.

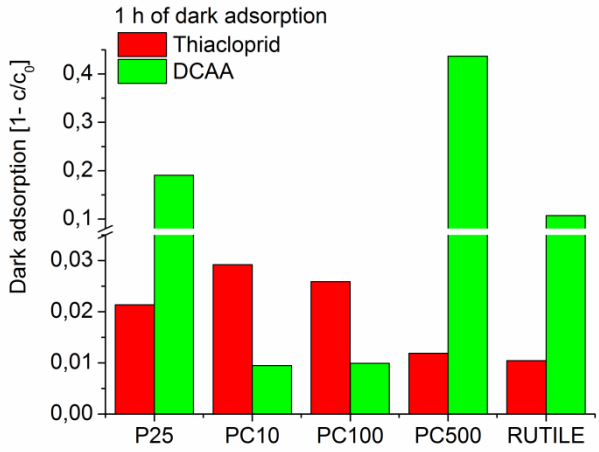

Figure 15. Dimensionless proportion of thiacloprid and DCAA adsorbed on surface of different TiO_2 after 1 h of dark adsorption.

The total organic carbon (TOC) instrument doesn't differentiate between TOC contribution of DCAA and thiacloprid, so the additional experiments (not shown here) were done, which prove that DCAA degradation corresponds to its TOC removal. This is in accordance with the observations of others (Czili and Horvath 2009), where the stoichiometric decrease of TOC in the

liquid phase indicates that there is no significant amount of intermediates containing carbon atom(s) during the photodecomposition of DCAA. This allows correlating DCAA degradation to its mineralization and consequently to calculate the TOC corresponding to thiacloprid (TOC_{THIA}), which represents the difference (Equation 32) between total TOC_{TOT} and TOC corresponding to DCAA (TOC_{DCAA}).

$$TOC_{THIA} = TOC_{TOT} - TOC_{DCAA} \qquad \textbf{Equation 32}$$

The initial TOC concentration values were 84±1 mg/L for all experiments.

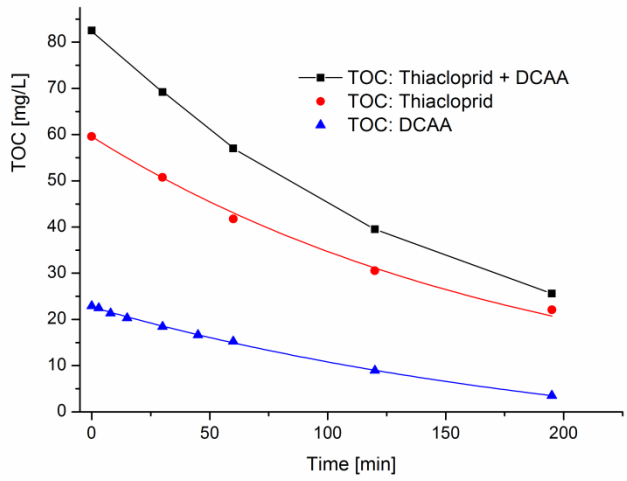

Figure 16. Modeling of DCAA and thiacloprid mineralization process. Figure presents calculated curves for Thiacloprid and DCAA obtained for photocatalytic ozonation process (O_3/TiO_2/UVA) where PC100 (3 g/L) photocatalyst was used.

2.3.2.2 Photocatalytic degradation (O_2/TiO_2/UVA)

Results of initial degradation rate for photocatalytic degradation and mineralization (**Figure 17**) show that DCAA and thiacloprid are degraded by different degradation rates, which is indicating that different physicochemical conditions influence their degradation.

From the first look one can see that DCAA is degraded at least 3x faster when using PC500, photocatalyst with high BET surface area. In comparison to others and among Millennium photocatalysts, correlation with BET surface is suggested, but with deeper look (Figure 18) one can see that P25 and PC10 are the exceptions. These catalysts have lower BET but have higher efficiency per 1 m^2 of photocatalysts surface when comparing to PC100 or PC500, which was also shown by others (Hathway and Jenks 2008) using different pollutants. On the other side JRC-TiO-6 doesn't show almost any photocatalytic activity, which is also usually claimed for pure rutile photocatalysts. Similarly, Gumy et al. and Enriquez et al. (Gumy et al. 2008; Enriquez et al. 2007) observed that primary degradation kinetics of strongly adsorbed pollutants, i.e. those containing a carboxyl group, is enhanced by large BET, unlike those which does not adsorb to TiO_2. It was demonstrated (Czili and Horvath 2009) that the adsorption affinity of TiO_2 for chloroacetic acids decreases with increasing number of Cl atoms (1 → 3) and for DCAA is ca. 30% lower in comparison to monochloroacetic acid (MCAA). It was also shown by the same authors, that (BET) surface area and to a lesser extent presence of anatase have positive influence to the adsorption of DCAA. Shortly, DCAA degradation is bound to degradation reactions on or near to the TiO_2 surface, highlighting the importance of BET surface of the catalyst. As regards a degradation mechanism, there are two hypotheses: (I) direct attack on a pollutant by TiO_2 holes (Enriquez et al. 2004; Enriquez et al. 2007) or (II) reaction with •OH radicals (Equations 33, 34, 35) on or near the photocatalysts surface (Czili and Horvath 2009). The second route is the most probable since it was experimentally proven.

$$Ti - OH \; + \; h^+(TiO_2) \rightarrow Ti - OH^\bullet$$ **Equation 33**

$$h^+(TiO_2) + \; H_2O \rightarrow \; ^\bullet OH + \; H^+$$ **Equation 34**

$$Cl_2CH - COO^- + \; ^\bullet OH_{surf} \rightarrow Cl_2C^\bullet - COO^- + H_2O$$ **Equation 35**

They claim that a role of the third reaction is significantly higher in comparison to reactions of electron transfer through molecular oxygen or direct electron transfer to DCAA.

As it was already mentioned, thiacloprid is a neutral molecule, which doesn't adsorb on TiO_2, consequently its degradation takes place predominantly in the solution bulk or near to catalysts surface and is initiated mainly by less reactive radicals which are not consumed in reactions with DCAA (Equations 34, 36, 22) (Pichat et al. 2000; Wang et al. 2002; Czili and Horvath 2009):

$$O_2 + \; e_{cb}^-(TiO_2) \rightarrow O_2^{-\bullet} + \; TiO_2$$ **Equation 36**

It was shown (Beltran et al. 2008) that peroxide is formed during O_2/TiO_2/UV process and in the case of thiacloprid hydrogen peroxide is an important oxidizing agent, which can in some cases slightly improve its photocatalytic degradation (Banic et al. 2011).

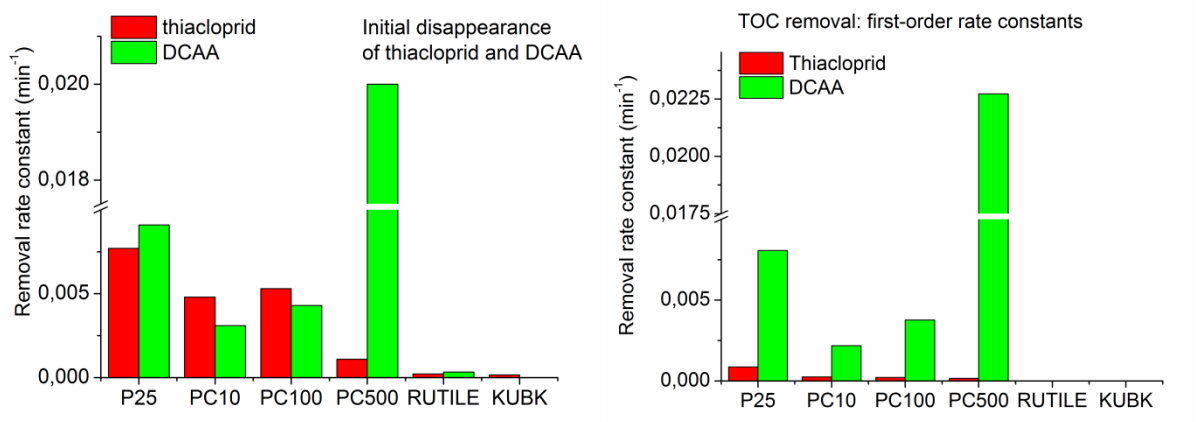

Figure 17. Comparison of initial photocatalytic degradation rates of thiacloprid and DCAA in the presence of five different TiO_2 powders (left) and initial degradation rate of TOC represented by two model compounds (right), during photocatalytic degradation. KUBK is a blank experiment performed without TiO_2.

The results of thiacloprid photocatalytic degradation (Figure 17) don't show any correlation of rate constants to BET surface area and increase in the order: Blank (KUBK) < JRC-TiO-6 < PC500 < PC10 < PC100 < P25. Out of these results we can draw the same conclusion as Hathway and Jenks (Hathway and Jenks 2008), so that adsorption to special reactive sites is not required and large surface area (BET) is consequently not mandatory to degrade pollutants with a weak or no adsorption on TiO_2 surface (Agrios and Pichat 2006; Enriquez et al. 2007; Gumy et al. 2008). If we take into account that PC10 has almost 9x lower BET in comparison to PC100 and 29x to PC500, thiacloprid degradation results obtained by using Millennium PC photocatalysts show, that the reaction rate increases in order of increasing sintering temperature (PC500 → PC10). Similar findings were published by Agrios and Pichat (Agrios and Pichat 2006) for phenol degradation. They justified these phenomena by gradual improvement of TiO_2 crystalinity and increasing of small proportions of rutile with sintering temperature, leading to a decrease of electron-hole recombination. These assumptions could also be supported from our site, since the results of PC10 and PC100 thiacloprid photocatalytic degradation show faster reaction in comparison to PC500 (Figures 17, 18). Because the DCAA is adsorbed on or is positioned near the TiO_2 surface, it is in closer contact with more reactive but also less stable and short-living radicals. On the other hand the thiacloprid is consequently not reached by these radicals, but most probably by more stable and less reactive oxidizing species which can still attack its molecule. In the case of PC10 and PC100 more radicals are formed due to their high crystalinity, so the degradation rates

are more dependent on the kinetics of the radicals decomposition and sensitivity of the organic molecule rather than just by the TiO_2 BET surface.

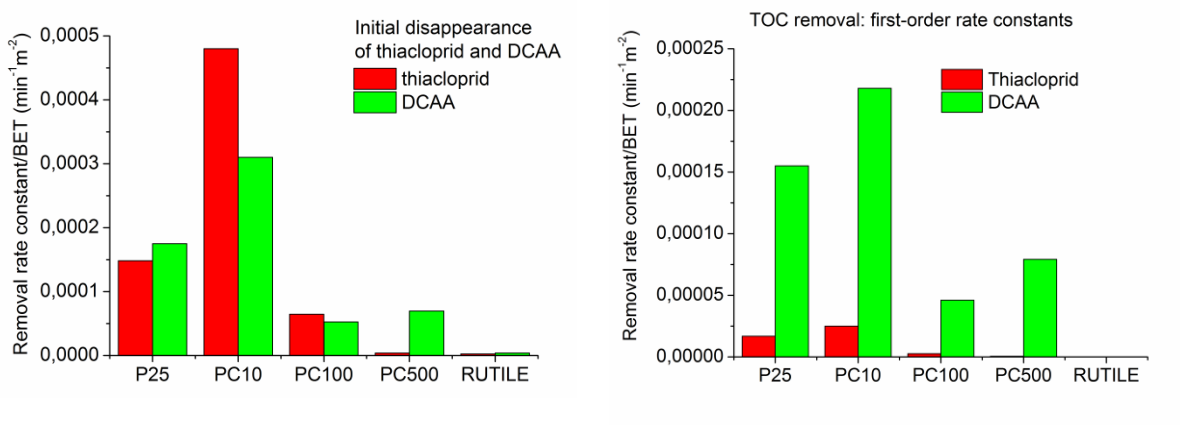

Figure 18. Initial degradation rates of parent compounds (left) and TOC represented by thiacloprid and DCAA (right), normalized to 1 m^2 of photocatalysts BET surface area ($min^{-1}m^{-2}$).

Another important factor is dark adsorption (**Figure 15**) which goes in line with photocatalytic degradation results and confirms that photocatalytic process is predominantly bound to TiO_2 surface, so the adsorbed molecules are degraded faster.

When comparing mineralization rate constants one can see that thiacloprid TOC degradation rates are just 5 to 10 % of a size for DCAA (**Figure 17**). This indicates, similarly as was already discussed, that DCAA positioned close to the TiO_2 surface and consequently its degradation products are degraded faster than thiacloprid situated in more distant surroundings. DCAA is also much smaller molecule and is consequently mineralized faster. Because of this, the mineralization of thiacloprid takes place mainly in TiO_2 particle surrounding and is thus slower. Due to slow reaction it is most probable that during experiment time (3 h) the intermediates which are more easily adsorbed to TiO_2 surface are not formed, which gives obvious preference to DCAA. It was shown by others (Gumy et al. 2008), that high BET is beneficial for TOC removal which is in agreement with some of our results (**Figure 17**,) but when comparing its efficiency per surface area (**Figure 18**) one can conclude, that PC10 and P25 are much more effective.

High adsorption affinity of charged compounds to the TiO_2 and its high BET surface area are otherwise main causes for faster mineralization, since this process is dominantly linked to surface reactions with •OH radicals (Equation 33). This was clearly demonstrated by PC500 photocatalyst, which outperforms all others used (**Figure 17**).

2.3.2.3 Catalytic ozonation degradation (O_3/TiO_2)

It has already been proven that the addition of TiO_2 powders in the ozonation system (dark conditions) accelerated the generation of hydroxyl radicals. This improvement originates from catalytic degradation of ozone (Equations 37, 38).

In acidic environment ozone decomposes to hydroxyl radicals due to the electrostatic forces and hydrogen bonding to TiO_2 (Zhao et al. 2009):

$$TiO_2 - OH_2^+ + O_{3(ads)} \rightarrow TiO_2 - O^{\bullet}H^+ + HO_3^{\bullet} \qquad \textbf{Equation 37}$$

$$TiO_2 - O^{\bullet}H^+ + H_2O \rightarrow TiO_2 - OH_2^+ + {}^{\bullet}OH \qquad \textbf{Equation 38}$$

The mechanism involves the adsorption–decomposition of ozone on TiO_2 catalytic surface sites (surface OH groups), which act in acidic conditions as Lewis adsorption sites for the ozone (Beltran et al. 2002), followed by the reaction of non-adsorbed ozone on oxidized sites (Rosal et al. 2006). These reactions generate unstable species, like ozone anion radicals, which can further

act as the promoter of chain reactions to produce hydroxyl radicals (Yang et al. 2007; Rosal et al. 2008) and other active species (Rosal et al. 2006). On the other hand these oxidation species, namely hydroxyl radicals, are generated manly in the solution (Yang et al. 2007), so it can be suggested that their formation is not necessarily linked to TiO_2 surface.

There was no DCAA degradation or TOC decrease in the absence or presence of any type of TiO_2, when performing dark experiments. These results are not expected, since some chloroacetic acids (MCAA) are degraded slowly in the presence of ozone (Kopf et al. 2000). This finding shows that DCAA positioned on or near TiO_2 surface is not reached by radicals. Thiacloprid, on the other hand, was decomposed by different rates in all cases (**Figure 19**), even without the catalyst present, where it reacts with molecular ozone by electrophilic substitution or dipolar cycloaddition (Beltran et al. 2009; Colombo et al. 2012), which resulted in hydrogen peroxide production. Thiacloprid was degraded also if TiO_2 was not present in reaction mixture, which can be due to indirect hydroxyl radical-mediated oxidation (Rosal et al. 2008) :

$$Thia + O_3 \rightarrow Products + H_2O_2 \qquad \textbf{Equation 39}$$

$$H_2O_2 \leftrightarrow HO_2^- + H^+ \qquad \textbf{Equation 40}$$

$$O_3 + HO_2^- \rightarrow HO_2^{\bullet} + O_3^{-\bullet} \rightarrow \cdots \rightarrow {}^{\bullet}OH \qquad \textbf{Equation 41}$$

It was shown (Beltran et al. 2008), that in the case of O_3/UV process, the concentration of hydrogen peroxide faster increases and drops in comparison to normal photocatalysis. This fact suggests the similar mechanism also for our case, so that H_2O_2 concentration increases due to reactions with aromatic rings and decreases, when thiacloprid is degraded to more stable intermediates. In this stage the hydrogen peroxide reaction with ozone (Equation 41) is dominant, which reflects in decrease of peroxide concentration and free radical formation.

The results of catalytic degradation (**Figure 19**) show accelerated degradation of thiacloprid in comparison to ozonation alone, which was also shown by others (Yang et al. 2007). Degradation rates don't depend on TiO_2 BET surface, but more likely on the crystalline phase composition (anatase, rutile). Many studies (Ohtani et al. 1992; Rosal et al. 2006; Yang et al. 2007; Rosal et al. 2008; Song et al. 2010) show, that surface OH groups density positively influences the catalytic degradation of ozone (Equations 37, 38) which results in production of different active species (Rosal et al. 2008). Some of the mentioned studies (Yang et al. 2007; Song et al. 2010) show, that rutile crystalline phase and even amorphous TiO_2 are more appropriate for catalytic ozonation degradation since they possess higher surface OH group density. Indeed, the obtained results (**Figure 19**) show that a proportion of rutile in TiO_2 catalyst (JRC-TiO-6, P25) is beneficial for catalytic ozonation degradation, which is in a good agreement with mentioned literature and other results which are not shown in present work. On the other hand the presented measurements of surface OH (**Figure 13**) don't prove that TiO_2 samples containing rutile (JRC-TiO-6, P25) possess higher surface density of surface hydroxyls. In the case of PC100 this correlation could be drawn since this photocatalyst has much higher surface hydroxyl density and higher catalytic decomposition of thiacloprid in comparison to other PC catalysts, but this is not reflected proportionally. It was shown by Ohtani et al. (Ohtani et al. 1992), that replacement of surface hydroxyls with F^- ions suppresses the catalytic decomposition by half, so it can be concluded that surface OH groups influence the reaction just to some degree. Since it is shown that in present case BET and amount of surface OH per exact mass of photocatalyst lose importance, there are most probably additional factors that influence the process. Possible explanation is agglomeration of nanoparticles. The results in fact show the same trend as the exposed surface area (**Figure 14**): PC500 < PC10 < PC100 < P25 < JRC-TiO-6. This can be explained by the fact, that larger agglomerates provide less exposed surface hydroxyls per mass of TiO_2 available for O_3 decomposition (Imamura et al. 1991; Cernigoj et al. 2010b), which leads to decreased catalytic production of "solution bulk" radicals.

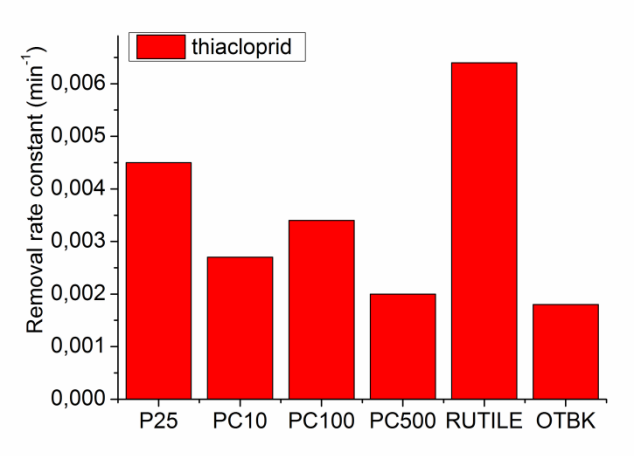

Figure 19. Initial degradation rates of thiacloprid during catalytic ozonation degradation without (OTBK) or in presence of different commercial TiO_2 powders.

On the other hand is thiacloprid most probably degraded by less reactive oxidation species produced on the TiO_2 agglomerate surface produced from O_3 which doesn't affect DCAA. Additionally, as it was already mentioned, thiacloprid may directly react with ozone or peroxide (Equations 39, 40, 41) in solution bulk, but this reaction is slow since the concentration of O_3 during blank experiment remains constant.

2.3.2.4 Photocatalytic ozonation degradation (O_3/TiO_2/UVA)

During photocatalytic ozonation experiments we monitored different reaction parameters to provide stable conditions, which allow a comparative study of different photocatalysts. **Figure 20** presents one typical experiment of photocatalytic ozonation using P25 TiO_2 photocatalyst with monitoring the ozone concentration in the solution, the concentration of thiacloprid and DCAA, the TOC and the pH value of the solution. The experiment could be divided into two phases – the first 30 min period with very high consumption of ozone and the second period, where mostly the mineralization takes place. Immediately after starting the experiment, just after the addition of DCAA + thiacloprid solution containing TiO_2 and turning on the lights, the O_3 concentration dropped (Beltran et al. 2008) and is kept low the first 30 min of the reaction despite constant purging of the solution with fresh ozone. The effect does not belong to the dilution effect, but is a consequence of an efficient O_3 consumption in different types of reactions with the easily oxidizable carbons from thiacloprid and its intermediate degradation products. Together with an ozone decrease a slight decrease of pH is observed, resulting from the production of acidic intermediate degradation products (Lucas et al. 2009). The mineralization rate is similar to the degradation rate of DCAA and is much slower compared to thiacloprid disappearance, confirming that the degradation of parent compounds to their intermediate degradation products prevail over the mineralization reactions in the beginning. This part of experiment is followed by the second part where O_3 concentration starts to increase and eventually stabilizes around $\gamma(O_3)$ = 4 mg/L, which was the set value in the reactor before the introduction of organic compounds and TiO_2. The ozone is not being consumed so efficiently in the second phase due to the absence of easily oxidizable carbons and due to the lower TOC. In this part of experiment the pH slightly increases, indicating that organic acids are being degraded, what correlates with the TOC decrease to almost 90 % after 3.5 h of the reaction.

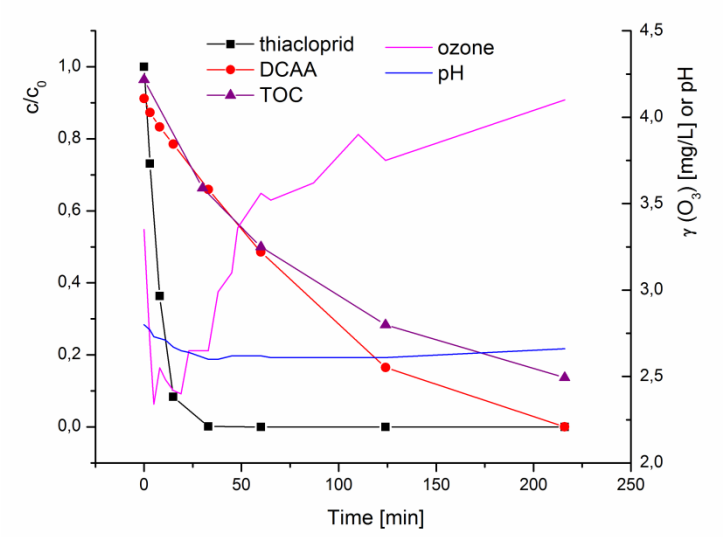

Figure 20. Experiment of photocatalytic ozonation (O_3/TiO_2/UVA) using P25 TiO_2 photocatalyst (3 g/L). The graph presents all variables monitored during the degradation experiments. The ozone concentrations in the case of photocatalytic degradation (O_2/TiO_2/UVA) experiments were not monitored.

Similar experiments were performed for all the catalysts used and the degradation rates were calculated. As a measure of a parent compound disappearance rate a line coefficient from the first 30 % of degraded molecules versus time was calculated, while as a measure of TOC decrease a degradation curve was fitted according to the first order kinetics and the reaction constant was obtained as a final result. The differentiation between the TOC value belonging to thiacloprid or DCAA molecules was possible due to the reasons explained in 2.3.2.1 section. The overall results of the photocatalytic ozonation experiments of the solutions containing a mixture of thiacloprid and DCAA are gathered in **Figure 21**.

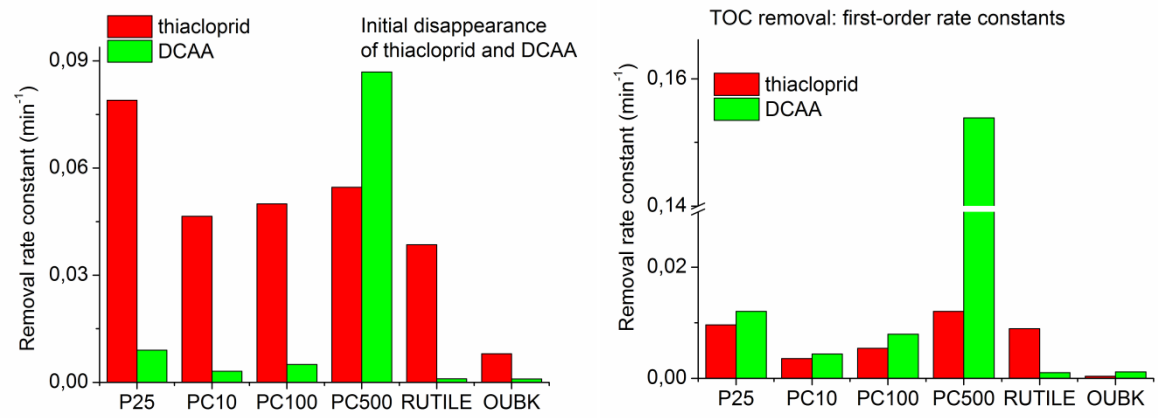

Figure 21. Comparison of initial photocatalytic ozonation degradation rates of thiacloprid and DCAA in the presence of five different TiO_2 powders (left) and initial degradation rates of TOC represented by thiacloprid and DCAA (right). OUBK – photo-ozonation is a blank experiment performed without TiO_2.

In the case of DCAA degradation (**Figure 21**), there is a clear trend of increasing degradation rate with increasing BET surface area, since the surface efficiencies (Figure 22) for majority of photocatalysts (P25, PC10, PC500) are of the similar size, with the exception of PC100. In comparison to normal photocatalysis the efficiencies are of the same rang for almost all TiO_2 samples, meaning that ozone doesn't increase reaction rate significantly. Rutile TiO_2 (JRC-TiO-6) on the other hand was not successful in the decommissioning of DCAA, the same as the experiment without TiO_2 (OUBK). Apparently rutile does not help in photocatalytic ozonation process of more persistent molecules, which indicates that catalytic/photocatalytic decomposition of O_3 on its surface doesn't lead to formation of stronger oxidative species. This is suggesting and

was proved by others (Czili and Horvath 2009), that degradation of DCAA is possible only with the presence of oxidant species with high oxidizing potential (Kopf et al. 2000; Enriquez et al. 2007), eg. $^{\bullet}OH$ radicals (Czili and Horvath 2009), onto or near the surface, which are in case of rutile not formed. Unlike the DCAA, thiacloprid reacts with weak and long-living radicals, which are consequently present in the solution bulk. As an addition to above mentioned surface reactions (Equations 33, 34, 35), the DCAA can be degraded in PH-OZ process also by surface •OH radicals produced by reaction of O_3 with photo activated TiO_2 (Kopf et al. 2000; Rivas et al. 2012):

$$Ti(IV) + e_{cb}^{-}(TiO_2) + O_3 \rightarrow Ti(IV) - O_3^{-\bullet} \quad \textbf{Equation 42}$$

$$Ti(IV) - O_3^{-\bullet} \underset{H^+}{\rightarrow} Ti(IV) - HO_3^{\bullet} \quad \textbf{Equation 43}$$

$$Ti(IV) - HO_3^{\bullet} \rightarrow Ti(IV) - OH^{\bullet} + O_2 \quad \textbf{Equation 44}$$

Overall, the photocatalytic activity trend is clear and logic, since the DCAA decomposition is bound to surface or near to the photocatalysts surface zone (Enriquez et al. 2007; Czili and Horvath 2009).

As it was shown, BET is playing a key role when the DCAA degradation is taking place, which is on the other hand again not true for thiacloprid. This is proven by significantly different surface efficiencies (**Figure 22**). The line coefficients (**Figure 21**) increase in order: Blank (OUBK) < JRC-TiO-6 < PC10 < PC100 < PC500 < P25. While in catalytic ozonation experiments the rutile shows the fastest thiacloprid degradation, it loses importance in photocatalytic experiments, but is in the case of PH-OZ process still competitive player and comparable to other photocatalysts. This probably means that it has suitable structure, which can lead to the formation of singlet oxygen or other relatively weak radicals but not $^{\bullet}OH$ radicals. Rutile has also lower electron-hole separation ability in comparison to anatase (Sumita et al. 2002) which consequently means that it cannot react with the ozone in the way as anatase (Equations 42, 43, 44). This anatase ability can thus lead to higher concentration of the most reactive species due to O_3 degradation (Beltran et al. 2009). We suppose that the most important reaction is the production of ozonide radical anions, which in the consequent steps result in hydroxyl radical formation (Equation 45).

$$O_{3\,(ads)} + e_{cb}^{-}(TiO_2) \rightarrow O_3^{-\bullet} \rightarrow \cdots \rightarrow {}^{\bullet}OH \quad \textbf{Equation 45}$$

As it was already mentioned, thiacloprid reacts on one side with weaker radicals which are formed on TiO_2 surface, but on the other side with radicals formed in solution bulk (Equations 39, 40, 41), which are not necessarily weak. Since there is no direct correlation of BET surface with thiacloprid degradation, all mentioned reactions predominantly take place in the solution bulk. During PH-OZ process the concentration of H_2O_2 increases and decreases rapidly (Beltran et al. 2008), meaning fast reaction between thiacloprid, O_3 and H_2O_2, stimulated by ozonide anion radical, which is in acidic environment the main promoter for radical production (Hernandez-Alonso et al. 2002):

$$O_3^{-\bullet} + H^+ \rightarrow HO_3^{\bullet} \quad \textbf{Equation 46}$$

$$HO_3^{\bullet} \rightarrow O_2 + {}^{\bullet}OH \quad \textbf{Equation 47}$$

Molecular oxygen, if present, can also act as electron scavenger and its further reaction with ozone gives hydroxyl radical in consecutive steps (Kopf et al. 2000):

$$O_2 + e_{cb}^{-}(TiO_2) \rightarrow O_2^{-\bullet} + TiO_2 \quad \textbf{Equation 48}$$

$$O_2^{-\bullet} + O_3 \rightarrow O_3^{-\bullet} + O_2 \quad \textbf{Equation 49}$$

Normalization of degradation rates constant to 1 m^2 of TiO_2 shows, that PC10 and P25 have much higher surface efficiencies (**Figure 22**) in comparison to others which is similar as in case of photocatalysis and is due to reasons already described above (Section 2.3.2.2). These efficiencies are in comparison to PC experiments increased by factor of 10 for all catalysts, which is a completely different trend in comparison to DCAA.

Similarly as in case of DCAA degradation, TOC removal rate constants (**Figure 21**) are in good correlation with BET of TiO_2 samples, which is in accordance with the results published by others (Gumy et al. 2008). The ratio between the TOC removal rates corresponding to DCAA and thiacloprid is comparable for P25, PC10 and PC100, which suggests the same mineralization mechanism present but with different surface efficiency (**Figure 22**). On the opposite to mentioned photocatalysts, PC500 shows mineralization ability, which is much more in favor of DCAA. The combination of DCAA and O_3 adsorption to PC500 high BET surface area most probably contribute to significantly higher mineralization performance in comparison to others. JRC-TiO-6, rutile photocatalyst, on the other hand is inefficient for DCAA photocatalytic ozonation degradation and mineralization in general, which is true also for all other types of experiments performed by this photocatalyst. Therefore is unexpected that in PH-OZ process it promotes thiacloprid mineralization. Since there are no $^{\bullet}OH$ radicals, which will react also with DCAA, thiacloprid is mineralized by reaction of weak oxidative species with less resistant carbon atoms in its molecule. This path could result in direct CO_2 evolution and without production of acidic intermediate.

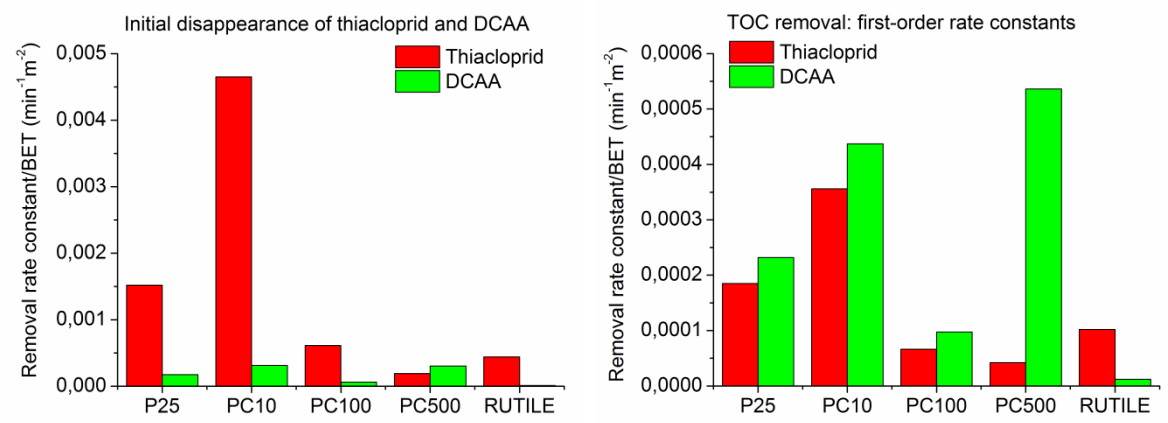

Figure 22. Removal rate constants of thiacloprid, DCAA (left) and corresponding TOC (right) normalized to 1 m^2 of TiO_2 surface.

It is interesting that surface efficiency in case of thiacloprid mineralization increases by 10 – 15 times in comparison to photocatalysis, while for DCAA this factor is 1.5 – 2, with the exception of PC500 (7x). At the same time the order of photocatalytic activity remains the same. Out of these data it can be concluded, that DCAA is much less involved in PH-OZ process than thiacloprid. Additionally, if one looks at the degradation efficiencies of parent compounds and compare them to mineralization efficiencies (**Figure 22**), can notice that these are practically the same for DCAA, while they decrease for 8 – 12 times in case of thiacloprid. The second conclusion is that DCAA is mineralized faster due to its adsorption to TiO_2 surface from the beginning, while thiacloprid larger molecule needs to be degraded to acidic intermediates which are able to adsorb.

As it was mentioned in previous section, the degree of agglomeration could be one additional factor. Since the exposed catalysts surface influences the degree of PH-OZ synergy (Cernigoj et al. 2010b) it is possible that only exposed surface area of agglomerate is actually involved in the PH-OZ process. In this case the distribution of two molecules in agglomerate, its surface and solution bulk play an important role.

To sum up the photocatalytic experiments, the suspension of PC500 is definitely the best choice among tested TiO_2 samples, when degradation of acidic organic molecules and mineralization reactions are in progress, while P25 is the catalyst, which is optimal to use for the first degradation step of neutral molecules with low adsorption affinity to titania.

2.3.3 Photocatalytic ozonation – synergistic process

It was shown (Cernigoj et al. 2007a; Beltran et al. 2008; Cernigoj et al. 2010b; Jing et al. 2011; Rivas et al. 2012; Tomova et al. 2012; Shin et al. 2013; Zsilak et al. 2014), that PH-OZ is often more efficient in comparison to sum of photo-ozonation and photocatalysis or catalytic ozonation, which is attributed to synergistic effect of this process. As it is presented (Figures 23, 24), the degree of synergy varies from catalyst to catalyst and to a large extent also depends on the type of pollutant and stage of its degradation process.

When comparing PH-OZ degradation rates of thiacloprid, with the sum of separate AOPs (photocatalysis, photo ozonation and catalytic ozonation, **Figure 23**), the initial degradation is enhanced by factor 2.5 to 5, where PC500 and P25 show the greater degree of synergism. This enhancement is even more emphasized when it comes to a stage of thiacloprid mineralization, where the TOC decrease during PH-OZ process is 6 to 24 times faster in comparison to the sum of O_3/UV + O_2/TiO_2/UV processes. PC500 shows the highest synergism among all tested photocatalysts regardless the thiacloprid disappearance or mineralization.

In case of DCAA PH-OZ degradation (**Figure 24**) there is no synergy detected, except for PC500, which exhibits 4 times higher activity in comparison to sum of photo-ozonation and photocatalysis processes. On the other hand, the DCAA TOC data show minor synergism (1.2 to 1.5x) for the majority of photocatalysts (P25, PC10, PC100), but markedly enhanced synergism is noticed just for PC500 (6.2x). This photocatalyst shows higher synergy for DCAA mineralization in comparison to its first degradation stage, which is similarly as in case of thiacloprid, with an exception of lower enhancement factor.

A - Thiacloprid degradation

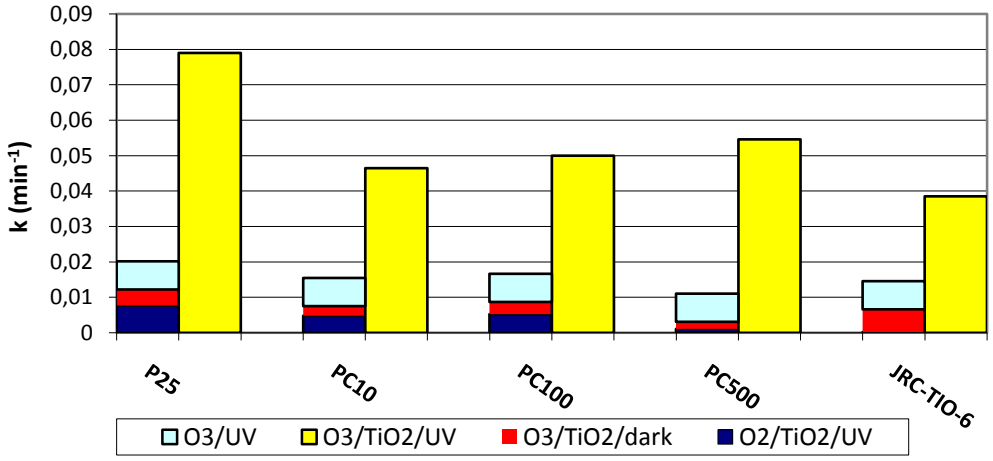

B - Thiacloprid TOC

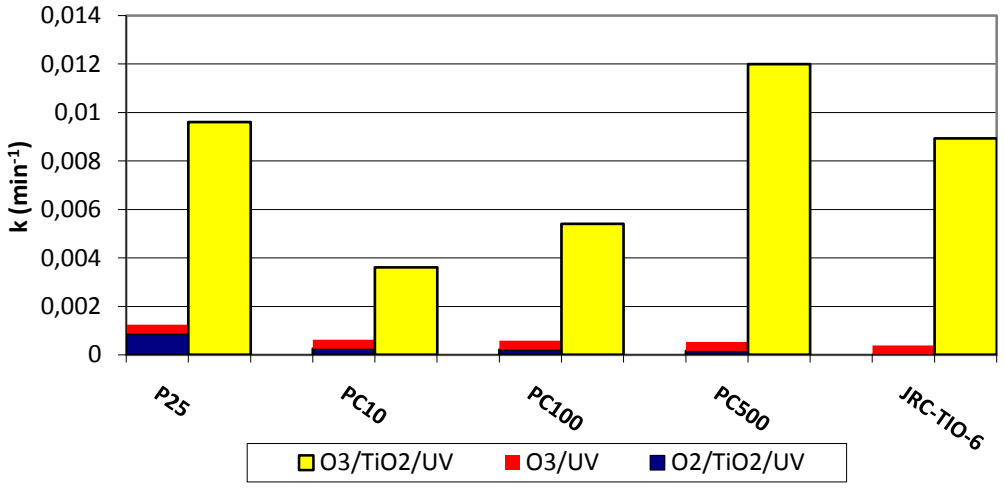

Figure 23. Comparison of initial degradation rates of thiacloprid photocatalytic ozonation ($O_3/TiO_2/UV$) to the sum of all other AOPs used (O_3/UV, $O_3/TiO_2/dark$, $O_2/TiO_2/UV$). Comparison of thiacloprid first stage degradation (A) and its mineralization initial degradation rates (B).

The analysis of the data obtained by three different kinds of catalytic experiments reveals that the greater synergy was detected in the case of thiacloprid, neutral molecule, which doesn't adsorb to TiO_2 surface but is at the same time less stable. In contrast, DCAA degradation and mineralization during PH-OZ process is not enhanced, except in case of PC500. Decreased effect of synergy in case of DCAA (Equations 42, 43, 44), when comparing to thiacloprid could be the consequence of: (I) direct reaction with $^{\bullet}OH$ (Equation 35), which could prevail since DCAA is adsorbed and/or (II) particles agglomeration, which decreases TiO_2 surface exposed to solution and limits access of O_3 to TiO_2 surface active sites (surface OH groups) inside the agglomerate. On the other hand, PC500 shows significant synergism also in the case of DCAA, what can be attributed to photocatalysts high BET surface and O_3/DCAA simultaneous adsorption. In this case ozonide directly reacts with adsorbed molecule, which in turn significantly accelerates the decomposition of DCAA and TOC decrease (Rivas et al. 2012):

$$Ti(IV) - O_3^{-\bullet} + TOC_{ads} \xrightarrow[H^+]{} CO_2 + H_2O \qquad \textbf{Equation 50}$$

A - DCAA degradation

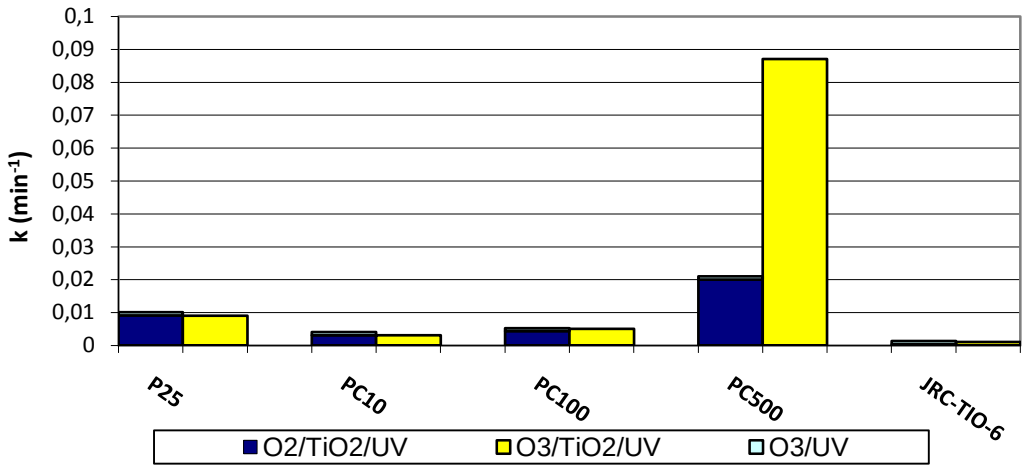

B - DCAA TOC

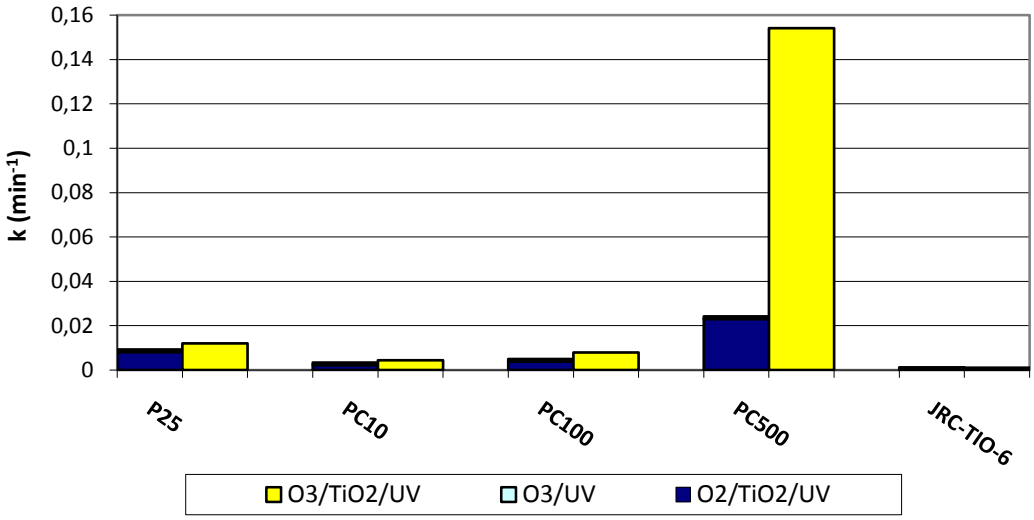

Figure 24. Comparison of initial degradation rates of DCAA photocatalytic ozonation (O_3/TiO_2/UV) to the sum of all other AOPs used (O_3/UV, O_3/TiO_2/dark, and $O2/TiO_2$/UV). Comparison of DCAA first stage degradation (A) and its mineralization initial degradation rates (B).

Enhanced synergy in the case of thiacloprid has its origin in the interaction of ozone with TiO_2 agglomerate surface exposed to solution, which leads to chain decomposition reactions of ozone. Result of these reactions is formation of different radicals, which are able to oxidize thiacloprid, since it is less stable molecule than DCAA. This can be partly confirmed by PH-OZ experiments conducted with rutile photocatalyst (JRC-TiO-6), which exhibits high synergistic effect and high ability to degrade and mineralize thiacloprid. It is well known that rutile weak point is the charge separation and consequently high recombination rate of photo excited electrons and holes, but in presence of ozone, which is good electron scavenger, rutile is able to produce enough radicals.

The present study shows, that photocatalytic ozonation process requires sufficiently high BET surface, while in the case of primary degradation stage other physicochemical properties like: crystallinity, efficient charge separation, efficient ozone decomposition on larger exposed surface and degree of TiO_2 nanoparticles agglomeration are more important. Out of the results presented,

it can be concluded, that combination of PC500 and P25 photocatalysts seems to be good and potentially more efficient when used in combination with ozone in acidic conditions.

2.4 Conclusions

Photocatalytic ozonation conducted in acidic environment is already very efficient under low UVA illumination intensity, since the ozone enhances the photocatalyst's efficiency of charge separation and radical production. Another fact, which was noticed, is that inefficient catalyst in oxygenated photocatalysis does not imply low efficiency in photocatalytic ozonation. This was observed in case of rutile photocatalyst (JRC-TiO-6), which shows negligible photocatalytic activity in presence of oxygen, while on the other hand is its thiacloprid degradation activity comparable to other photocatalysts, when it was used in the PH-OZ process. In the same type of AOP, we would expect noticeable influence of photocatalyst's surface area (BET), which has proved to be not so important, except in case of DCAA degradation and its mineralization, where PC500 outperforms all other TiO_2 samples. In the case of PC500 was shown, that adsorption of organic molecules (DCAA, other organic acids) onto TiO_2 surface accelerates photocatalytic ozone degradation and consequently the organic oxidation.

General comparison of degradation and mineralization rate constants of DCAA and thiacloprid shows that DCAA is degraded onto or near the photocatalysts surface, while thiacloprid not. One can observe that even in the case of PH-OZ process reactions near the TiO_2 surface are much faster than those in the solution bulk, which is logic since the $^{\bullet}OH$ radicals are highly reactive species and consequently react with the nearest organic molecules, eg. adsorbed to TiO_2 surface. On the other hand, the synergistic effect is much more emphasized in the solution bulk, which implies that ozone reacts just with exposed surface of TiO_2 agglomerates. Finally, P25 seems to be preferable for the early stages of organic degradation, because of its high photocatalytic activity in case of neutral molecules with low adsorption affinity, while PC500 for the mineralization step, which can be justified by its superfast mineralization of organic acids having high adsorption affinity to titania surface.

3 Part B: Highly active photocatalytic coatings prepared by a low-temperature method

3.1 Introduction

The most practical and frequently used immobilization methods to produce thick highly active layers for air/water treatment are sol-gel (Mallak et al. 2007; Novotna et al. 2008; Kesmez et al. 2009; Lopez et al. 2013; Sampaio et al. 2013), powder modified titania sol (Chen and Dionysiou 2006; Chen and Dionysiou 2008; Miranda-Garcia et al. 2010; Šuligoj et al. 2010; Miranda-Garcia et al. 2011) and sol-spray (Neti et al. 2010; Dostanic et al. 2013). With these three methods the commercial photocatalytic nanoparticles can be immobilized efficiently only if high temperature (≥ 400°C) is used during immobilization procedure. In addition to these, effective immobilization could also be achieved by a low-temperature hybrid sol suspension method (Šuligoj et al. 2010). Compared to others, this procedure has several advantages including easy replication, simplicity, low temperature treatment (≤ 150°C) and the possibility of application to various substrates (aluminum, stainless steel, glass, glass fibers/spheres, quartz wool, Al_2O_3 monoliths). In this section it is presented that the hybrid sol-suspension method can be successfully used to prepare stable, thick and highly active photocatalytic layers using different commercial TiO_2 nanoparticles. This part of the doctoral thesis was also published in Environmental Science and Pollution Research scientific journal (Kete et al. 2014).

3.2 Experimental details

3.2.1 Chemicals

The following chemicals were used as purchased: terephthalic acid (TPA) from Alfa Aesar, HCl (37%), NaOH and NaF (≥99%) from Sigma-Aldrich, hydroxyethyl-cellulose (HEC), titanium tetraisopropoxide (TTIP) from Fluka, tetraethyl orthosilicate (TEOS) from J.T. Baker, Levasil 200/30% colloidal SiO_2 from H.C. Starck, absolute ethanol from Sigma-Aldrich, 96% ethanol from Itrij. All aqueous solutions were prepared using highly pure water from the NANOpure system (Barnstead). Commercial TiO_2 nanopowders were obtained from: Evonik Degussa (Aeroxide® P25 and P90), Cristal Global (Millennium/CristalACTiV™ PC500), Kronos (KRONOClean 7000 – C doped), Tipe (VPC-10 – N doped), Sachtleben Chemie GmbH (Hombitan LO-CR-S-M).

3.2.2 Sol-suspension preparation and deposition

The sol suspensions of commercial nanoparticles of TiO_2 were prepared according to the patented procedure (Šuligoj et al. 2010). Titanium tetraisopropoxide (TTIP, 30 mL) in ethanolic solution (5 mL) was hydrolyzed in an $HClO_4$ (70%, 1 mL) aqueous solution (90 mL), where acid catalyzes the hydrolysis and stabilizes the sol. During hydrolysis and condensation reaction of TTIP, a white precipitate of hydrated amorphous TiO_2 was formed, which was then refluxed for 48 h, causing the crystallization and disaggregation of TiO_2, which results in a stable nanocrystalline titania sol. Separately, a homogeneous silica sol was prepared from TEOS (3.72 mL), deionized water (2 mL) and HCl (31%, 15.5 µL). The nanocrystalline titania sol (8.4 mL), the silica sol (1.2 mL), colloidal SiO_2 (2 mL) and ethanol (8 mL) were gradually mixed together to give a binder sol. Finally, 3.2 g of the corresponding commercial titania powder or mixture (1:1) of two powders was suspended in the binder sol. The titania/binder sol was then placed in a cold ultrasonic bath for 10 min to obtain the final sol-suspension containing 17.8 wt.% total TiO_2. Photocatalytic layers were immobilized on microscope slides (76 mm x 26 mm x 1 mm, Technische Glaswerke Ilmenau GmbH, Germany) by the dip-coating technique with a pulling speed of 10 cm/min. After deposition, the layer was dried using an air dryer and finally treated in a furnace (EUP-K 6/1200 Laboratory furnace, Bosio d.o.o., Slovenia) at 150 °C for 1h. Dip-coating and heating cycles were repeated until the required surface density of the catalyst was obtained (0.5 – 0.8 mg/cm^2), which means 2 to 3 cycles. Photocatalyst surface density was determined by weighing the substrate before and after immobilization procedure, where the mass difference was divided by geometric area of covered support. The obtained layers were named after the used commercial photocatalyst or mixture. The layer of P25 without the binder was deposited in the same way as mentioned above, but using a suspension of P25 in ethanol (80 g/L) instead of the sol-suspension.

3.2.3 Characterization of the layers – physicochemical properties

3.2.3.1 Mechanical resistance of the layers

The mechanical resistance and adhesion of each layer was tested by two different tests: (I) Wolff-Wilborn pencil scratch test (ISO 15184) with highest available pencil hardness 6H and (II) "Sonication test". The second test was made similarly to Nawi and Zain (Nawi and Zain 2012), so the sample was placed in a 50 mL beaker filled with highly pure water, which was then placed in an ultrasonic bath. After a certain time of sonication (0.5, 1, 2, 3, 5 and 10 min), the layer was washed with highly pure water, dried (120 °C, 20 min) and weighed. Mass loss was determined from mass difference and geometrical surface of the photocatalytic layer (per 1 cm^2).

3.2.3.2 Layer thickness

The thickness of photocatalytic layers was determined using a Taylor–Hobson Talysurf profilometer.

3.2.3.3 Dynamic light scattering (DLS) – agglomerates size

Sizes of nanoparticle agglomerates were measured using a particle size analyzer 90Plus (*Brookhaven Instruments Corporation*). The suspensions used for measurements were prepared by dispersing a small amount of nanopowder in highly pure water (c≈36±10 mg/L), sonicated for 3-4 min in an ultrasonic bath and measured for 2 min.

3.2.3.4 AFM and SEM investigations

The coatings topography was investigated with an atomic force microscope (AFM) Veeco CP-II instrument *(tip model NSC15-AlBS, MikroMasch, USA)*, operating in non-contact mode in atmospheric conditions. The probe tip radius was approximately 10 nm. The micrographs of different samples were acquired approximately at the same position in the center of the film, consequently avoiding any possible border effects. The one-dimensional autocorrelation function was calculated along the fast scanning axis and averaged over the slow scanning axis. The autocorrelation function was modeled with the Gaussian function

$$G(X) = \sigma e^{\left(\frac{-x^2}{T^2}\right)}$$ **Equation 51**

where σ denotes root mean square deviation of the heights and T is the autocorrelation length. We used autocorrelation length in order to determine characteristic lateral size of clusters. This approach is argued based on the calculation of the autocorrelation function of topography image of randomly distributed grains of approximately similar diameter. In such particular situation, the autocorrelation function exhibits Gaussian shape with the width equal to the radius of grains. Recently, Fekete et. al. (Fekete et al. 2012) presented a method to calculate the lateral size distribution from the autocorrelation function analysis.

SEM was performed by the same instrument depicted in section 2.2.4.

3.2.3.5 Band gap determination

The diffuse reflectance UV/Vis absorption spectra were measured on prepared titania layers using a UV/Vis spectrophotometer equipped with an integrating sphere *(LAMBDA 650 UV/Vis with 150 mm integrating sphere, Perkin Elmer, USA)*. Indirect band gap energies were determined by plotting the Kubelka–Munk transformation of the original diffuse reflectance spectra vs. photon energy (Tauc plot) (Murphy 2007).

3.2.3.6 BET surface area

These measurements were done in the same way as described in Section 2.2.4, with the exception that for these measurements “film powder” samples, obtained by carefully scratching a number of coatings and collecting the powder, were used.

3.2.3.7 XRD characterization

The X-ray powder diffraction (XRD) patterns of “film powders” were obtained on X-ray diffractometer *(X'Pert PRO MPD, PANalytical, Netherlands)* using CuK_α radiation with a step size of 0.017° 2θ and a fully opened X'Celerator detector. The diffractograms were collected in continuous mode in the 2θ range of 5.01–89.98° while rotating the sample. The average crystallite sizes, i.e. effective sizes of coherently scattering domains, were determined from the broadening of the anatase diffraction peak (101) at 2θ = 25.1°, using Scherrer's equation (Klug and Alexander 1974).The phase composition of samples was checked using the library included in the instrument software.

3.2.3.8 Surface OH

The amount of surface OH groups was estimated in the same way as already described (Section 2.2.4), by using commercial nanopowders (2 g) as received and without any pretreatment.

3.2.4 Photocatalytic activity determination

Photocatalytic tests were carried out in a UVA photochamber reactor, equipped with UVA lamps (two CLEO 20 W, 438 mm×26 mm, Philips; and one EVERSUN L40W/79K, 590 mm×38 mm, Osram) (Cernigoj et al. 2010a), and a solar simulator *(Suntest XLS+, Atlas, USA)* chamber with simulated solar irradiation source (Xenon lamp), using daylight filter. Each type of film was tested at four different irradiation conditions: (I) in the photochamber at 2.3 mW/cm^2 (300–400 nm), (II) in Suntest XLS+ at 28.7 mW/cm^2 (300–800 nm) containing 2.6 mW/cm^2 of UVA (300–400 nm),(III) in Suntest XLS+ at 45.0 mW/cm^2 (300–800 nm) containing 3.8 mW/cm^2 of UVA (300–400 nm), and (IV) in Suntest XLS+ at 75.0 mW/cm^2 (300–800 nm) containing 6.1 mW/cm^2 of UVA (300–400 nm). The UV radiation flux in the photochamber and Suntest XLS+ was measured using a UV radiometer (*XenoCal BB 300–400nm UV detector, Atlas, USA)*. The solar simulator allows to set the radiation flux (300–800 nm), which is then sustained and auto controlled during the experiment by the integrated irradiance control.

The prepared titania-silica layers were first pre-irradiated in the UVA photochamber reactor for 2 h in order for surface impurities to be removed and then their photocatalytic activity was tested using a highly sensitive fluorescence-based method (Cernigoj et al. 2010a; Bekermann et al. 2012), which is founded on the deposition of a thin transparent solid layer of terephthalic acid (TPA) over the photocatalytically active titania layer. After irradiation, the highly fluorescent 2-hydroxyterephthalic acid (HTPA) is formed as an intermediate product (**Figure 25**).

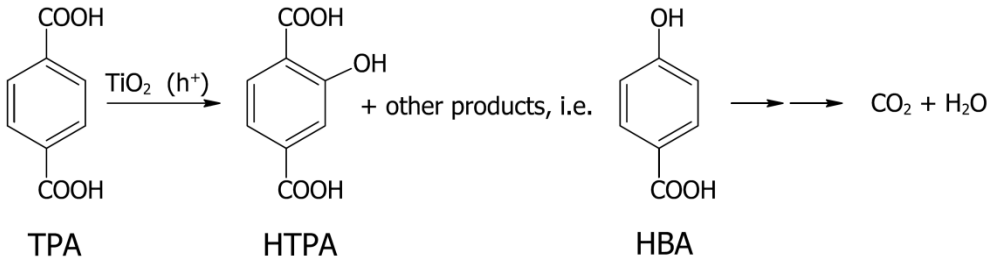

Figure 25. Fluorescent HTPA, formed during photocatalytic decomposition of TPA, is further degraded to other products and eventually to CO_2 and water.

In order to make the analytical procedure rapid, a special plastic holder (**Figure 26**) with holes was used, which was attached to the layer system using silicon grease, with the purpose of creating wells with a photocatalytic bottom. This allowed us to take a sample after different irradiation times using the same coating. Samples were obtained by washing the wells with an automatic pipette using a fixed volume (159 µL) of an ethanol/water mixture. These solutions were transferred into microtiter plate wells *(microtiter plate with 96 wells, flat bottom, black)* for fluorescence measurements using a microplate reader in fluorescence mode *(Infinite F200 Microplate reader, Tecan, Switzerland)*. The wavelength of excitation was 320 nm (filter bandwidth: 25 nm) and emission was measured at 430 nm (filter bandwidth: 35 nm). The

instrument was operating in top mode with 25 reads per well, with 20 µs integration time. The amplification factor for the photomultiplier tube was 56 or 78. For each layer, at least two parallel photocatalytic tests were done to calculate average and standard deviation. TPA photostability was tested on a clean microscope slide placed in Suntest (75.0 mW/cm^2, 300–800 nm) and used as blank experiment.

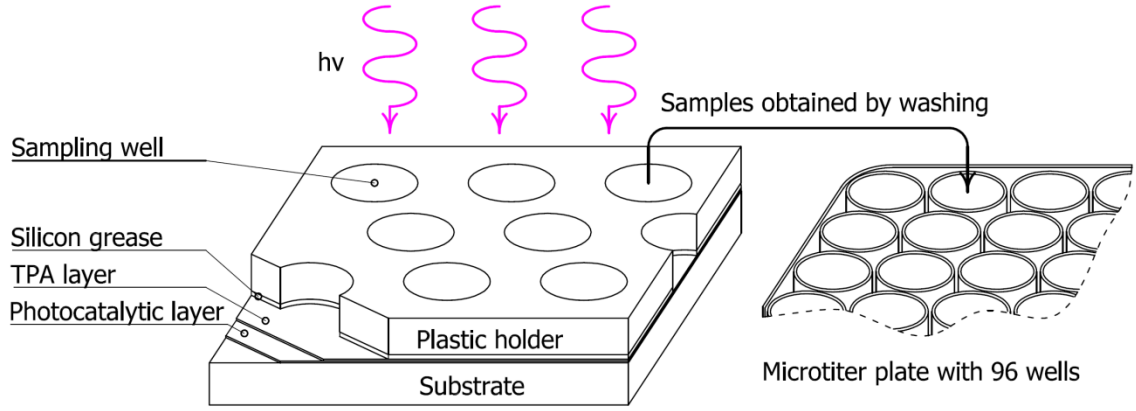

Figure 26. Plastic holder for creating wells (10-14) with photocatalytic bottom attached on photocatalytic layer coated with TPA. Hole diameter 9 mm (0.636 cm^2). Each well represents a sampling site.

3.3 Results and discussion

3.3.1 Physicochemical properties

The performed measurements gave markedly different data for the different prepared photocatalytic layers (**Table 2**). Despite similar film loading (0.65 ± 0.10 mg/cm^2), thicknesses of the layers varied significantly (1.9–5.5 µm). The variation of layer thickness is most probably the consequence of particle size, size of agglomerates, and resulting porosity. Despite this thickness variability, they can be reliably compared to each other in their photocatalytic performance, according to the results of Krysa (Krysa et al. 2005). They report that a layer thickness between 1 and 1.5 µm is enough to absorb more than 90% of UVA (355 nm) radiation. It was shown that there was no increase of oxalic acid degradation rate when the thickness of the photocatalytic layer was above 1.0 µm (Krysa et al. 2005). All the films presented here are thicker than 1.9 µm and have a similar catalyst loading.

Table 2. Physical characteristics of photocatalytic layers and commercial TiO_2 powder sources.

Photocatalytic layer	Surface density [mg/cm^2]	Thickness [µm]	Crystallite size[nm](1)	Average primary particle size [nm] (2)	Indirect band gap [eV] Anatase	BET of photocatalyst with binder [m^2/g]	BET of commercial TiO_2 powder [m^2/g]
P25	0.68 ± 0.03	4.5	21.3	20 – 32	3.02	96	52.4
P90	0.76 ± 0.02	3.2	13.1	11 – 16	3.05	130	100
PC500	0.57 ± 0.06	1.9	6.0	5 – 11	3.24	241	286
Hombitan LO-CR-S-M	0.55 ± 0.02	3.4	77.0	110 – 355	3.07	56	6.5
VPC-10	0.61 ± 0.04	3.7	17.3	20 – 50	3.15	85	50
KRONOClean 7000	0.77 ± 0.05	5.5	6.3	5 – 14	3.21	220	240
P25 + PC500	0.61 ± 0.03	3.5	13.4	/	3.11	173	/
P25 + KRONOClean 7000	0.68 ± 0.02	4.1	12.7	/	3.14	169	/
P90+Hombitan LO-CR-S-M	0.61 ± 0.04	2.2	28.9	/	3.12	89	/

(1) From XRD measurements of a sample with the binder
(2) From SEM analysis

Mechanical stability tests (**Figure 27**) revealed that the type of photocatalyst somehow influences the mechanical resistance significantly. In some cases the hardness of a photocatalyst mixture is a compromise of the two photocatalysts (P25+PC500), or the mixture demonstrates lower mechanical resistance (P25+KRONOClean 7000). The correlations between two different mechanical tests can be made, since the same layers which had better scratch resistance are also more stable during sonication test (Hombitan LO-CR-S-M, P90+Hombitan LO-CR-S-M and VPC10) and, on the opposite, layers with low scratch resistance are also less stable during sonication (P25+KRONOClean 7000, PC500, P25-no binder). Some layers (P25 and P25+PC500) with intermediate mechanical resistance exhibit better stability during sonication in comparison to scratch resistance, while others the opposite. Differences in mechanical resistance may origin in agglomeration of nanoparticles, already present in sol suspension (Peng et al. 2008). The SEM analysis and DLS measurements (**Table 3**) reveal that particles used for more stable layers (P25, P90 and VPC10 – **Figure 28**) form smaller nano-agglomerates (≤170 nm), or can be very good dispersed (Hombitan – **Figure 28**) so that they do not form agglomerates. In contrast, those particles used to produce layers with lower stability have generally high BET surface area (PC500 and KRONOClean 7000 – **Figure 28**), so have smaller primary particle size and form bigger nano-agglomerates (≥330 nm). One possible explanation of mechanical stability (Chen and Dionysiou 2006) is that when these agglomerates/particles of photocatalysts are introduced into the binder sol they are “wetted” only on the surface and binder does not penetrate to inter-particle space of agglomerates even if the sol-suspension is sonicated.

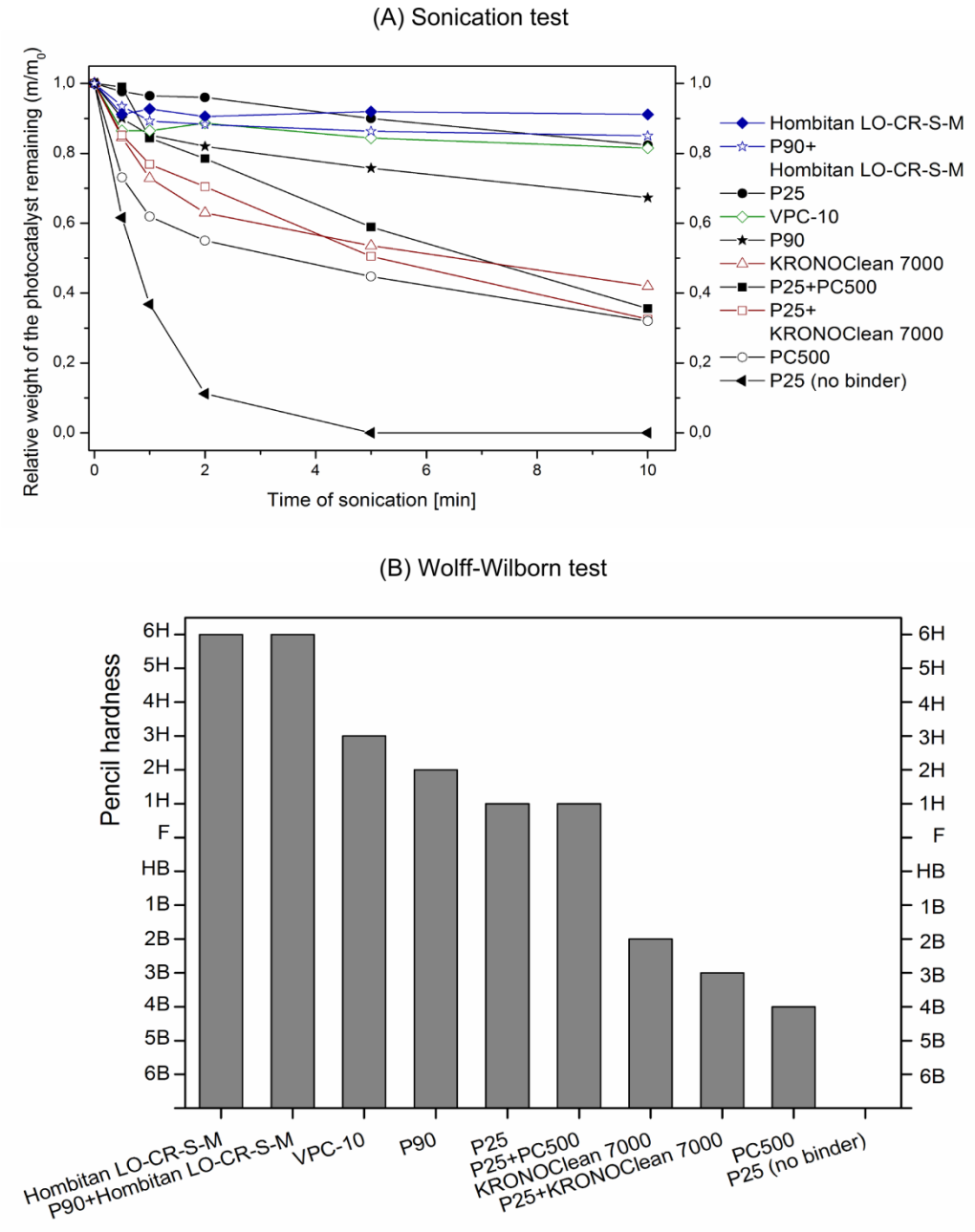

Figure 27. Mechanical resistances of the layers determined by two different tests: (A) ”Sonication test” and (B) Wolff-Wilborn test (ISO 15184).

Consequently the particles in agglomerate are not bound, leading to lower mechanical resistance. On the contrary, if particles form smaller agglomerates or are well dispersed they are immobilized more efficiently (Chen and Dionysiou 2008). In case of Hombitan the particles are completely covered by the binder which is reflected in the layer mechanical stability. When comparing photocatalytic layers using binder with that of P25 without the binder, it is very clear that the immobilization procedure is successful and particles which can be efficiently dispersed exhibit much longer durability and higher resistance towards mechanical stress.

HOMBITAN LO-CR-S-M

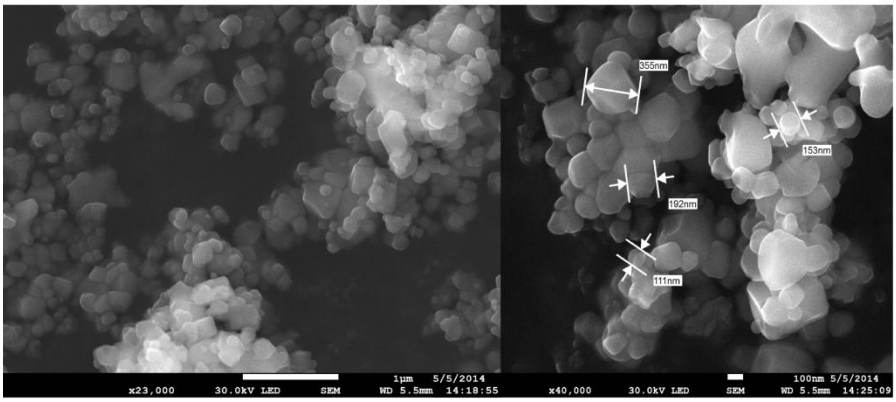

VPC-10

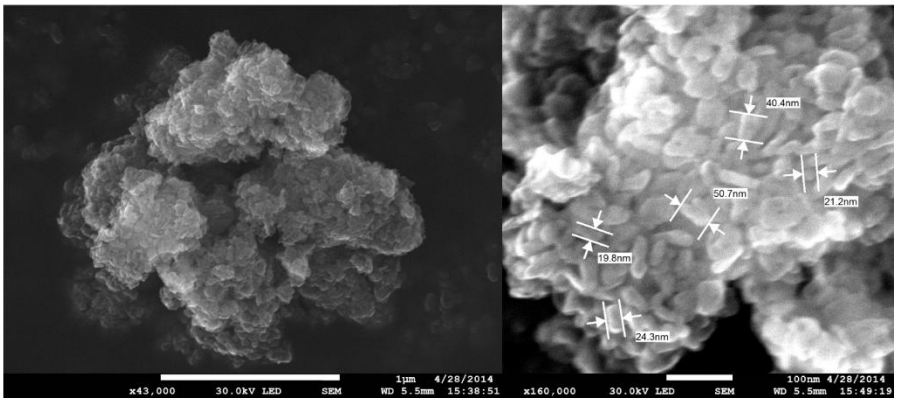

P25

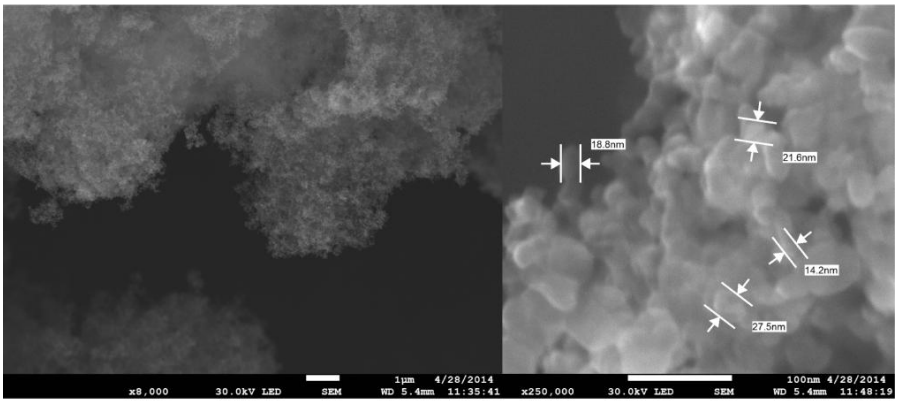

P90

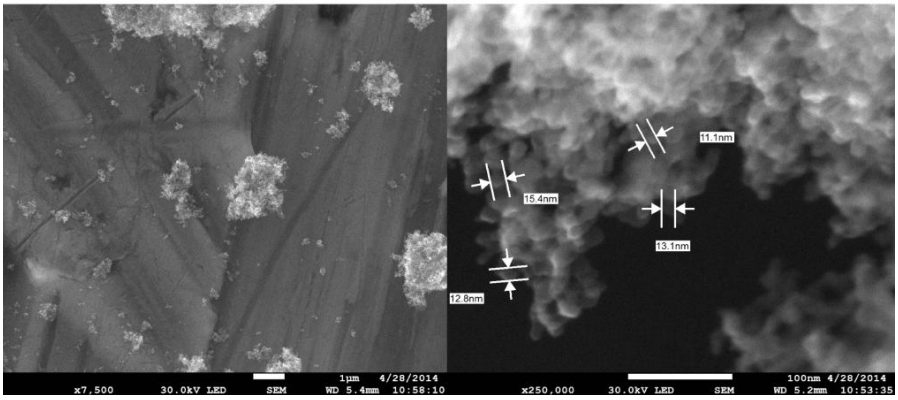

PC500

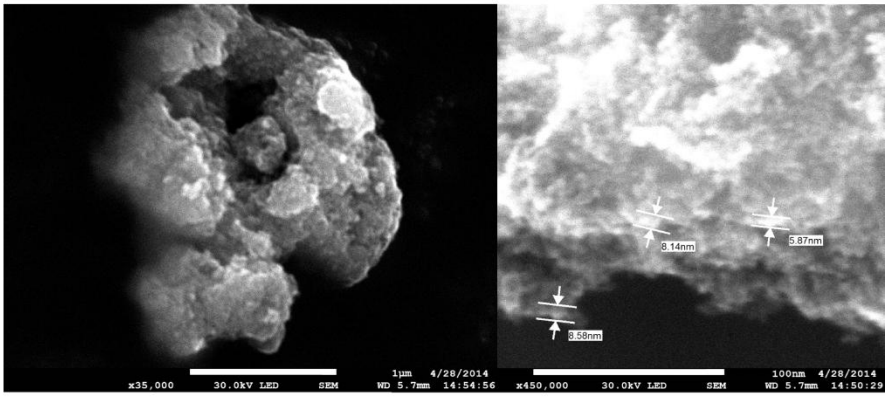

KRONOClean 7000

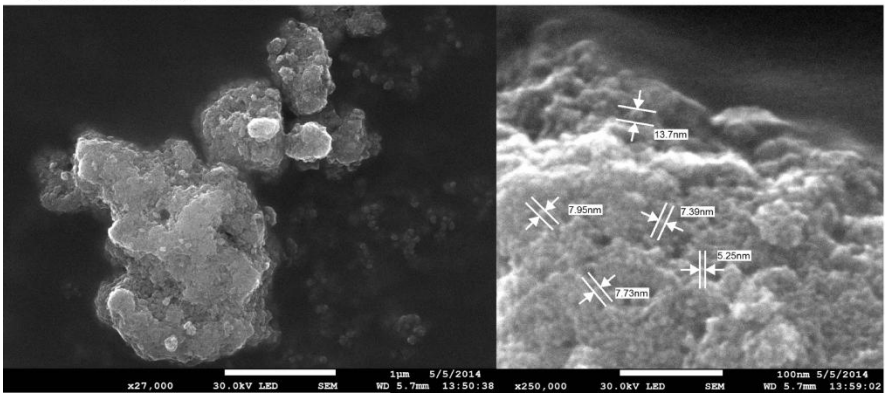

Figure 28. SEM analysis of commercial TiO_2 nanopowders (HOMBITAN LO-CR-S-M, VPC-10, P25, P90, PC500, KRONOClean 7000). Analyzed as received.

Table 3. Roughness of photocatalytic layers (2 µm × 2 µm) (AFM measurements) and agglomerate/particle sizes of source titania nanopowders dispersed in water (DLS measurements).

Sample	Rms [nm]	Agglomerate/particle size [nm]
Hombitan LO-CR-S-M	122	302±5 (particle size)
KRONOClean 7000	152	338±3
KRONOClean 7000 + P25	76.2	/
P25	44.4	52±4
PC500	87.1	392±5
P25 + PC500	96.1	/
VPC-10	70.0	168±3
P90	23.2	90±7
P90+Hombitan LO-CR-S-M	78.2	/

Stable layers of nano-TiO_2 can thus be prepared successfully in a relatively simple way and their good mechanical resistances will allow them to be further tested in a water photocatalytic reactor as a fixed photocatalyst. In some cases, higher mechanical stability could be achieved by the addition of Hombitan LO-CR-S-M (pigment), but resulting in a decrease of photocatalytic activity (see “photocatalytic activity evaluation” part). In other studies (Chen and Dionysiou 2006; Qiu and Zheng 2007; Chen and Dionysiou 2008; Peng et al. 2008; Neti et al. 2010; Miranda-Garcia et al. 2011; Nawi and Zain 2012; Cerna et al. 2013; Dostanic et al. 2013; Souzanchi et al. 2013) where commercial photocatalysts (P25, Hombikat UV100) were used to prepare thick photocatalytic layers (0.5 – 110 µm), immobilized on different substrates by high temperature (400 – 700°C) or

low temperature (150°C) procedure, there are not many data about layer mechanical stability. Pencil hardness tests were done just in some cases when layers were prepared at high temperatures. The hardness of that layers was defined to be 1B for layers heat treated at 500°C (Cerna et al. 2013) and 6H for those treated at 600°C (Chen and Dionysiou 2006). Comparing to these data, our immobilization method provides high mechanical stability although low temperature is used to cure the layers.

AFM analysis was intended to verify the surface repeatability of the present immobilization method for different commercial nanopowders. The surface roughnesses of the coatings are presented in terms of root mean square deviation (RMS) of heights on a 2 μm x 2 μm area in **Table 2**. It can be noted that the roughness ranges between 23 nm and 150 nm. We experienced that it is very difficult to control the process of immobilization to such an extent as to produce layers with similar RMS, since RMS depends on the viscosity of sol suspension, which in turn depends heavily on the photocatalyst particle size, its zeta potential and degree of agglomeration/aggregation, which varies among photocatalysts. 3D topography scans of photocatalytic layers (**Figure 29**) gave additional information about the surface morphologies. It can be observed that both layers using P90 have surface structure with finer grains/nano-agglomerates and small aggregates in comparison to others, while Hombitan LO-CR-S-M, VPC-10 and P25 have smoother surfaces with larger aggregates of nanoparticles (0.3 – 1.5 μm).

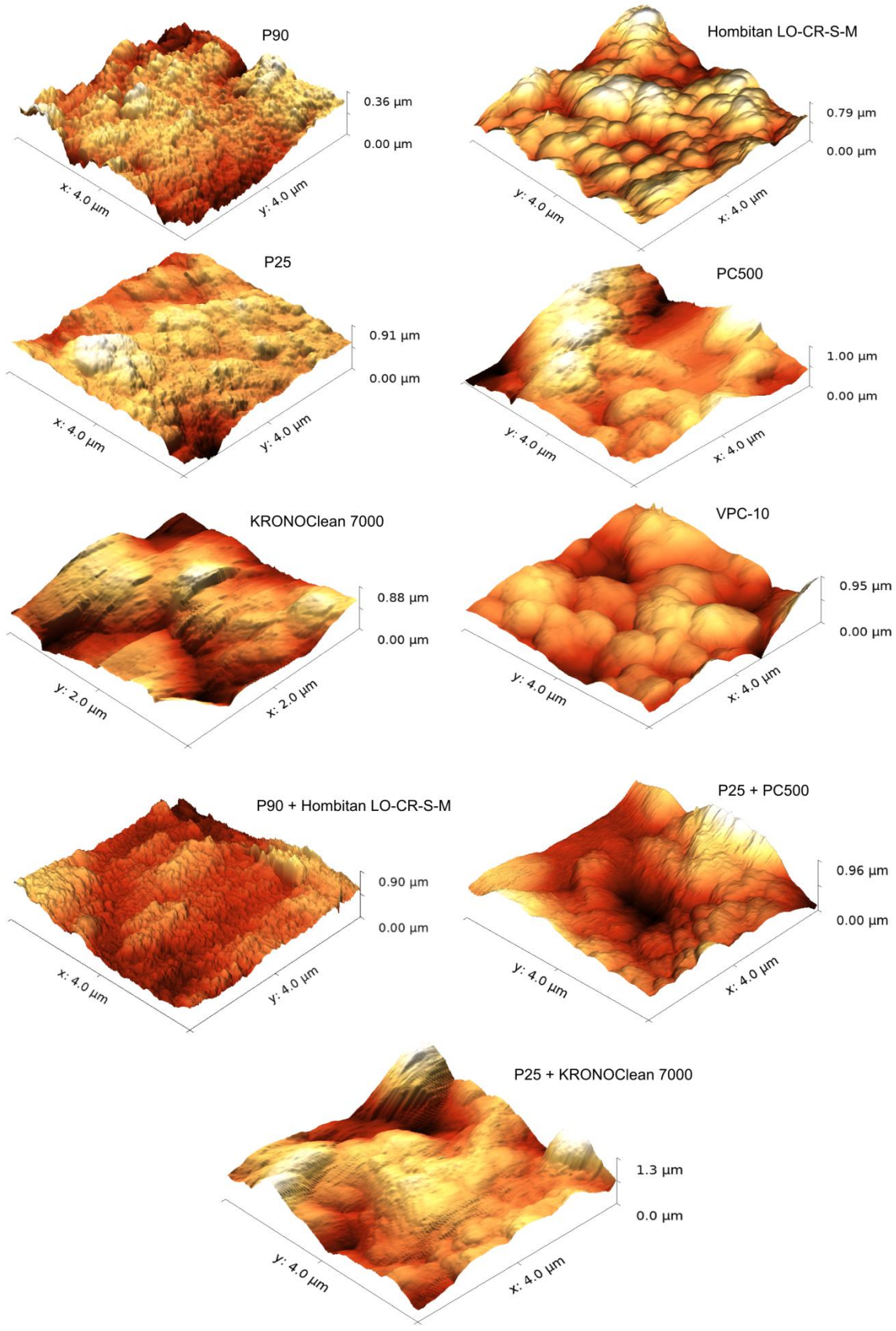

Figure 29. AFM micrograph images (4 µm × 4 µm) of photocatalytic layers. KRONOClean 7000 coating was too rough to allow scan at these dimensions.

All other layers exhibit higher surface roughness and on some of them aggregates greater than 2 μm were found (PC500 and KRONOClean 7000). Layer roughnesses for different photocatalytic layers show that, similarly as in case of mechanical resistance, agglomeration of nanoparticles and particle size influence this parameter. The bigger are the aggregates of nano-agglomerates/particles, the higher is the surface roughness. Finally, it is worth to mention, that AFM micrographs of 10 μm x 10 μm area and position pictures obtained by AFM did not show any cracks for the majority of analyzed layers, except for layer prepared from P90 (**Figure 29**).

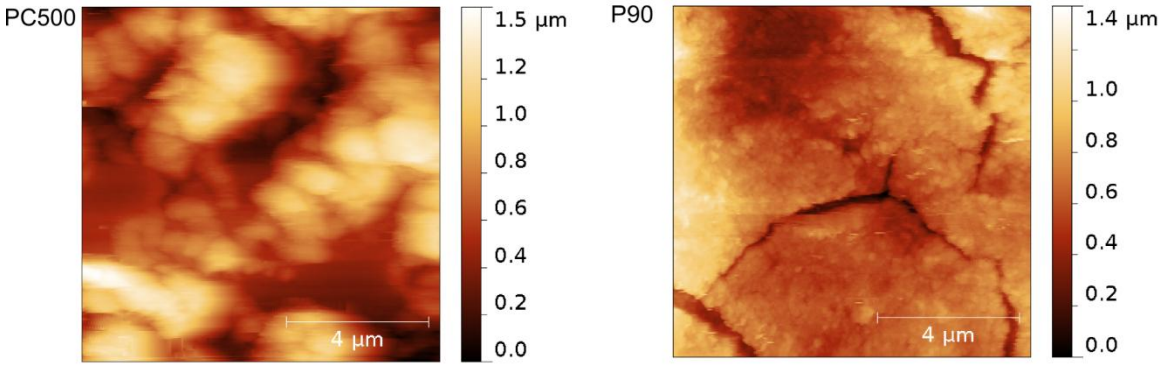

Figure 30. AFM micrograph images (10 μm × 10 μm) of PC500 and P90 photocatalytic layers.

The BET surface area of "film powder" samples changed in comparison to their raw commercial powder counterparts (**Table 2**) due to the contribution of the titania/silica binder (BET 195 m^2/g). In all cases, the surface area of the final photocatalyst/binder system is a compromise between the values corresponding to the commercial catalyst and the binder itself, which was also noticed by other authors (Peng et al. 2008; Miranda-Garcia et al. 2011). As a result, increased surface area is obtained for catalysts with a relatively low one (P25, P90, Hombitan, VPC-10) while no dramatic loss occurs in the case of high surface area catalysts (PC500, KRONOClean 7000). From these data one can conclude that no negative effect on the surface area of the commercial catalyst is provoked by the fixation procedure.

Using XRD analysis (**Figure 31**) of "film powder" samples, they can be clearly distinguished by their crystalline structure into those with pure anatase phase and those with mixed anatase/rutile phases. Samples PC500, KRONOClean 7000 and VPC-10 are single-phase (anatase) photocatalysts, while Hombitan LO-CR-S-M, P25 and P90 additionally contain rutile in proportions 26%, 13% and 18%, respectively. According to data obtained from producers, there are different proportions of amorphous phase (0% - 12%), where KRONOClean 7000 contains the highest proportion. According to crystallite sizes, layers prepared using single source commercial photocatalysts could be ranked in order from smaller to larger: PC500, KRONOClean 7000, P90, VPC-10, P25 and Hombitan LO-CR-S-M. As we show in our previous publication (Tasbihi et al. 2012), there is no perceived impact on XRD patterns with respect to photocatalysts without the binder, since the treatment of the samples takes place at low temperature.

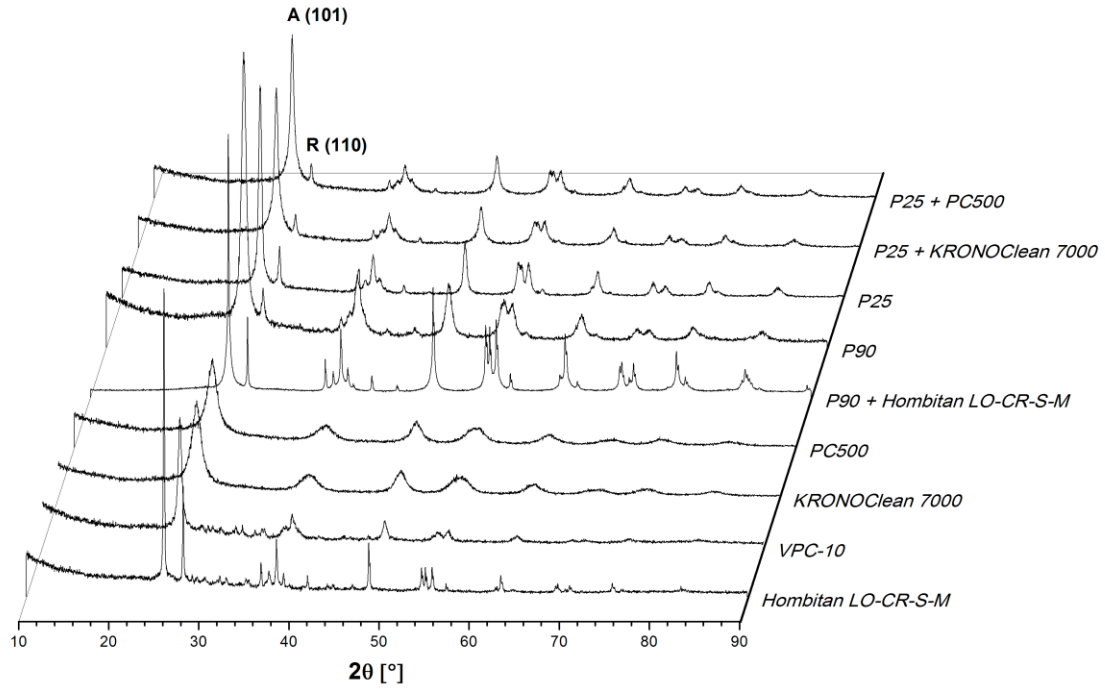

Figure 31. XRD results of different layers. The most characteristic peak of each crystalline phase, anatase-A at 2θ = 25.07° and rutile-R at 2θ = 27.45° is labeled.

Indirect band gap calculations (**Figure 32**) reveal that both Aeroxide® P25 and P90 photocatalysts have the lowest anatase band-gap energy (3.02–3.05 eV → 410 nm) which probably has its origin in the phase composition (Nair et al. 2011). It was found that all photocatalysts which contain rutile have a second band-gap, which is in the 2.9–3.0 eV region and corresponds to this crystalline phase (Murphy 2007). On the other hand, doped photocatalysts (KRONOClean 7000, VPC-10) need photoactivation photons with even higher energies.

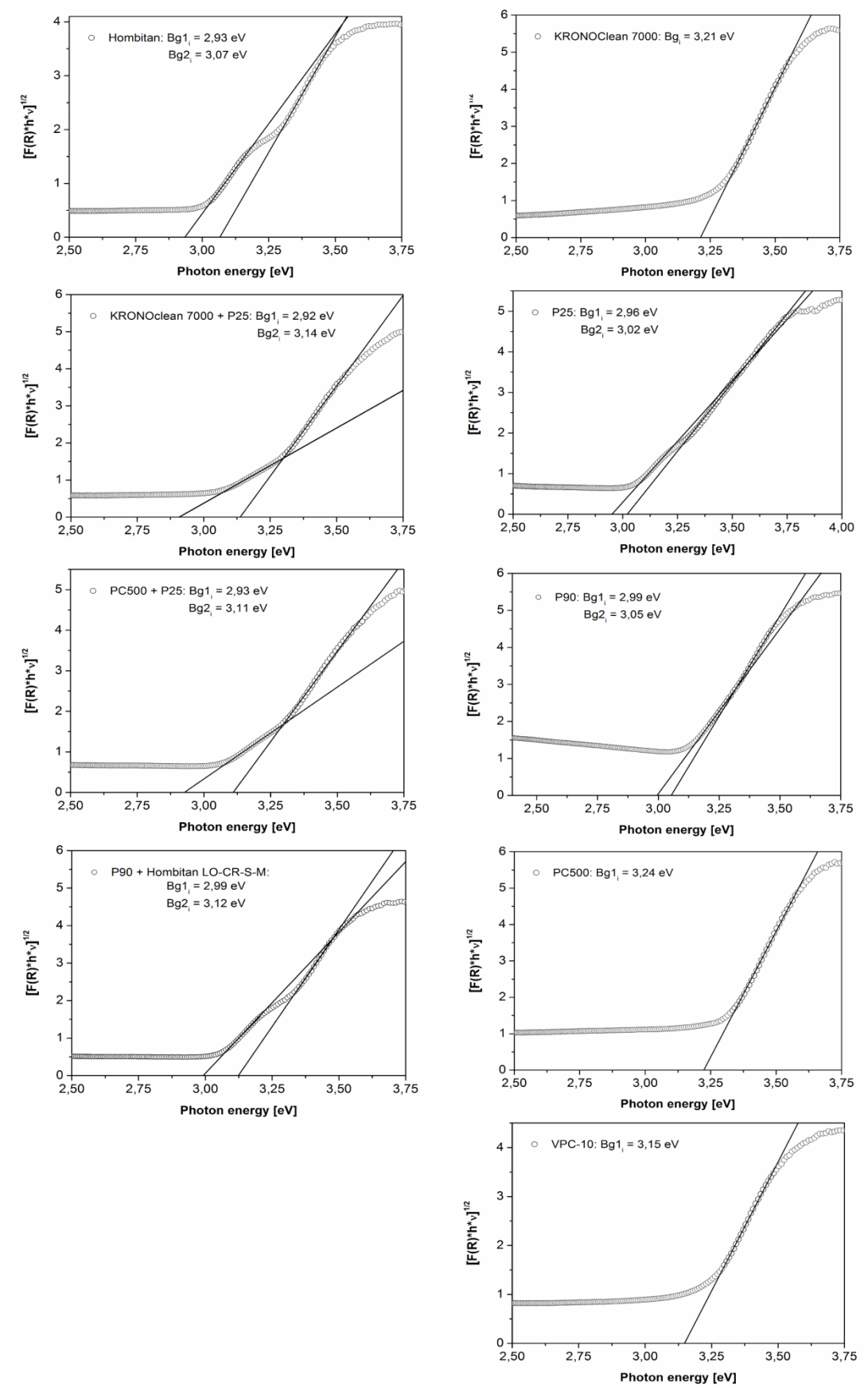

Figure 32. Indirect band gap energies determined by plotting the Kubelka–Munk transformation of the original diffuse reflectance spectra vs. photon energy (Tauc plot) for all prepared layers.

The UV-Vis diffuse reflectance measurements showed an increase in absorbance under 480 nm (VPC-10) and 550 nm (KRONOClean 7000 and P25+KRONOClean 7000), but this does not result in a lower band-gap according to the present calculations. Ohtani (Ohtani 2010) highlighted two major problems regarding doping of photocatalysts: (I) in many cases the modification occurs in the surface, so it is not actually doped and (II) estimation of band-gap energy, especially for doped samples, is very difficult due to the influence of impurities or surface electronic states on absorption spectra. These phenomena seem to appear in our case of doped photocatalysts, since there is no effect on narrowing of band-gap energy (**Table 2**). Although the quantum size effect on TiO_2 is somewhat controversial (Almquist and Biswas 2002), several authors have reported an increase in band gap energy for particles <10 nm (Anpo et al. 1987; Maira et al. 2000; Lin et al. 2006), which is in good correlation with our band-gap measurements (see PC500 and KRONOClean 7000).

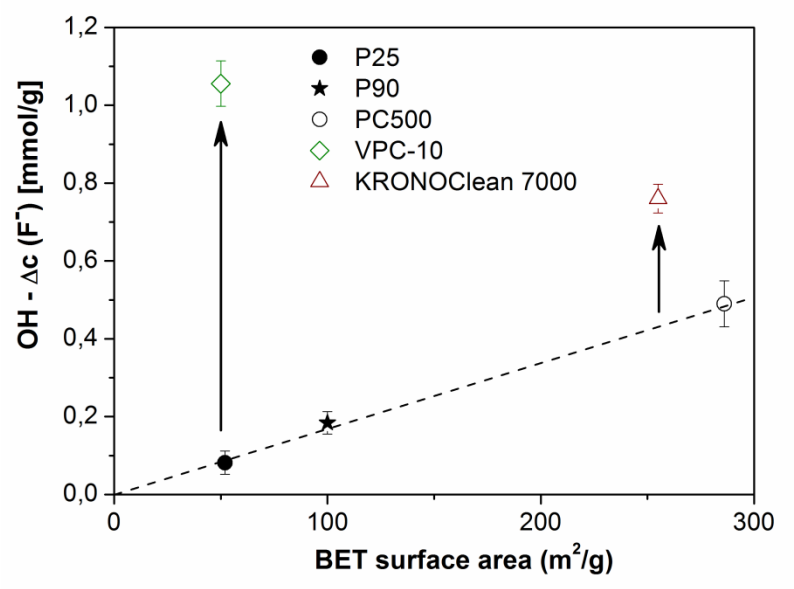

Figure 33. Concentration of hydroxyls in dependence of photocatalysts BET surface area. The concentration of F^- adsorbed corresponds to OH concentration.

Determination of surface hydroxyls (**Figure 33**) was done to verify if their surface density influences the photocatalytic activity. Similarly as Paola et al. (Paola et al. 2014) and Ohtani et al. (Ohtani et al. 1992), we observed increasing linear trend in amount of surface hydroxyls versus BET surface area for pure TiO_2 photocatalysts. In fact, if the corresponding concentration of OH groups is divided by the photocatalyst surface area, all pure TiO_2 samples possess similar surface hydroxyl density (1.7±0.1 μmol/m^2). On the other hand, for doped photocatalysts (KRONOClean 7000 and VPC-10) the amount of OH per square meter of photocatalyst was 2 and 11 times, respectively, higher than that expected from their surface areas according to the pure-titania correlation, suggesting that these two samples have a modified surface that could be traced back to the doping process. In addition, according to the study of surface hydroxyls by Paola et al. (Paola et al. 2014) a higher amorphous phase content in KRONOClean 7000 may also lead to higher surface density of OH groups. In any case, these authors also clarify the important fact that, in addition to hydroxyl group surface density, the structural properties of individual photocatalyst plays an important role, highlighting the importance of nanoparticle crystallinity. According to datasheets, P25, P90 and PC500 are highly crystalline (>99 %), while KRONOClean 7000 contains 12% of amorphous phase.

3.3.2 Photocatalytic activity evaluation

The evaluation of photocatalytic activity was done by following the formation of hydroxyterephthalic acid (HTPA), which is in this case the first degradation product of terephthalic acid (TPA). In the first minutes of experiment, there is excess of TPA and the concentration of HTPA rapidly increases (first reaction step – formation of HTPA, rate constant k_1) due to oxidation of TPA by holes and/or hydroxyl radicals formed on the surface of photocatalytic layer. With the

increasing of the HTPA concentration also its degradation rate (k_2) increases (second reaction step). A plateau is reached, when the rates of formation and degradation of HTPA are of the same size. By HTPA degradation, forming other intermediate degradation products (e.g. hydoxybenzoic acid – HBA), its concentration starts to decrease (**Figure 34**). On this basis a simplified kinetic model for HTPA was proposed (Cernigoj et al. 2010a):

$$\frac{d[HTPA]}{dt} = k_1 - k_2[HTPA] \qquad \textbf{Equation 52}$$

A fitting of the data for the initial formation of HTPA (until reaching the plateau), according to this simplified kinetic model, was performed by solving Equation 52. The fitting function is represented by the equation:

$$[HTPA] = \frac{k_1}{k_2}(1 - e^{-k_2 t}) \qquad \textbf{Equation 53}$$

where [HTPA] represents molar concentration of HTPA. In the proposed kinetic model, the HTPA formation follows zero-order kinetics and HTPA degradation pseudo-first order kinetics (Cernigoj et al. 2010a).

For catalyst comparison purposes, only the initial rate constant k_1 (first reaction step) will be considered. **Figure 34** shows measured HTPA concentrations and fitted curves for some photocatalytic layers and a blank experiment in which HTPA is not formed.

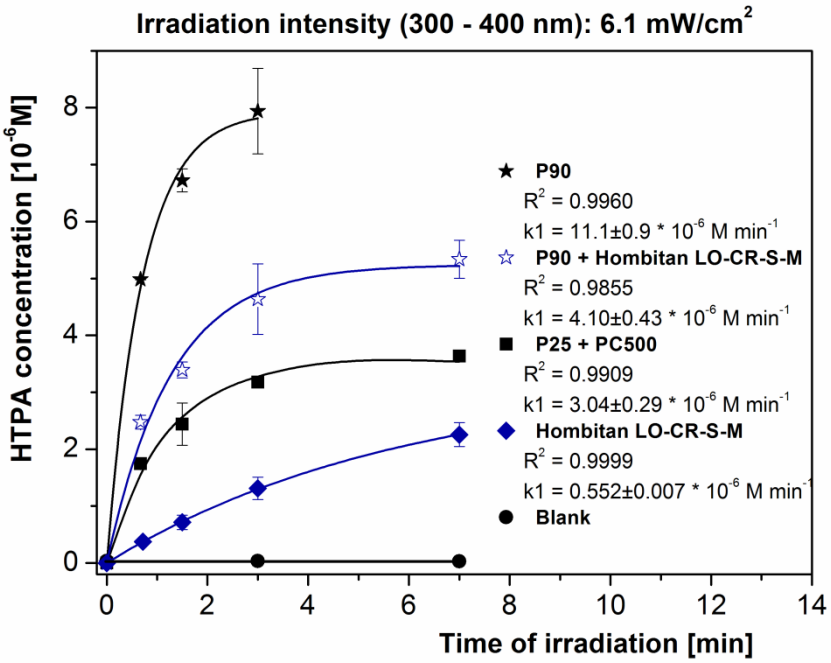

Figure 34. HTPA formation during TPA degradation on various photocatalysts. In the first minutes the concentration of HTPA rapidly increases (k_1). Due to consumption of TPA and consequent HTPA degradation (k_2), the concentration of HTPA reaches a plateau and eventually starts to decrease.

HTPA formation constants under different irradiation conditions are reported in **Figure 35** and

Table 4 for all the tested photocatalysts (6 single source and 3 mixtures). Regarding the single-source catalysts, the results show that P90 is the most active one at all irradiation conditions. As it can be observed, the change in proportionality of the rate constant – irradiance curve (Herrmann 2010) is reached at different irradiance values depending on the employed photocatalyst. For most of the photocatalysts, this limit is achieved at a moderately low irradiance (2.6 mW/cm^2), which is similar to what Brosillon et al. (Brosillon et al. 2008) obtained in a liquid phase, while for KRONOClean 7000 it is in the range between 2.6 and 6.1 mW/cm^2. Regarding this carbon-doped photocatalyst and the nitrogen-doped VPC-10, no increased activity is observed with respect to the undoped ones even if the tests with Φ ≥2.6 mW/cm^2 UV irradiation were performed in a solar simulator with a high proportion of visible irradiation. In any case, to confirm the presence or absence of visible-light-induced activity of these doped photocatalysts, further experiments would be needed. The photocatalyst with the lowest activity was in all cases Hombitan LO-CR-S-M, which is not actually meant to be used as a photocatalyst but rather as a weather resistant pigment additive. When comparing layers with comparable BET surface area, P25 to VPC–10 or PC500 to KRONOClean 7000, one can observe that pure TiO_2 photocatalysts are more active in broad range of irradiance intensities in comparison to those containing N or C.

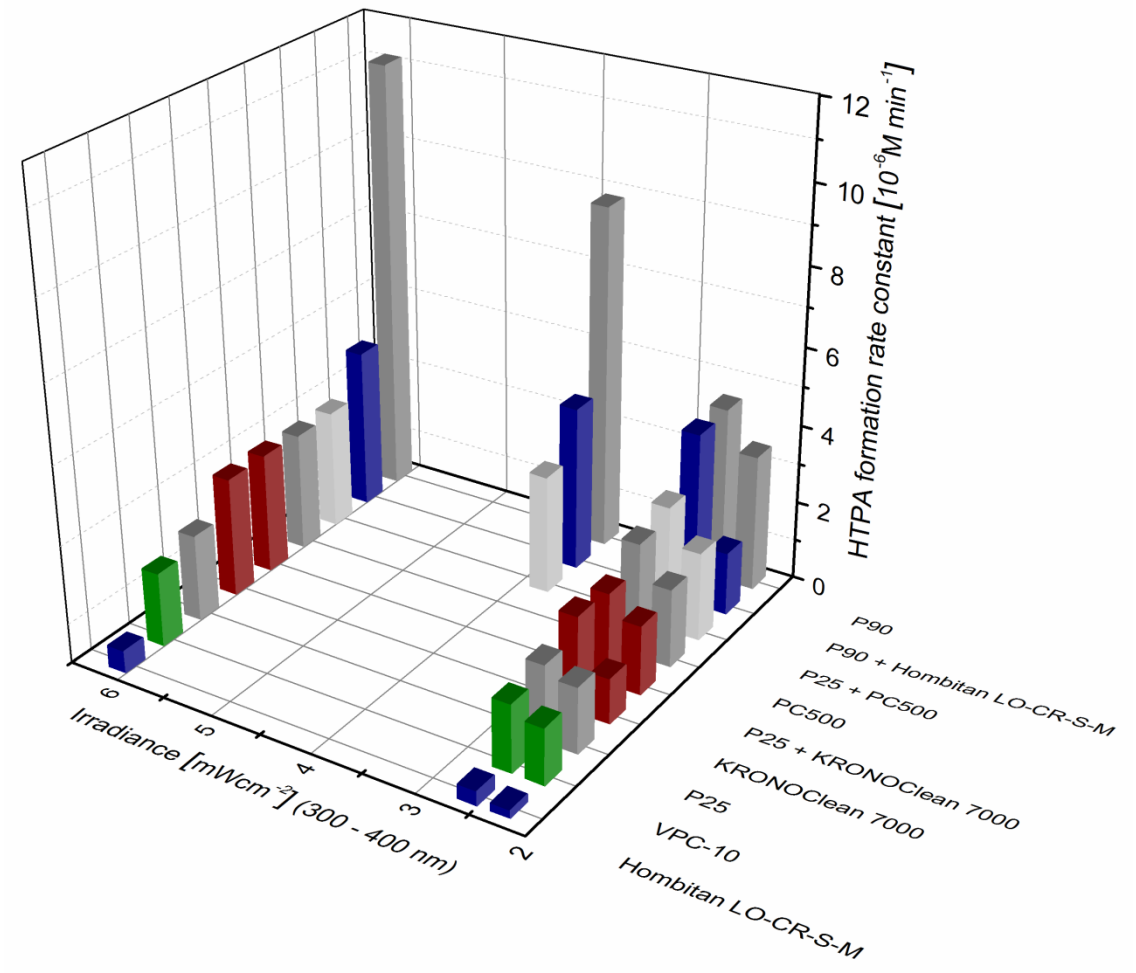

Figure 35. HTPA formation rate constants as a function of UV radiation intensities for different photocatalysts.

Table 4. HTPA formation rate constants obtained under different UV radiation intensities for different photocatalysts.

Photocatalytic layer	HTPA formation rate constant [10^{-6} Mmin^{-1}]			
	Photochamber 2.3 mW/cm^2 (1)	Suntest XLS+ 2.6 mW/cm^2 (1)	3.8 mW/cm^2 (1)	6.1 mW/cm^2 (1)
P25	1.66 ± 0.18	1.93 ± 0.13	/	2.19 ± 0.09
P90	3.46 ± 0.51	4.47 ± 0.28	8.8 ± 1.0	11.1 ± 0.9
PC500	1.97 ± 0.25	2.88 ± 0.38	/	3.01 ± 0.13
Hombitan LO-CR-S-M	0.197 ± 0.008	0.36 ± 0.04	/	0.552 ± 0.007
VPC-10	1.41 ± 0.07	1.71 ± 0.03	/	1.87 ± 0.06
KRONOClean 7000	1.14 ± 0.17	2.42 ± 0.21	/	3.04 ± 0.22
P25 + PC500	2.24 ± 0.10	3.17 ± 0.37	3.03 ± 0.25	3.04 ± 0.29
P25 + KRONOClean 7000	1.74 ± 0.10	2.30 ± 0.32	/	3.06 ± 0.06
P90+Hombitan LO-CR-S-M	1.52 ± 0.25	4.41 ± 0.21	4.21 ± 0.20	4.10 ± 0.43

(1) UVA (300 – 400 nm) radiation flux

These results may reflect the concerns about crystallinity, meaning that samples which are partly amorphous are less photocatalytically active. Overall, photocatalytic activity evaluation experiments revealed that P90 immobilized following the present procedure shows the highest activity under all tested irradiation conditions. Moreover, it exhibits a completely different dependence of photocatalytic activity on irradiance with an increase in HTPA formation constant upon increasing irradiance even in the range where the rest of catalysts have reached a limit in activity. Since electron-hole recombination is expected to be dominant at high irradiances (Herrmann 2010), this behavior may be indicative of an improved charge carrier separation in P90.

Plotting HTPA formation constants versus BET surface area (**Figure 36**) revealed a good correlation between photocatalytic activity and the surface area of most of the photocatalysts. Apparently, BET surface areas higher than ca. 170 m^2/g do not contribute significantly to higher photocatalytic activity. This seems to be the case with immobilized photocatalytic nanoparticles which are more or less agglomerated and, despite smaller particles and higher BET surface area, do not offer better contact with the adsorbed organic coating of TPA. Thus, it can be concluded that surface area of the attached photocatalyst affects photocatalytic activity only to some extent. As an additional factor to photocatalysts surface area, surface OH groups and crystallinity of nanoparticles affect the photocatalytic activity. In any case, P90 deviates considerably from the trend of other tested layers, suggesting that additional factors to those mentioned above exert an influence on the high activity of this catalyst. In this respect, activity vs. irradiance data suggest an improved charge separation in this material.

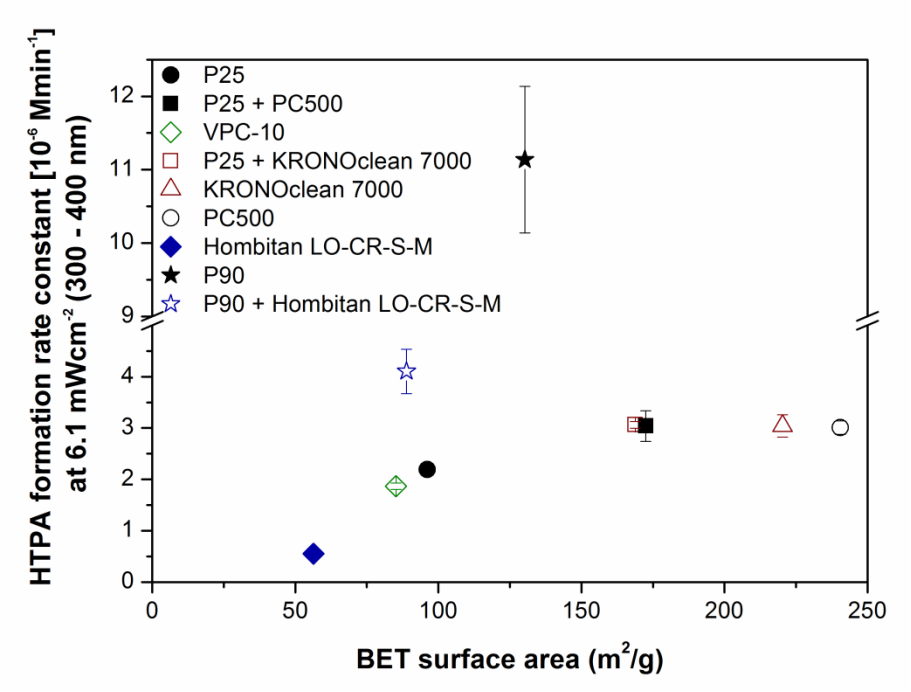

Figure 36. HTPA formation constants presented as a function of BET surface area of different photocatalysts ("film powder" samples). Irradiation intensity in Suntest was 75.0 mW/cm^2, which corresponds to 6.1 mW/cm^2 of UVA.

In addition to the single photocatalysts, binary systems of three different catalysts were tested in order to check for possible improvements with respect to a single component. The activity of P25+PC500 mixture is slightly higher in comparison to pure PC500, but still within the standard deviation and no synergistic effects were observed. For the other two tested mixtures it can be concluded that photocatalytic activity decreases in comparison to photocatalytic activities of pure photocatalysts and mixing does not lead to synergistic effects. As mentioned earlier, the addition of Hombitan LO-CR-S-M results in an improved mechanical resistance, but at the expense of photocatalytic activity, as observed in **Figure 35** and **Figure 36**. It is interesting to note, however, that this loss of activity is only evident at high irradiances, which, although the reasons are not clear for the time being, may lead to an interesting compromise between mechanical resistance and photocatalytic activity in low-irradiance application such as indoor air cleaning.

3.4 Conclusions

From the present research we can conclude that the low-temperature sol-suspension procedure reported here can be successfully used to immobilize TiO_2 nanopowders. Photocatalysts which are easily dispersed to particle-like size or small agglomerates (<170 nm) form highly mechanically stable layers, in our case these layers were prepared from Hombitan LO-CR-S-M, P25, P90 and VPC-10. In the case of immobilized photocatalysts, high BET surface area or surface hydroxyl density of the nanopowder itself is not necessarily providing better photocatalytic activity. Clear evidence for this is Aeroxide® P90 immobilized by the present procedure, which is, despite lower BET surface area (130 m^2/g) and the same hydroxyl surface density in comparison to other immobilized photocatalysts, the most photocatalytically active layer throughout the whole range of UVA irradiance (2.3 mW/cm^2 – 6.1 mW/cm^2). The obtained activity-irradiance curves suggest that, compared to the rest of tested catalysts, P90 probably presents an improved electron-hole separation, which allows the whole process of photocatalysis to be more efficient at higher UVA irradiation intensities. Due to stability and good mechanical resistance of selected photocatalytic layers (P90, P25, and VPC-10) as well as their high activity towards organic deposits degradation, they can be further used and tested in water photocatalytic purification reactions.

4 PART C: Photocatalytic compact reactor for waste water treatment – development and construction

4.1 Introduction

In this part of a thesis I present construction of prototype reactor system based on knowledge from the past, as well as the main idea and construction/realization of compact reactor. With (I) utilization of custom made Al_2O_3 reticulated monolith foams used as TiO_2 carriers, offering high photocatalytically active surface and (II) placement of irradiation source (lamps) inside the reactor, significant reduction in dimensions was achieved in comparison to prototype reactor. Although the size is significantly reduced, the overall photocatalytic cleaning capacity increases (Section 5). The constructed compact reactor also represents the flexible concept and can be easily adapted to specific requirements, concerning its dimensions and cleaning capacity.

4.2 Prototype reactor system

The prototype reactor system was designed according to knowledge from the past (Cernigoj et al. 2007b), so its shape is similar to Carrbery type photoreactor and glass slides were used as support for immobilization of TiO_2 nanoparticles. The main goal was to develop more compact reactor, which could be used in real application of waste water treatment. The mentioned reactor design was for this purpose downscaled but on the other side the reactor cell volume was increased to provide more cleaning capacity.

The photocatalytic cell for prototype reactor consists of a DURAN glass (**Figure 37**). The total length is 400 mm and inner diameter 80 mm. On both sides it has standard connector GL14 for connection with the other components in the reactor system. At lower connection port there is a valve in order to facilitate handling with the reactor cell. The effective volume of the reactor cell is around 1.5 L. The basket for holding immobilized catalyst is made exclusively of Teflon. 12 glass slides (280 mm × 28 mm × 2 mm) with immobilized catalyst (12 × 169.1 cm^2) can be fastened around the axis (10 mm in diameter, 300 mm long) with the help of two holders (**Figure 38**).

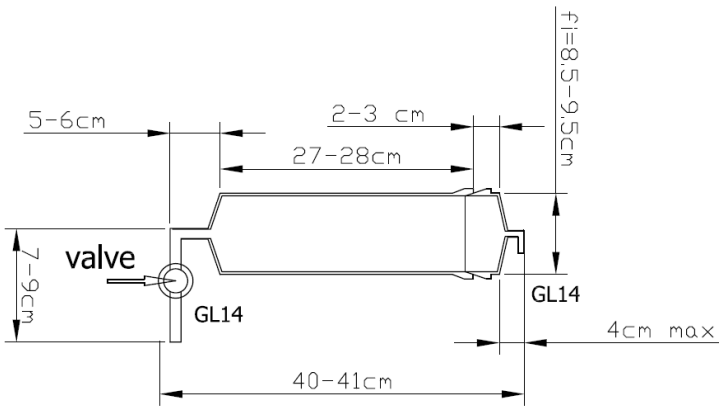

Figure 37. Sketch of photocatalytic cell for prototype reactor.

The geometry of the photoreactor is of a Carrbery type. Peristaltic pump allows circulation of the analyte solution (0.9 L/min) and there is also a sampling point (**Figure 39**A). Photocatalytic activity of the prepared films was evaluated using three UVA low-pressure mercury fluorescent lamps with 45 W of overall power (CLEO compact 15 W, 288 mm×16 mm, Philips; broad maximum at 355 nm). The UV (290 – 390 nm) irradiation intensity in reactor at cell position was 16±4 W/m^2 measured by UVA radiometer.

All three main components of the reactor, reactor cell, pump and sampling point are connected with Teflon tubes, so total volume of the reactor is 1.75 L. The geometrical surface to volume ratio between surface of the catalyst and volume of the whole reactor when using glass slides is 1.16 cm^2/mL.

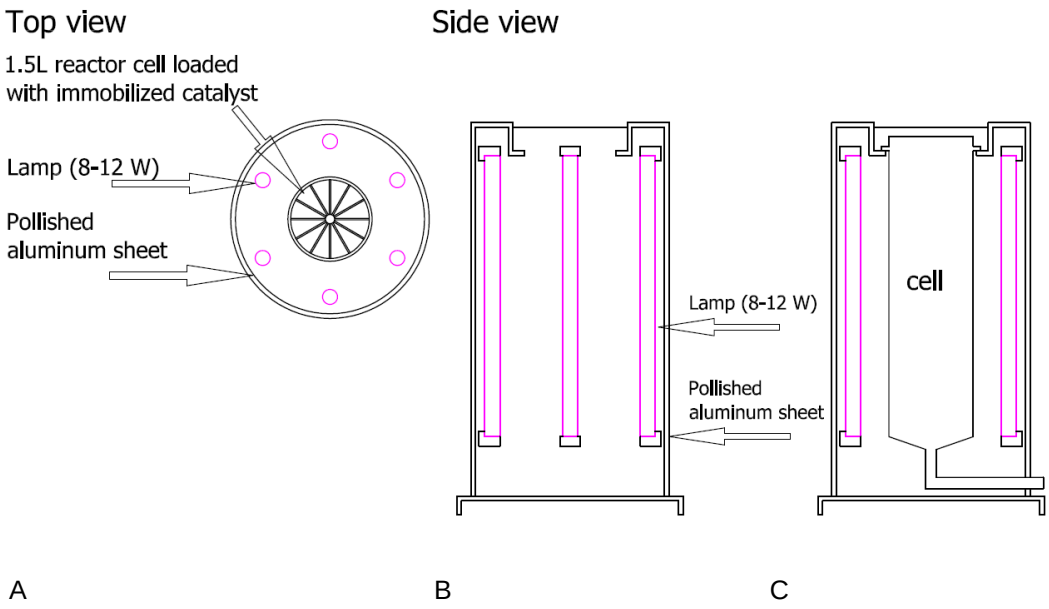

Figure 38. Prototype reactor: top view (A), side view (B) and side view with reactor cell (C).

This reactor was used to test the degradation kinetics of RB19, phenol, LAS and PBIS under different conditions.

A

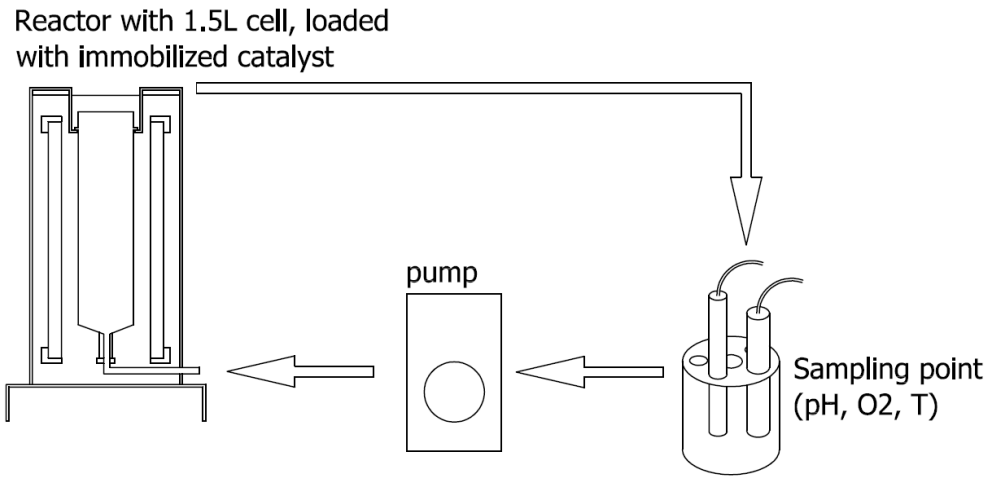

B

Figure 39. Prototype reactor system with pump and sampling point, where pH, T and O_2 measurements take place (A). Photo of prototype reactor system (B).

4.3 Development of compact reactor: main concept

The main idea was to develop compact photocatalytic reactor, which is small enough to use in different kind of applications, eg. treatment of household grey water, removal of pharmaceuticals or drinking water pretreatment process. Within this, the use of immobilized TiO_2 photocatalyst is suggested to be the elegant solution, since the filtration step is avoided which usually increases system dimensions and complexity. The main drawbacks of immobilization step are decrease of surface area available for photocatalytic reactions and decreased distribution of irradiation in reactor. To increase photocatalyticaly active surface, support with high geometric surface area should be used. The last but not least, the light irradiation should achieve whole photocatalytic surface, which requires uniform light distribution in whole reactor volume.

To satisfy all mentioned conditions the following concept of reactor system was first proposed. The compact reactor basically consists of three main parts (**Figure 40A**): (I) housing with ability to reflect light, (II) foamed ceramic monolith with immobilized photocatalyst and (III) lamp system.

As mentioned, foamed ceramic monolith was the choice for TiO_2 support, because this kind of material is commonly known as substrates with relatively high surface area for bulk material (1 – 2 m^2/g) and high stability up to 1000 – 1500°C since they are used for aluminum alloy filtering. According to some publications (Twigg and Richardson 2007), geometrical surface of monolith per volume as a function of number of pores per inch (PPI) can be:

- 10 PPI → 17.6 m^2/L of monolith
- 15 PPI → 20.9 m^2/L of monolith (estimated according to 10 and 20 PPI)
- 20 PPI → 24.1 m^2/L of monolith.

Volume of monolith in proposed reactor is 0.56 L, which means that in case of monolith with 10 PPI porosity, total photocatalyst geometrical surface will be around 9.8 m^2, which is much higher in comparison to previously used glass slides. The surface to volume ratio in case of treating 1L of contaminated water is 98 cm^2/mL, while in case of 10L this ratio is still 9.8 cm^2/mL.

Materials for foamed monoliths production (Al_2O_3, SiC, ZrO_2) are nontransparent, which means that light penetrates in monolith through pores. Consequently the depth of light penetration in such foamed ceramic monolith is relatively low (1 – 2 cm) and we propose to use 6 lamps in the reactor system placed inside the monolith to provide uniform light distribution.

As it was already mentioned intensity of irradiation influences the photocatalytic process just to some degree and must be optimized for the reactor system. It was shown in chapter 3.2.4 that UV irradiation intensity above 2.6 mW/cm^2 does not positively influence on photocatalytic activity of majority of photocatalysts. So if lamps with theoretical 100% efficiency are used, the theoretical value of irradiation power output should be:

$$P_{opt.} = Photocatalyst\ surface * 0.0026\ \frac{W}{cm^2} = 98000\ cm^2 * 0.0026 \frac{W}{cm^2} = 254.8\ W$$

meaning approximately 42 W per lamp. On the other hand it was shown (Chapter 2), that photocatalytic ozonation process can be efficiently conducted also at low irradiation intensities, which allows to use the lamps with lower irradiation flux. For best light utilization it is suggested to use lamps with narrow irradiation spectrum near TiO_2 bandgap (3.2 eV) wavelengths with maximum at 350 - 370 nm. This is due to decrease of number of emitted photons with shortening of λ at a constant power of a lamp, so with shorter λ lower number of excitons is produced, which are necessary for reduction/oxidation reactions.

In comparison to reactors with suspended photocatalyst particles, reactors with immobilized photocatalysts suffer from mass transfer limitation. In the case of proposed reactor this limitation is decreased by using support with high surface area and turbulent flow. The turbulent flow is achieved with tangential inflow of polluted water, which is forcing the liquid to circulate around the monolith, but to pass through its pores it has to change direction. The randomly distributed pores

then mix the water which is passing to the center of monolith and further to reactor outflow (**Figure 40**)

A

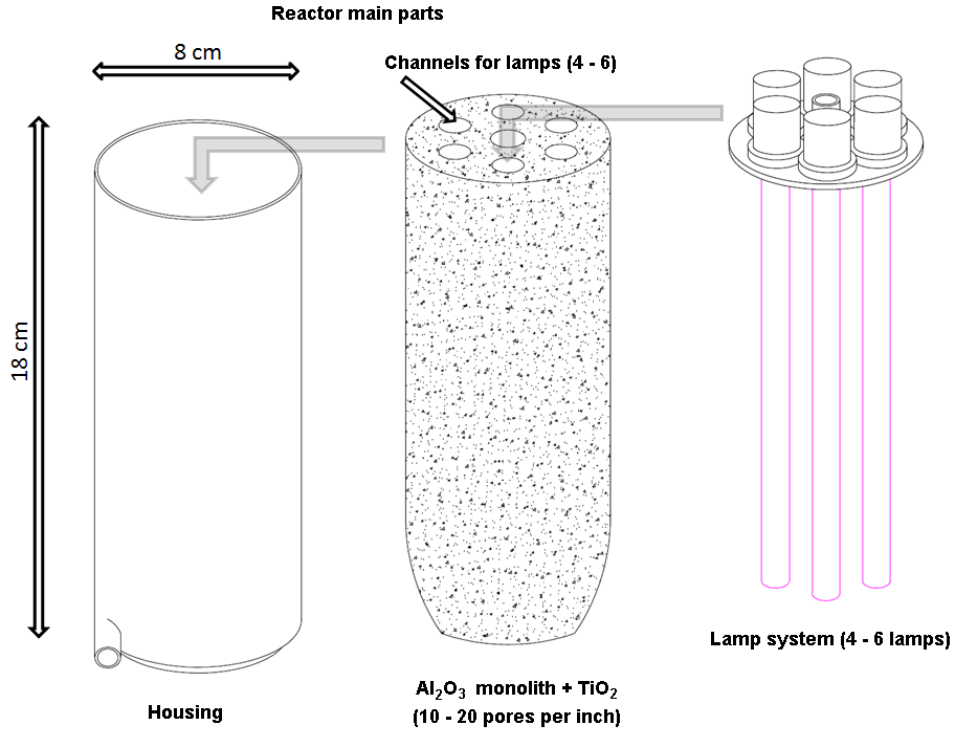

B

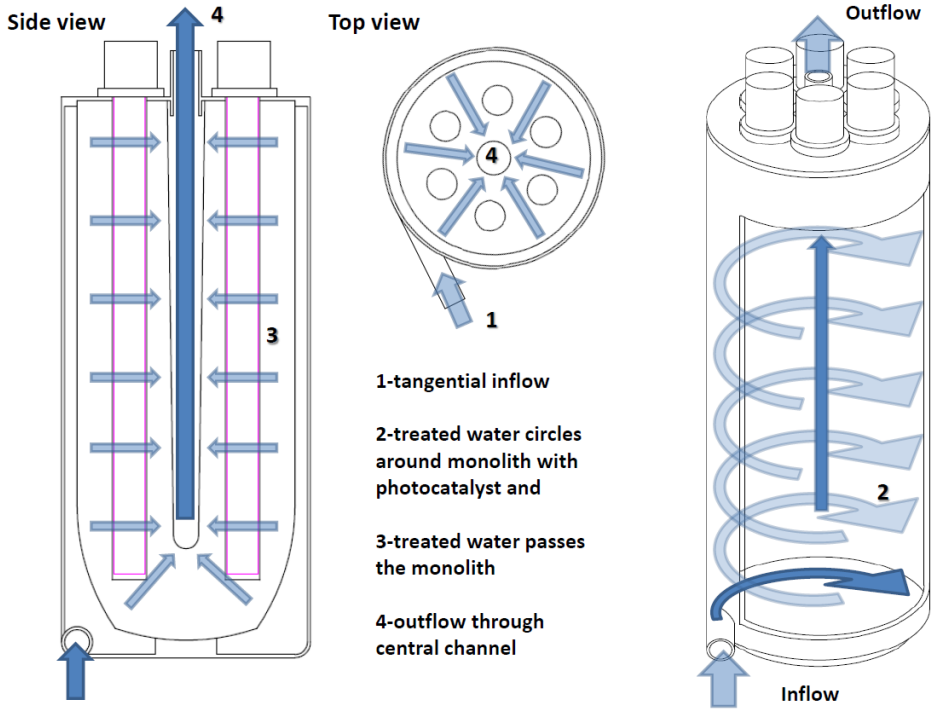

Figure 40. Geometry and composition of proposed reactor (A) and its operation (B).

4.4 Compact photocatalytic reactor – realization

4.4.1 Geometry and composition

The final compact reactor did not follow the initial idea literally, because during its construction some technological obstacles and high prices of some parts (eg. lamps, Al_2O_3 monolith) influenced the final product. Anyway, the main concept has been maintained. The reactor is composed of following parts (**Figure 41**):

- Two circle aluminum parts with holes for lamps or outflow with tube connections, glass tubes for lamps and housing from borosilicate glass. Geometry of the glass housing is based on the idea, that tube reactor wall forces the inflow water to circle. It is of a very common shape, easily produced from different inorganic compounds, which is in our case borosilicate glass. This type of glass is used because it is transparent to UVA and offers insight into the reactor system.

- Three units of foamed Al_2O_3 10 PPI monolith with immobilized photocatalyst which were made especially for this reactor and are designed to fit inside. The porosity was chosen on basis of some references (Raupp et al. 2001; Vargova et al. 2011; Plesch et al. 2012) and some irradiation penetration qualitative tests done on different monolith porosities (10, 20, 30 PPI) with exact thickness (10, 15, 20 mm), which were easily available.

- Lamp system consists of three weak low-pressure mercury lamps (Philips TL 4W G5 BLB Black Light UV), since they were more easily available and if necessary can be anyway replaced by different types (UV-A, -B, -C) and/or more powerful lamps. Their number was decreased since the irradiation penetrates relatively deep in 10 PPI monolith and are positioned in the monolith in a way to illuminate the surface of the photocatalyst to the highest extent possible. In order to prevent the loss of photons, which pass the monolith, the outer side of the reactor system was covered by polished aluminum to reflect irradiation back.

- Reflector made of polished aluminum sheet which is rolled around glass cylinder.

Outside reactor diameter is 120 mm and its length together with lamp connections is around 200 mm, but total volume of monoliths was lower in comparison to initial concept. If it is taken into account that monolith with 10 PPI porosity offers 17.6 m^2/L of geometrical surface, it can be calculated that volume of three monolith units in proposed reactor (0.230 L) has approximately 4.05 m^2 of total geometrical surface to immobilize photocatalyst. This surface available for TiO_2 immobilization is high and in the case of treating of 1L of contaminated water the theoretical surface to volume ratio is 40.5 cm^2/mL and 4.05 cm^2/mL in the case of 10L.

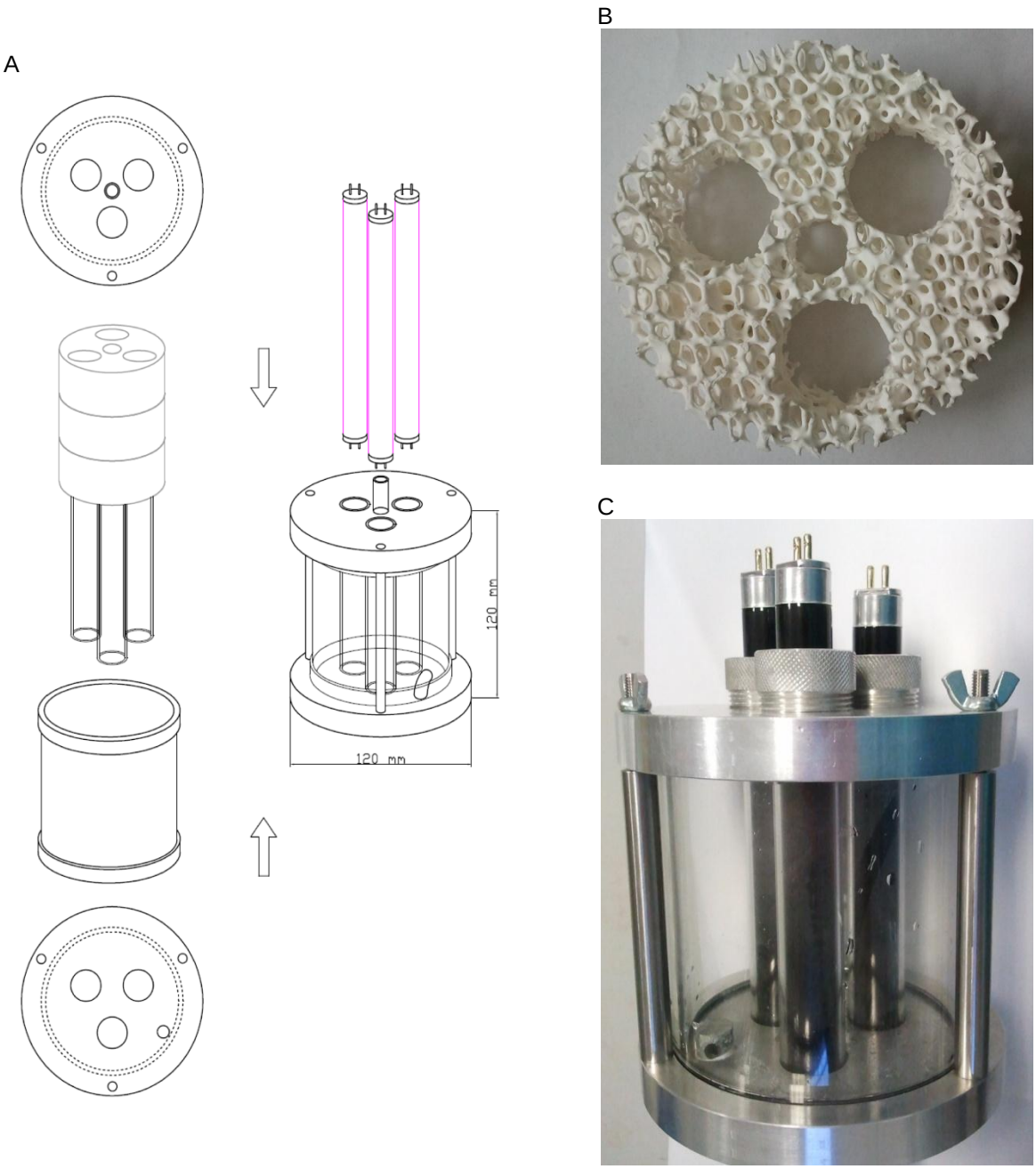

Figure 41. Composition of monolith photocatalytic reactor (A) and photos of foamed ceramic insert (B) and constructed reactor (C).

4.4.2 Operation

The proposed reactor with fixed photocatalytic phase can operate as single pass flow reactor or circular flow reactor and can be used for water or, with some modifications, air photocatalytic treatment. Since we are focused on photocatalytic water treatment, it will be used for water photocatalytic purification.

The reactor is expected to operate similarly as was predicted by its concept in chapter above. The horizontal tangential inflow of water to cylindrical reactor cell with high flow rate (1 – 2 L/min) is forcing the inflow water to circle around the monolith (**Figure 42**). Before passing through the monolith, velocity and direction of circulating water is significantly changed – perpendicularly to inflow, which will result in turbulent flow through the monolith to the center of reactor and further to outflow (**Figure 42**B). In photocatalytic reactors turbulent flow is of great importance, especially in case of immobilized photocatalyst since it decreases external diffusion layer. Despite turbulent flow through the monolith, its open three-dimensional network structure with an interconnecting porosity offers a good permeability (Richardson et al. 2000) and a significant pressure drop is not expected.

In present case the reactor operated in batch mode, so the peristaltic pump was used (0.9 L/min) allowing circulation of the analyte solution (**Figure 39**A) and a sampling point designed for placing the electrodes (O_3, O_2, pH, T). All three main components of the reactor, reactor cell, pump and sampling point are connected with Teflon tubes, so total volume of the reactor system is 0.69 L.

A

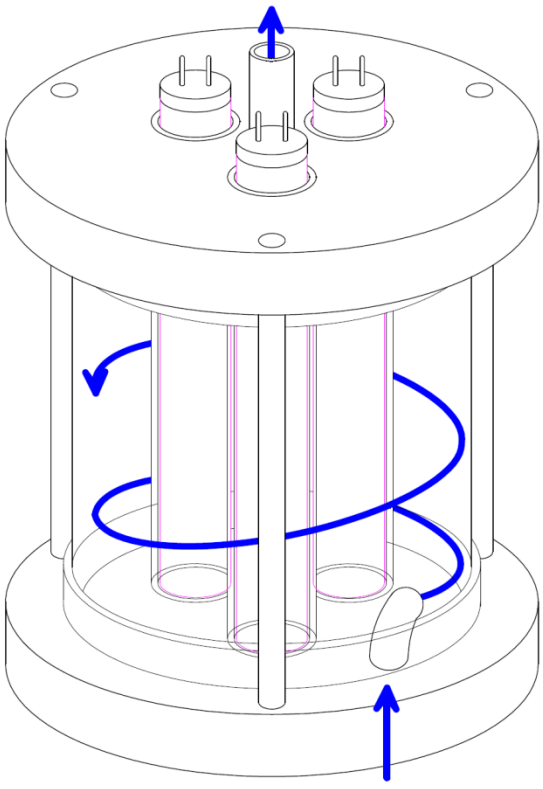

B

Figure 42. Principle of monolith photocatalytic reactor operation. Tangential inflow forces the water to circle around the monolith (A) and then passes the monolith with immobilized photocatalyst (B).

5 PART D: Degradation experiments: LAS, PBIS, RB19, Phenol

5.1 Introduction

With degradation of LAS+PBIS and RB 19 as representatives of surfactants and dyes respectively, commonly found in domestic/household waste water and phenol as trace contaminant, an evaluation of PH-OZ and PC processes in prototype and compact reactor has been performed. Experiments conducted in prototype reactor in presence of immobilized P25+PC500, P25 or P90 photocatalysts on glass were performed to check dark adsorption, differences in degradation kinetics among pollutants according to AOPs used and influence of pH to RB 19 degradation. These results were then used to explain and compare the photocatalytic efficiency of compact reactor, where three different photocatalysts and one mixture (P25, P90, PC500 and P25+PC500) were immobilized on foamed Al_2O_3 monolith.

5.2 Chemicals

The chemicals used to conduct degradation experiments in prototype and compact reactor were: Reactive blue 19 (Bezema), sodium dodecylbenzenesulfonate ($CH_3(CH_2)_{11}C_6H_4SO_3Na$), sodium tetraborate decahydrate ($Na_2B_4O_7x10H_2O$, ≥99.5%) and phenol (C_6H_5OH, ≥98%) purchased from Fluka, 2-phenyl-5-benzimidazolesulfonic acid ($C_{13}H_{10}N_2O_3S$, 96%), sodium hydroxide (NaOH, ≥99%) and hydrochloric acid (HCl, 37%) purchased from Sigma-Aldrich, acetonitrile (HPLC grade) from J.T. Baker and ammonium acetate ($C_2H_7NO_2$, ≥96%) from Merck. All aqueous solutions were prepared using highly pure water (2xd H_2O) from the NANOpure system (Barnstead). Chemicals used to prepare the layers are already listed in section 3.2.1. Custom made ceramic Al_2O_3 reticulated foams Vukopor$^@$ A with porosity of 10 PPI used as photocatalyst supports were purchased from Lanik, a.s. (Techservis Boskovice, Czech Republic).

5.3 Immobilization of TiO_2

Immobilization of different commercial TiO_2 nanoparticles on glass slides was conducted by the same procedure as described in section 3.2.2, just that the sol-suspension was applied by brush so that the surface density of catalyst was 1.1 mg/cm^2. On the other hand for Al_2O_3 monoliths the procedure was modified so that the amount of absolute ethanol was double in comparison to patented procedure described previously. The modification was done to decrease the viscosity of sol-suspension, which allows easy application by dip coating. The immobilization procedure included dipping of a Al_2O_3 monolith into sol-suspension placed in ultrasound bath, draining the excess of sol-suspension from the monolith and after that drying with air drier and finally heating to 150°C for 1h. This procedure was repeated once or twice and final mass of immobilized TiO_2 was 1.7 – 2.3 g per one monolith. Before use in compact reactor, the three monoliths were washed by ultrapure water to remove poorly attached catalyst particles.

5.4 Materials and procedures

Four different model compounds (Figure 43) were used for photocatalytic assessment of titania layers and additionally, a model waste water sample with a mixture of contaminants:

- Reactive blue 19 – textile dye
- LAS: Sodium dodecylbenzenesulfonate - surfactant
- PBIS: 2-Phenyl-5-benzimidazolesulfonic acid
- Phenol - trace contaminant
- Simulated waste water (Reactive blue 19, LAS, PBIS and phenol).

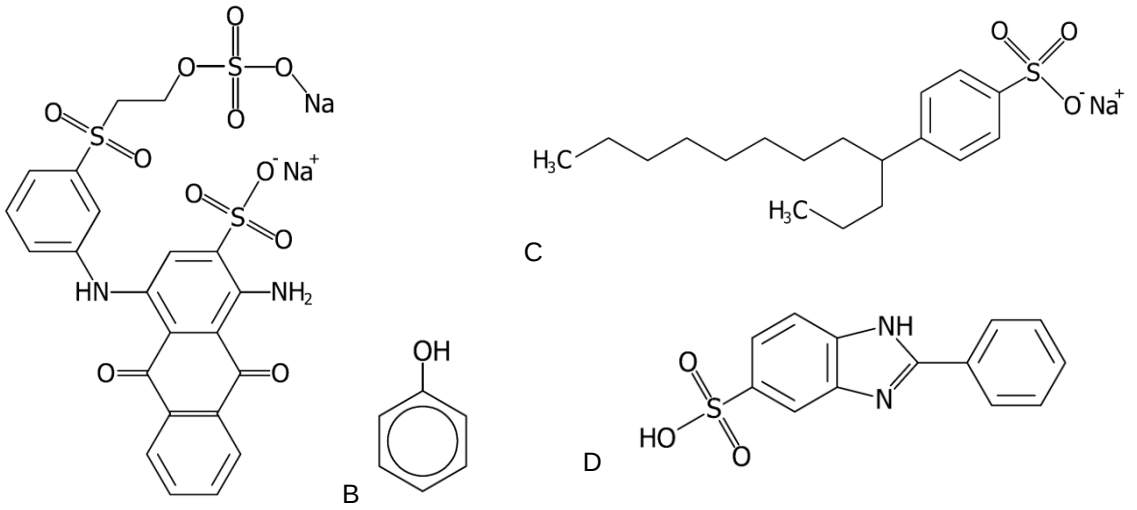

Figure 43. Chemical structures of: Reactive blue 19 (A), phenol (B), LAS: Sodium dodecylbenzenesulfonate (C) and PBIS: 2-Phenyl-5-benzimidazolesulfonic acid (D).

It was shown in a previous part of this work (Section 2), that polarity of molecule greatly influences its removal rate constant and a degree of synergy in PH-OZ process. Listed chemicals were therefore used to check if this is so also in case of immobilized photocatalyst. Reactive blue 19 and phenol have in comparison to other two the most polar molecules which is the result of high relative proportion of oxygen. On the other hand LAS and PBIS are more neutral molecules. From model contaminants mentioned, only LAS has long nonpolar tail with polar head and in water most probably forms micelles.

From these four model compounds we prepared three types of solutions in double deionized water, which were used to estimate degradation and mineralization rates in photoreactors:

- Reactive blue 19 solution: c = 25.0±0.5 mg/L in both reactors
- LAS + PBIS solution (also called unique solution):
    - c = 72±1 mg/L (LAS) + 4.6±0.3 mg/L (PBIS) in prototype reactor or
    - c = 32.0±1.0 mg/L (LAS) + 4.0±0.2 mg/L (PBIS) in compact reactor
- Phenol solution: c = 25.0±0.5 mg/L in prototype reactor
- Simulated waste water using tap water: Reactive blue 19 (c = 25.0±0.5 mg/L), LAS (c = 32.0±1.0 mg/L), PBIS (c = 4.0±0.2 mg/L) and phenol (c = 25.0±0.5 mg/L) in compact reactor

5.4.1 LAS and PBIS solution preparation

First, two separate stock solutions of surfactants were prepared: LAS and PBIS. The solution of LAS (1000 mg/L) was prepared by simply dissolving 1000 mg of LAS in 1 L of water. PBIS solution was prepared in 1 L flask by dissolving 100 mg of PBIS in sodium hydroxide aqueous solution (V = 50 mL; [NaOH] = 10.0 mM or 20 mg/50 mL). If concentration is not exactly the same, but is higher, one should recalculate the volume of NaOH solution added to PBIS following standardized equation (AS/NZS 2040.1:2005 2005):

$$V_{NaOH} = \frac{M_{NaOHSpecified}}{M_{NaOHActual}} \times 50$$

V_{NaOH} … volume (mL) of NaOH to be drawn off for adding to the PBIS dose

$M_{NaOH\ Specified}$ …20 mg of NaOH

$M_{NaOH\ Actual}$ …the actual mass of NaOH used to produce the 50 mL solution

After that we half filled the flask with water and swirled to completely dissolve the PBIS. Finally we added purified water up to the mark and mixed thoroughly. Then certain volume of both stock solutions and water was taken to get desired higher or lower concentration of LAS+PBIS, 72 mg/L+4.6 mg/L or 32 mg/L+4 mg/L, respectively.

All other solutions were prepared simply by dissolving certain mass in a given volume. In all cases double deionized water was used to prepare solutions.

5.4.2 Analytical methods and procedures

For sample analysis we used three different types of analytical procedures: (I) UV-Vis absorbance spectroscopy, (II) HPLC DAD analysis and (III) total organic carbon (TOC) analysis.

Photos of Al_2O_3 monolith surface with or without TiO_2 layers were obtained by Bresser Optik Researcher 5803100 and Motic B1-223 A microscope equipped with digital camera Moticam 5 with a 5MP resolution, coupled with ShiftCapture system installed on PC. Magnifications used were 20, 40 and 100x.

Hewlett Packard 8453 UV-visible spectroscopy system was used for UV-Vis measurements. With this method the degradation of Reactive blue 19 and LAS + PBIS (unique) solutions was monitored. Characteristic wavelengths for absorbance measurements were: 590 nm to measure Reactive blue 19, 223 nm for LAS and 302 nm to measure PBIS.

To get linear response in case of unique solution, the samples with high concentration were diluted using deionized water before measurement and then concentration was recalculated to initial value.

Agilent 1100 Series with DAD detector HPLC system was used for phenol analysis. The separations were done at 25 °C using Zorbax C8 column coupled with Alltech precolumn, using 10 mM ammonium acetate and acetonitrile as the eluents. In the first 4 min the mixture of 85:15 of NH_4OOCCH_3 to acetonitrile was used, from 4 to 16 minutes this ratio was changed by linear gradient to 30:70 and after 2 min a 5 min postrun followed. The eluent flow rate was 1.0 mL/min and injection volume 10 µL. Phenol was detected by measuring absorbance at 214 nm.

Analysis of total organic carbon – TOC was done using Analitik Jena AG MULTI N/C 3100 in the same way as already presented (Section 2.2.3).

5.5 Decomposition of ozone in compact reactor

These kind of experiments were done to check catalytic and photocatalytic ability of different commercial TiO_2 nanoparticles (P25+PC500, P25, PC500, P90) immobilized on Al_2O_3 monolith and monolith itself to decompose ozone. It is well known that different physicochemical properties influence this reaction (Section 2.3.2.3) and higher ability to decompose ozone could result in more efficient PH-OZ process.

Catalytic and photocatalytic decomposition experiments were carried out in compact reactor as follows: (I) first the reactor system was filled with 690 mL of 2xd H_2O, (II) during circulation (0.9 L/min) the system was in sampling vessel for 3 – 4 min purged with O_3 and once its concentration achieved 9.6±0.4 mg/L the frit purging system was removed, (III) when $\gamma(O_3)$ dropped to 8.5 mg/L the experiment started and lamps were switched on or left off. Concentration of dissolved ozone $\gamma(O_3)$ was monitored using ozone electrode (Multi-sensor Measuring Instrument MS 08, AMT Analysenmesstechnik GmbH) till its concentration was above 0.1 mg/L. Each test was made twice and ultrapure water between the experiments was replaced by fresh one. Because the temperature influences the O_3 solubility the experiments were conducted at the same conditions. Temperature during catalytic decomposition (UVA off) was from 22.6±0.4°C at the beginning to 22.9±0.4°C at the end and during photocatalytic decomposition (UVA on) from 23.2±0.4°C to

25.0±0.4°C which is the result of lamp heating. The ozone output during purging phase was for all experiments the same.

5.6 Degradation experiments details

5.6.1 Prototype reactor

Photocatalytic, catalytic, photocatalytic ozonation and ozonation removal experiments of different contaminants (RB 19, phenol, LAS+PBIS) in prototype reactor were performed in presence of P25+PC500 immobilized on glass slides. The intention of these experiments was to check influence of their chemical structure to their degradation rate constants, similarly as it was carried out using thiacloprid and DCAA (Section 2).

The reactor was before experiment filled with deionized water (1.65 L) and purged with synthetic air (79% N_2, 21% O_2) or ozone produced from oxygen using ozonator. After 5 to 10 min certain contaminant solution (100 mL) was added and for 2 min the solution was circulating in the system without illumination. Just before turning on the lights and consequently starting the experiment, the sample for TOC, UV-Vis or HPLC analysis was taken. The length of experiments was 4 or 5 h. The concentration of oxygen in the system was all the time around 9.0±1.5 mg/L. In case of photocatalytic ozonation experiments the reactor system was purged with ozone (10 – 15 min) before the addition of model compound solution till ozone concentration was stable. The concentrations in acidic conditions were $\gamma(O_3)$=5.0 mg/L and $\gamma(O_3)$=1.0 mg/L in alkaline. Ozone electrode was used to monitor $\gamma(O_3)$. The starting pHs during the experiments were 3.5 to 5.5 when using contaminants alone without addition of buffers or acids and 9.3 when the system was buffered by addition of sodium tetraborate buffer. After several hours of experiment the pH decreased to 4.0 – 4.5 and 9.0, respectively. Different starting pH in case of acidic environment was due to different acidity of pollutants when dissolved in water. Solutions of RB19 and phenol were more acidic, while solution of LAS and PBIS were more neutral. Low starting pH was additionally a consequence of adsorbed inorganic acids on photocatalytic layers, reactor cell walls and tubing, which reflected as slight increase of acidity after each experiment. Temperature of water solutions during experiments was rising in general and it was at the beginning around 19±1°C and at the end 23±1 °C. Temperature rise is mainly due to the lamps in the reactor, but differences of the end temperatures are due to other conditions in the laboratory.

5.6.2 Compact reactor

The goal of the present work was not just to construct the reactor potentially applicable for water treatment but also to evaluate its actual performance and to test scope of photocatalytic and PH-OZ processes realized in small reactor systems (Section 4.4). In order to test this, RB 19 and LAS+PBIS solutions were treated using photocatalysis, PH-OZ and ozonation processes. Simulated waste water was at the end treated by using the best photocatalytic system.

The experiments in compact reactor were conducted following almost identical procedure as in case of prototype reactor with some exceptions: (I) immobilized photocatalyst P25, P90, PC500 and P25+PC500 mixture were used, (II) reactor was first filled with 640 mL of water which was (III) purged with pure oxygen (5.1) instead of using synthetic one, so oxygen concentrations were higher, $\gamma(O_2)$=16 – 32mg/L, (IV) in the case of PH-OZ the ozone saturation concentration was lower, $\gamma(O_3)$=4.2±0.1mg/L, (V) the volume of contaminant solution (RB19 or LAS+PBIS) added before starting the experiment was 52 mL, (VI) starting and ending temperatures of solution were higher, 22.0±0.5 and 29±1°C respectively and (VII) experiments were done just at natural conditions without addition of buffer, where the starting pH was 4.9±0.2 and 4.4±0.3 at the end of experiments. Length of an experiment was adjusted to the AOP used, so that all experiments including ozone lasted for 2 h while photocatalytic experiment for 3 h.

In the case of simulated waste water, the volume of water was lower (562 mL), since the total added volume of four pollutants stock solutions was higher (118 mL). While the oxygen concentration was in the same range as in case of rest of the experiments, ozone starting concentration was due to higher pH (7.3 – 8.0) lower ($\gamma(O_3)$=1.4±0.1 mg/L).

5.7 Results

In this section results of photocatalytic, photocatalytic ozonation and ozonation experiments in prototype and compact reactor are discussed.

5.7.1 Prototype reactor: adsorption and photocatalytic degradation experiments

5.7.1.1 Adsorption of pollutants

Tests of model pollutants adsorption (**Figure 44**) to immobilized P25+PC500 were done to check if this factor in any manner influences their degradation kinetics as it was shown for DCAA and thiacloprid (Section 2.3). Degree of adsorption was measured in the same acidic pH conditions as already mentioned (Section 5.6.1) after 60 min of dark phase for all four model compounds in three solutions (Section 5.4), where the high concentration unique solution was used.

In agreement with others (Liu et al. 2010), from present results it can be concluded that Reactive blue 19 adsorb in much greater proportion (aprox. 4%) in comparison to phenol, whereas PBIS doesn't adsorb to TiO_2 surface. In the case of LAS the interpretation of data is not simple, since this surfactant was always foaming, especially at the beginning of the experiment, causing its loss from the system via openings in the cover of sampling vessel. The concentration decrease is therefore the result of adsorption and mentioned inconvenience, so it can be speculated, that adsorption level is actually lower and comparable to PBIS. Overall none of used pollutants is adsorbed in a large proportion to photocatalytic surface.

The small differences are consequence of different polarity of molecules since the surface of TiO_2 particles at this pH (pH=5.5±0.3) is more or less neutral because of the position of IEP, which is for majority of titania used in this work in a range from 5.7 to 7.0 (Section 2.3.1, **Table 1**). The results of adsorption proportions therefore follow the polarity of molecules, with an exception of LAS, which has probably lower affinity to TiO_2 surface than presented (**Figure 44**).

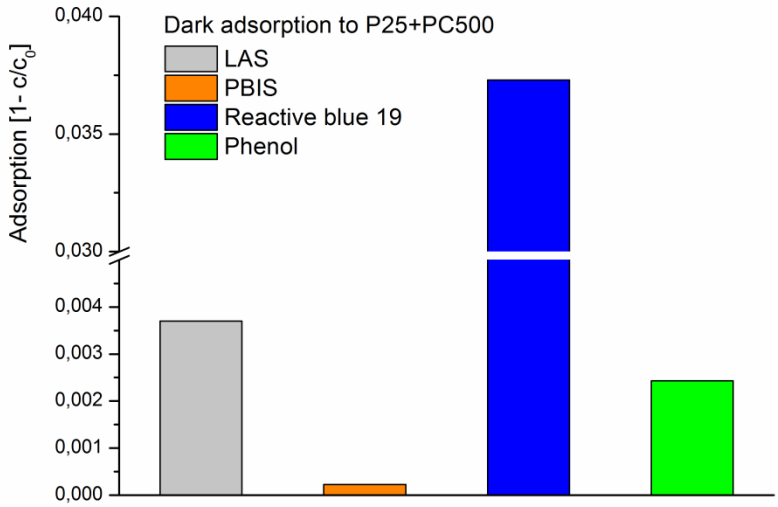

Figure 44. Proportion of adsorbed parent compounds after 60 min of circulation in prototype reactor in presence of P25+PC500 photocatalyst immobilized on glass slides.

5.7.1.2 Reactive blue 19

Degradation experiments of Reactive blue 19 were conducted by different types of advanced oxidation processes (AOPs, **Figure 45**): photocatalysis, catalysis, photocatalytic ozonation and ozonation. It can be observed, that in the case of parent compound degradation PH-OZ and ozonation processes are much more efficient in comparison to PC. This fast disappearance of RB 19 is most probably the consequence of O_3 fast reaction with the dye chromophores (He et al. 2008; Panda and Mathews 2014), especially in more acidic environment (Chen et al. 2009). From these results it can be reasonably stated, that in the first stage of RB 19 PH-OZ degradation,

photocatalysis doesn't even occur, since there is no difference in initial degradation rates of PH-OZ or ozonation process. The photocatalytic RB 19 degradation is on the other side more than 10x slower and is related to hydroxyl radicals attack to the C–N bond of the side chain on anthraquinone (Liu et al. 2010; Marques et al. 2010). Catalytic process (without UV irradiation) on the other hand does not affect the RB 19 concentration, which was somehow expected.

Unlike the first degradation stage, mineralization reaction during PH-OZ definitely requires presence of photocatalyst (Chen et al. 2014), since ozonation alone leads to very slow mineralization of RB 19. This is the proof that O_3 oxidation reactions result in stable degradation products (eg. quinones, phenols, maleic acid, oxalic acid, formic acid, acetic acid) (He et al. 2008; Marques et al. 2010), whereby the decomposition process stops. It was proved that oxalic acid is the major RB 19 degradation product (He et al. 2008) which is, similarly as phenol, very slowly mineralized by ozonation alone (Chen et al. 2014). Further mineralization reactions are obviously driven by stronger oxidative species (eg. $^{\bullet}OH$), which are in greater proportion present only during PC and PH-OZ processes. The mineralization initial degradation rate is in case of PH-OZ 3x higher in comparison to PC, which suggests the presence of already mentioned synergistic effect (Section 0).

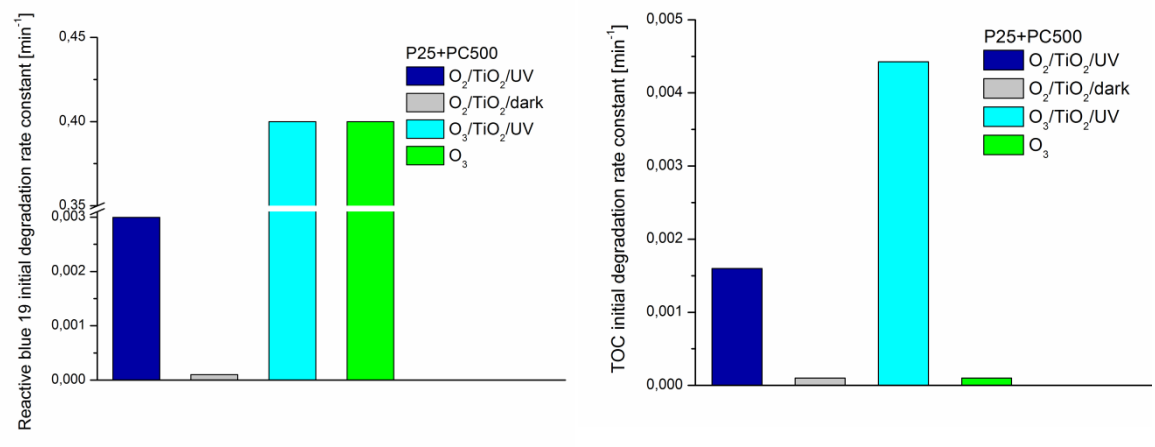

Figure 45. First order initial degradation rates of RB 19 and TOC (represented by RB 19) achieved in prototype reactor in the presence of immobilized P25+PC500 photocatalyst. Experiments were conducted by different types of advanced oxidation processes (AOP).

5.7.1.3 Phenol

Decomposition reactions of phenol were found to be of the first order, which was also shown for ozonation process by Turhan et al. (Turhan and Uzman 2008). In the case of PH-OZ degradation results (**Figure 46**) one can observe, that ozonation process alone contributes significant part in the first degradation stage, almost as high as in case of RB 19. For phenol it can be concluded, similarly as for RB 19, that it reacts with O_3 very fast (Chen et al. 2014). PH-OZ process is in comparison to ozonation slightly more effective (Chen et al. 2014) and if one takes into account the PC performance which is much lower, a barely noticeable synergy between PC and ozonation can be detected.

Mineralization using ozonation alone is fast at the beginning of experiment, but after 1 h the concentration reaches a plateau at 2/3 of starting TOC value. This indicates, that after initial O_3 cleavage of aromatic ring, it cannot be completely mineralized in direct ozonation (Turhan and Uzman 2008; Chen et al. 2014). In contrast initial mineralization rate constant in case of PH-OZ process is lower, but the process continues and after 4 h the TOC concentration drops under 10% of initial value. This is due to higher efficiency of PC/PH-OZ, where the intermediate products were more easily degraded. The higher mineralization extent in the PH-OZ mainly originated from oxidation by the holes induced from UV (Chen et al. 2014). Phenol mineralization process is faster in comparison to RB 19, which is the consequence of its simpler molecule and therefore requires fewer radicals to complete oxidation.

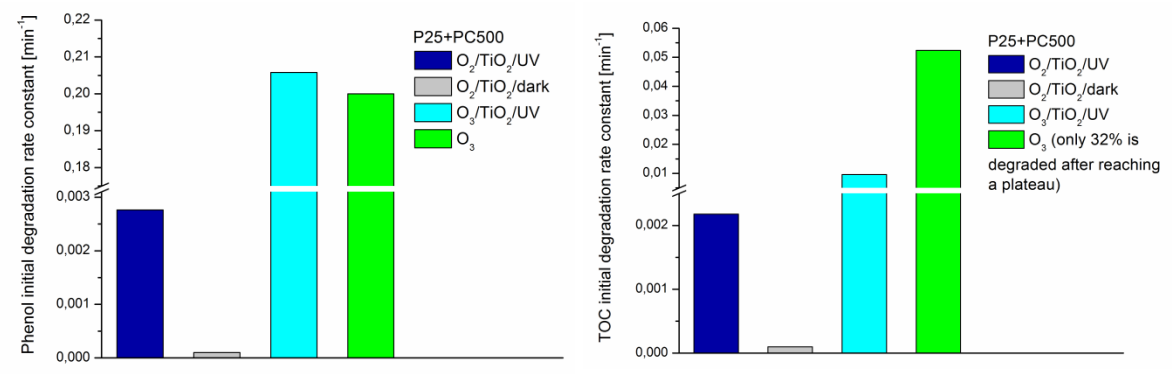

Figure 46. First order initial degradation rates of phenol and the corresponding TOC achieved in prototype reactor in the presence of immobilized P25+PC500 photocatalyst. Experiments were conducted by different types of advanced oxidation processes (AOP). Phenol mineralization in case of ozonation process stops after 1h of experiment and reaches a plateau at 68% of remaining TOC.

5.7.1.4 LAS + PBIS

Degradation results of LAS and PBIS (Figure 47) generally show that LAS is more resistant to degradation than PBIS regardless to AOP used. This is manly ascribed to its low content of aromatic rings and its characteristics to form micelles (Petrenko et al. 2010) which are positively charged and do not adsorb to positively charged TiO_2 surface. Degradation rates of LAS and PBIS simultaneously present in water are in the case of PC comparable to those of RB 19 and phenol while in the case of PH-OZ this is not so. Slower degradation in case of PH-OZ is due to molecules stability (Beltran et al. 2000; Hernandez-Leal et al. 2011), especially LAS and its higher resistance towards O_3 (Beltran et al. 2000), which is clearly seen from results of ozonation process. These experiments also show, that parent molecules can be degraded in presence of O_3 alone very efficiently and comparable to PC, but when it comes to their mineralization the process stops, which was also shown by others (Beltran et al. 2000). In this case molecular structure changes from initial organic matter to more inert degradation products, which cannot be degraded just by ozonation process. There is some decrease in TOC concentration (Figure 48), but this is mainly due to LAS foaming (Section 5.7.1.1), similarly to experiment with LAS as a single contaminant.

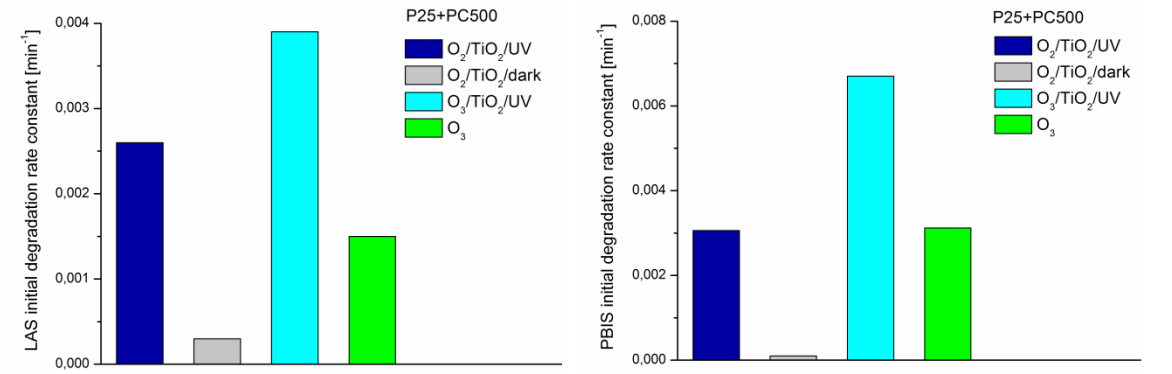

Figure 47. First order initial degradation rates of LAS and PBIS achieved in prototype reactor in the presence of immobilized P25+PC500 photocatalyst. Experiments were conducted by different types of advanced oxidation processes (AOP).

It can be concluded, that presence of photocatalyst is crucial for mineralization step (Figure 48) and that PH-OZ mineralization process actually results in synergistic effect which is not obvious for first degradation stage. Mineralization is for LAS+PBIS slower process in comparison to RB 19, which can be a consequence of RB 19 affinity to TiO_2 surface and its more reactive molecule. Phenol molecule is even simpler, which leads to its higher mineralization rate constant in comparison to mentioned three model compounds.

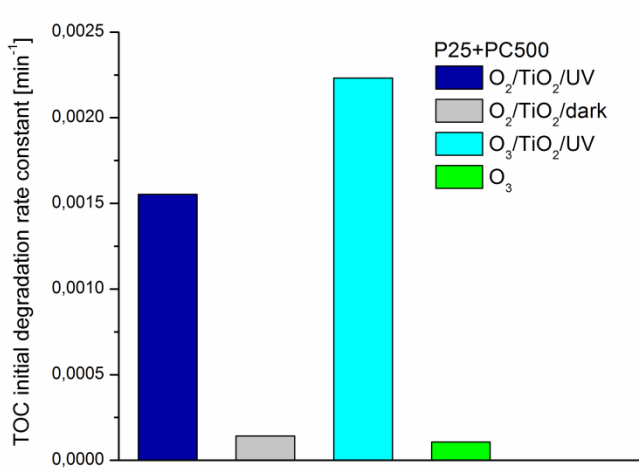

Figure 48. First order initial degradation rates of LAS+PBIS corresponding TOC achieved in prototype reactor in the presence of immobilized P25+PC500 photocatalyst. Experiments were conducted by different types of advanced oxidation processes (AOP).

5.7.1.5 Influence of pH on photocatalytic/photocatalytic ozonation processes

Influence of pH conditions on photocatalytic ozonation process was already studied by other authors (Glaze et al. 1987; Cernigoj et al. 2007a; Lucas et al. 2009), showing that PH-OZ process in acidic conditions often lead to synergistic effect, while at alkaline pH this synergy is lost due to self-decomposition or otherwise, noncatalytic decomposition of ozone. In present section, degradation of RB 19 during PH-OZ or PC process under different pH conditions was studied. The goal was to check if there are any pH limitations regarding blue dye degradation and mineralization. Experiments were conducted in presence of two types of photocatalysts – P25+PC500 mixture or P90 immobilized on glass slides, which were freshly prepared just for these experiments. Specific surface mass concentration was in case of both catalysts 1.2±0.2 mg/cm^2. Experiments were done at two different pH, natural ~4.1 and basic ~9.1. To establish alkaline conditions NaOH and $Na_2B_4O_7$ were used. During the experiments concentrations of RB19, TOC, oxygen/ozone and pH (**Figure 49** - 52) were followed.

PH-OZ degradation results (Figures 49, 50) show that RB 19 mineralization in alkaline conditions is in first 60 min comparable to that in acidic conditions (or decreased in case of P25+PC500 mixture), but after that it is highly reduced and TOC reaches a plateau. On the other hand RB19 is efficiently mineralized in acidic conditions. There could be several reasons for inhibition of mineralization process in alkaline solution: (I) fast disappearance of ozone, which is the main oxidative species (Chen et al. 2009) in the solution bulk due to presence of OH^-, (II) or disappearance of oxidative species produced on the photocatalysts surface and (III) TiO_2 surface is negatively charged because of photocatalysts low IEP, which hampers the adsorption of RB 19 degradation products and consequently prevents their further photocatalytic mineralization process. Contrary to mineralization process, the degradation of parent compound was instant, regardless pH, so that the kinetics could not be followed. This, as it was already discussed (Section 5.7.1.2), is most probably the result of its low stability against ozone (Chen et al. 2009), which was proved by $\gamma(O_3)$ fast decrease at the beginning of experiment (Panda and Mathews 2014), similarly as in case of thiacloprid (Section 2.3.2.4, **Figure 20**). Concentration of dissolved O_3 at alkaline pH was lower in comparison to acidic conditions despite the same purging conditions, which is a proof of O_3 self-decomposition at alkaline pH.

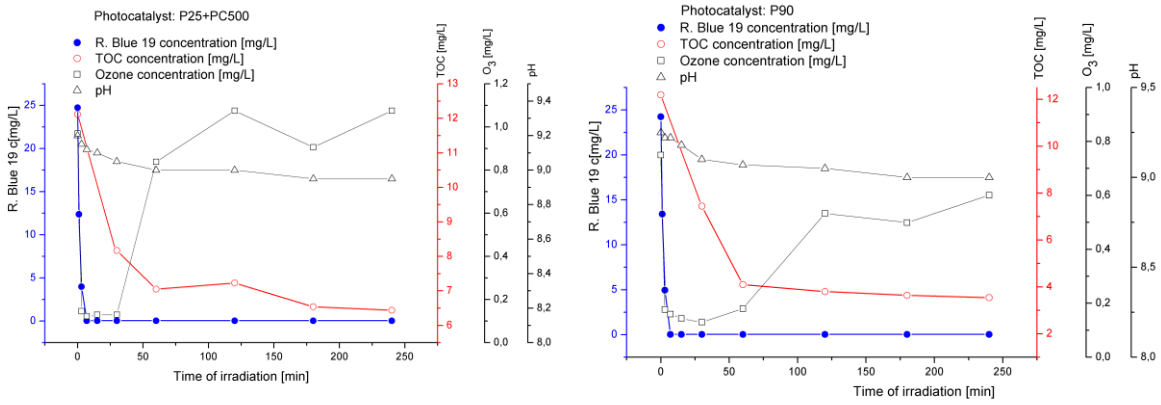

Figure 49. Photocatalytic ozonation degradation of RB 19 with two different photocatalysts, P25+PC500 and P90 in basic pH (pH=9.0 – 9.2).

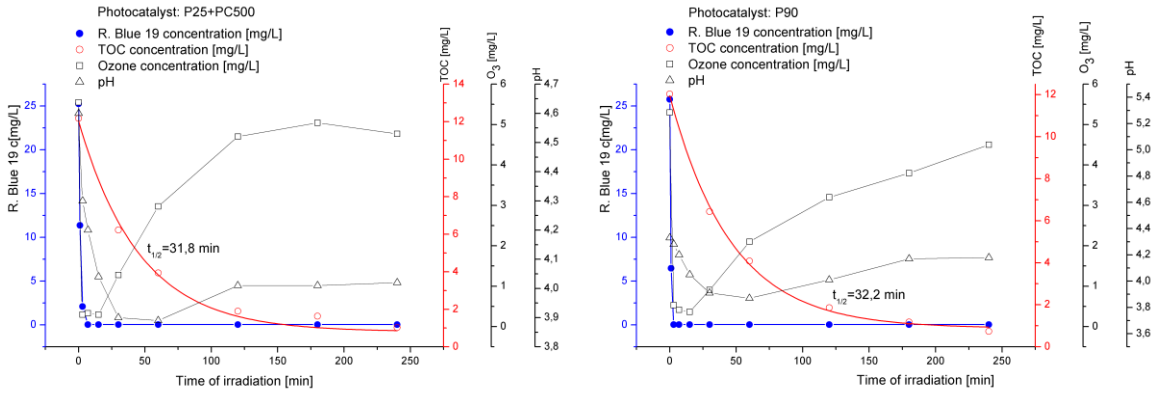

Figure 50. Photocatalytic ozonation degradation of RB 19 with two different photocatalysts, P25+PC500 and P90 in natural pH (pH=4.0 – 4.6).

Photocatalytic degradation of RB19 is in alkaline conditions, similarly as PH-OZ process, suppressed and the degradation rate is 8 – 9 times lower in comparison to reaction at low pH (**Figure 51**, **52**). Also there is no decrease in TOC, so mineralization doesn't occur. The reasons for this are the same as mentioned above, like TiO_2 surface charge and inhibition of oxidative species on its surface. As mentioned, in acidic environment both reactions are much more efficient. Reactions of mineralization are at the beginning faster than in the second stage, after 60 min. This can be explained by adsorption of RB 19 degradation products on the photocatalysts surface in second phase of degradation. In this case the molecules which are at the beginning adsorbed on or are located near the TiO_2 surface are initially degraded and the reaction follows the first order exponential degradation. After certain time (60 min) the layer of adsorbed degradation products molecules is thickened so just adsorbed molecules are degraded, which leads to zero order degradation. This limitation of photocatalytic process is not detected in case of PH-OZ, which has clear advantage thanks to faster production of oxidative species.

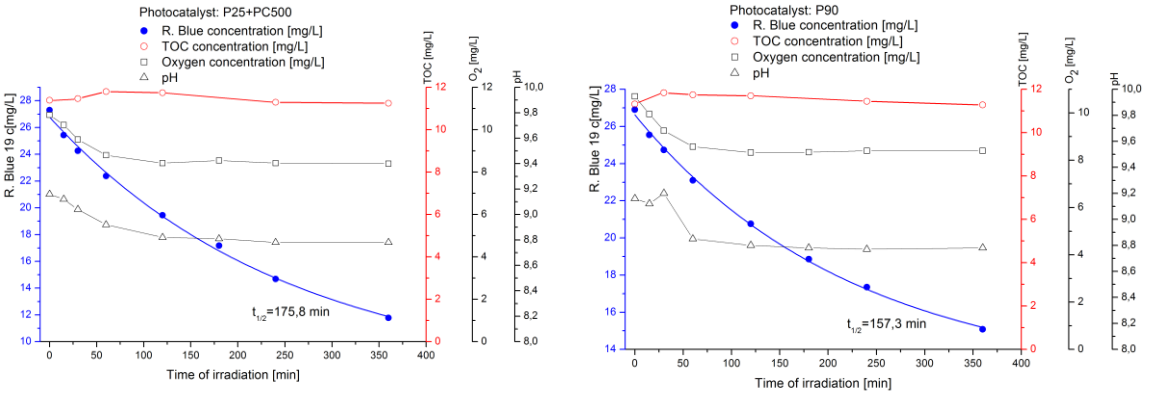

Figure 51. Photocatalytic degradation of RB 19 with two different photocatalysts, P25+PC500 and P90 in basic pH (pH=8.9 – 9.1).

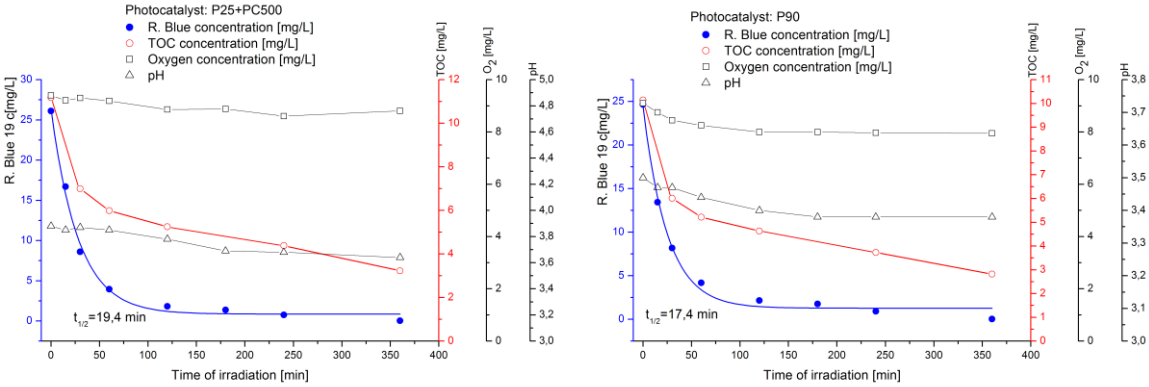

Figure 52. Photocatalytic degradation of RB 19 with two different photocatalysts, P25+PC500 and P90 in natural pH (pH=3.4 – 3.8).

Experiments conducted under different pH conditions show, that alkaline environment negatively influences both AOPs, photocatalysis and photocatalytic ozonation processes of RB 19. Similarly Chen et al. (Chen et al. 2009) show for ozonation alone that RB 19 is more efficiently oxidized in acidic environment due to higher $\gamma(O_3)$, the main oxidant in the initial reactions. The inhibition of mineralization when performing PH-OZ in alkaline conditions is obvious, but this process is still comparable to photocatalytic degradation at acidic pH, which gives to PH-OZ a head start in terms of flexibility, when it comes to pH fluctuations in reactor system.

5.7.2 Compact reactor: photocatalytic monoliths characteristics and cleaning performance

Photocatalytic performance in compact reactor was evaluated using two different aqueous solutions (RB 19 and LAS+PBIS), phenol solution was omitted because it is more easily degradable in comparison to others. Tests of catalytic/photocatalytic decomposition of O_3 were made to check its influence to pollutant removal.

5.7.2.1 Photocatalysts immobilized on Al_2O_3 monoliths

The mass fractions of immobilized photocatalysts on Al_2O_3 monoliths were determined (Table 5) to be in a range from 4.13 to 5.36 %. These differences in TiO_2 content may later result in photocatalytic activity, but it was presented by some authors (Vargova et al. 2011; Plesch et al. 2012) that this is not true, because the catalyst layer is already thick (~ 2 - 20 μm). Plesch et al. (Plesch et al. 2012) showed, that 60 or even 90% increase in mass of immobilized TiO_2 doesn't result in significantly higher photocatalytic activity. In addition, the mass fractions achieved herein are 2 to 3 times higher in comparison to those achieved by above mentioned authors. I would like to add, that just one layer of P90 was applied, owing to higher sol-suspension viscosity in comparison to other photocatalysts.

Table 5. The properties of films deposited from P25, P90, PC500 and mixture of P25+PC500 on reticulated Al_2O_3 monolith by sol-suspension method.

Photocatalyst	Mass of Al_2O_3 monolith/s [g]		Mass of immobilized catalyst [g]			Number of layers
	Monolith 1 / 2 / 3	Total	Avg. per monolith	Total	w(catalyst) [%]	
P25+PC500	43.97 / 41.30 / 42.05	127.32	1.76	5.28	4.15	2
P90	42.31 / 38.36 / 42.23	122.90	1.69	5.07	4.13	1
P25	43.92 / 46.54 / 43.62	134.08	2.21	6.64	4.95	2
PC500	42.30 / 43.65 / 42.38	128.33	2.29	6.88	5.36	2

Geometrical surface and BET surface area of monolith are another important factors that could influence pollutant conversion, since the exposed surface of photocatalyst with immobilization procedure decreases. According to Plesch et al. (Plesch et al. 2012), the Vukopor foam offers 0.3 m^2/g of BET surface. According to the mass this means that the total BET surface of three monoliths is between 38 to 40 m^2. When TiO_2 was applied to monolith by dipping to P25 suspension, the BET surface increased to 0.5 – 0.6 m^2/g (Ochuma et al. 2007; Vargova et al. 2011), so the total theoretical BET values of immobilized photocatalysts presented herein are assessed to be about: (I) 73 m^2 for P25+PC500, (II) 70 m^2 for P90, (III) 77 m^2 for P25 and (IV) 74 m^2 for PC500. These are in fact small differences and therefore couldn't be the decisive factor for the photocatalytic activity differences.

Exact surface area of monoliths is on the other hand not known and it can only be mathematically modeled. According to theoretical geometrical surface area of one monolith (Section 4.4.1), which is 1.35 m^2 (13500 cm^2), the surface density of photocatalyst is 0.15 mg/cm^2. On the other hand, if we take into account that two layers produced from patented sol-suspension (Section 3.2.2) result in surface density of 0.5 – 0.7 mg/cm^2 (Section 3.3.1, **Table 2**) and that sol-suspension in case of immobilization to monolith was diluted twice, the surface density would be about 0.3 mg/cm^2. In this case the actual geometric surface of one monolith would be 0.675 m^2. However, the exact geometrical surface of monolith remains unknown till present, so we assume that this value lies somewhere between 0.675 and 1.35 m^2 per one monolith unit and the surface density of immobilized TiO_2 lies in interval 0.15 – 0.3 mg/cm^2. We believe that the geometrical surface, similarly as BET surface, doesn't vary significantly between monolith units which allow us to compare the immobilized photocatalysts in compact reactor.

Figure 53 shows 20x, 40x and 100x magnification of pure Al_2O_3 monolith and monoliths with different immobilized titania. Photos were taken after all four degradation experiments were conducted. It can be noticed, that photocatalysts PC500 or mixture P25 + PC500 are not well adhered to monolith surface, since regions of detached photocatalytic layer can be seen. During observations of photocatalytic experiments it was noticed that just in case of PC500 there were deflashed particles sedimented to the bottom of reactor, while in case of P25 + PC500 this was not the case. From this it can be concluded, that P25 + PC500 layer is actually more stable despite observed result (**Figure 53**). From the presented figures it is not clear if these regions still contain TiO_2, but the experiment results didn't show any difference in photocatalytic activity. On the other hand P25 and especially P90 showed high mechanical stability and layer durability. The figures revealed cracked surface structure, which was already noticed for P90 immobilized on glass slides (Section 3.3.1). In the same part of the thesis it was already mentioned that these cracks didn't influence layer stability. It was shown that P25 and P90 were actually the more suitable to immobilize due to reasons already discussed and with the application to monoliths this is now confirmed. P90 immobilized on monolith showed the best result which is in correlation with previous results (**Figure 28**, Section 3.3.1).

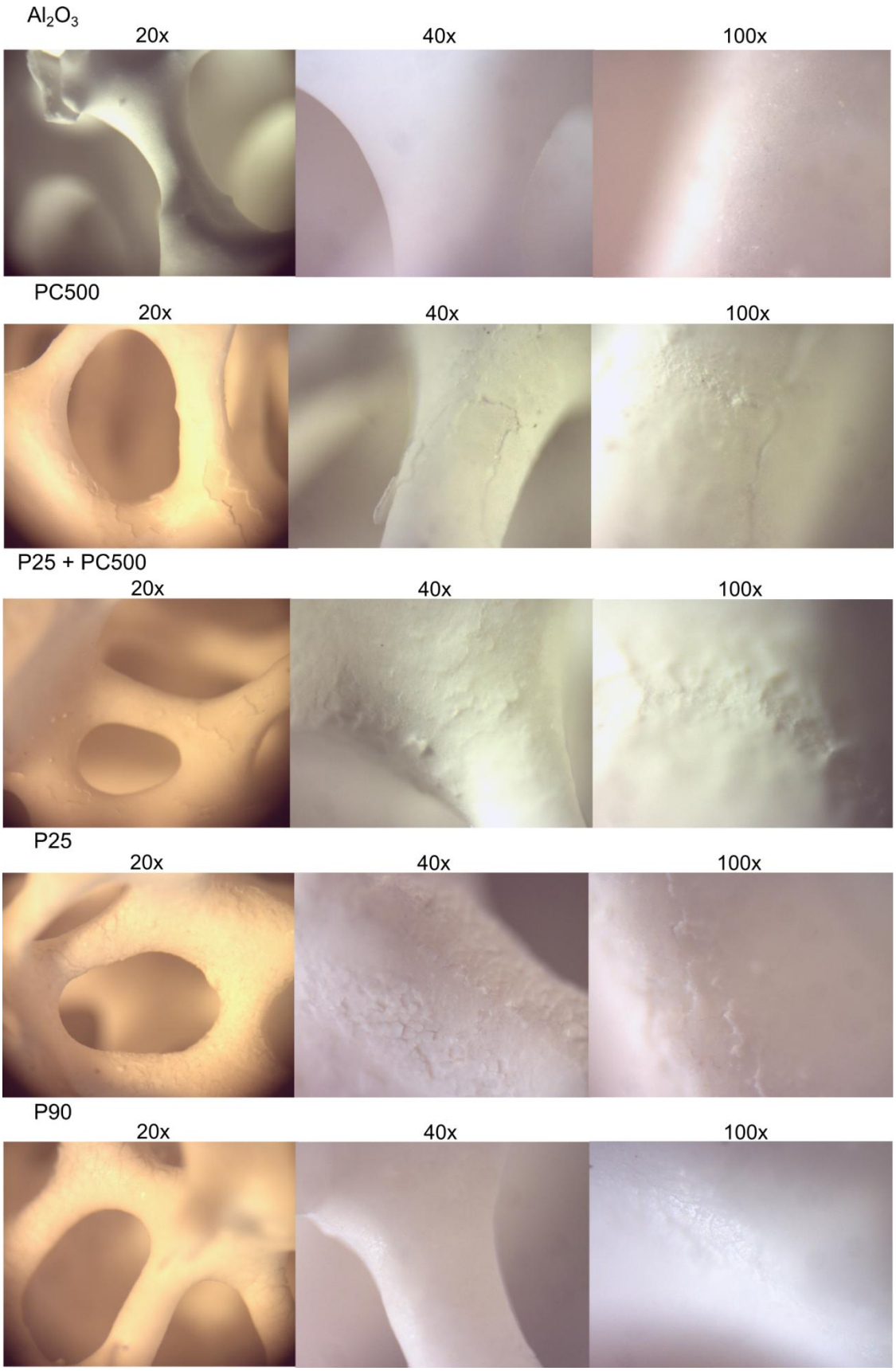

Figure 53. Photos of pure Al_2O_3 monolith and monoliths with different immobilized titania: PC500, P25 + PC500, P25 and P90. Magnifications used were 20x, 40x and 100x.

5.7.2.2 Decomposition of ozone

Photocatalytic decomposition experiments of O_3 in compact reactor in presence of different photocatalysts show, that all of them rapidly degrade ozone, especially P90 and PC500 (**Figure 54**). Since there has been no study performed, it is not known which physicochemical properties influence the differences between photocatalysts. Most probably they originate from inhomogeneity of layers and, since the photocatalytic decomposition of O_3 is related to TiO_2 surface, differences in layer roughness, geometrical surface of monoliths and differences in light distribution. Catalytic O_3 decomposition is again more rapid in presence of PC500, which could be due to its poor mechanical stability (Section 3.3.1). The particles present in solution thus increase active surface for O_3 decomposition. These experiments were performed to check, if ozone catalytic/photocatalytic decomposition ability influence the degradation kinetics of pollutants in the following experiments.

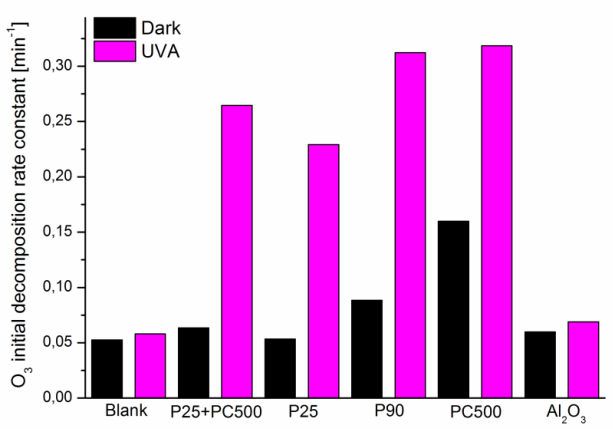

Figure 54. First-order decomposition constants of ozone in presence of different immobilized TiO_2 photocatalysts, obtained in compact photocatalytic reactor.

5.7.2.3 Reactive blue 19, LAS+PBIS – reaction evolution

Figure 55 presents the evolution of pollutant concentration (RB 19, LAS, PBIS, TOC), γ(O_3), pH and temperature during the PH-OZ processes. The reactions behind were already described and the two examples are presented just to compare and prove the statements above (Sections 5.7.1.2 and 5.7.1.4), so that slower degradation of LAS+PBIS in case of PH-OZ is most probably because of molecules stability and their higher resistance towards O_3 (Beltran et al. 2000; Hernandez-Leal et al. 2011), especially LAS. This is clearly presented with evolution of ozone concentration during the first 60 min of experiments. In case of RB 19 it drops to 0 mg/L (Panda and Mathews 2014), whereas during surfactants degradation the drop is not so dramatic.

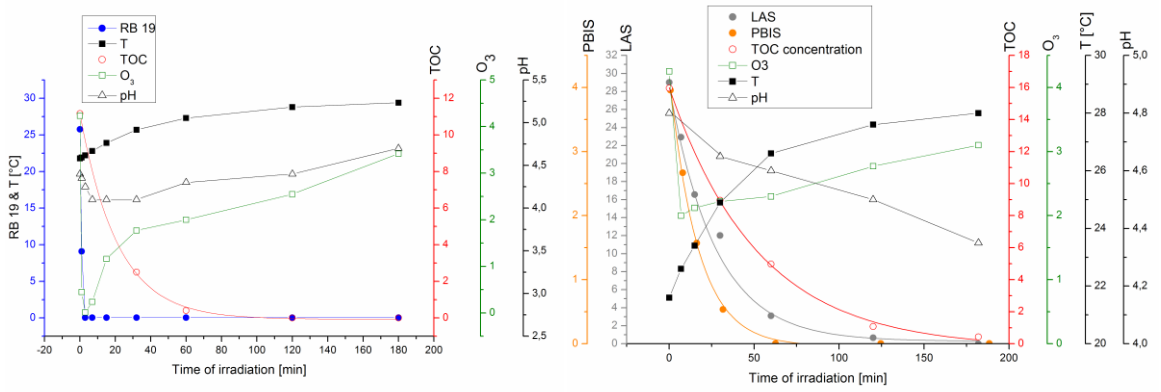

Figure 55. Experiment of photocatalytic ozonation (O_3/TiO_2/UVA) of RB19 (left) and LAS+PBIS (right) using P25+PC500 TiO_2 immobilized on Al_2O_3 monolith. The graph presents all variables monitored during the degradation experiments.

5.7.2.4 Reactive blue 19

Performance of compact reactor versus prototype was evaluated using RB 19 and LAS+PBIS solutions. The removal and mineralization rate of RB 19 (Figure 56) show, that PH-OZ process is generally more efficient. The data for PH-OZ degradation of RB 19 are even not shown, since this reaction is so fast that the kinetics was not possible to follow. Contrary, mineralization process during photocatalysis of RB 19 was slower (k = 0.06 – 0.14 min^{-1}) and a comparison to the same process in prototype reactor can be made. The degradation rate constant in compact reactor is in this case 20 – 40 times higher and the shortest half life was 5.0 min, achieved with P90. Mineralization is slower process and was during PC and PH-OZ easily followed. As it was expected, PH-OZ in compact reactor again shows advantage and when comparing its efficiency to prototype reactor, the coefficients are 10 – 12.5x higher and shortest half life achieved was 12.6 min. PC process on the other hand shows lower photocatalytic degradation and mineralization, but even higher enhancement factor (15x) in comparison to prototype.

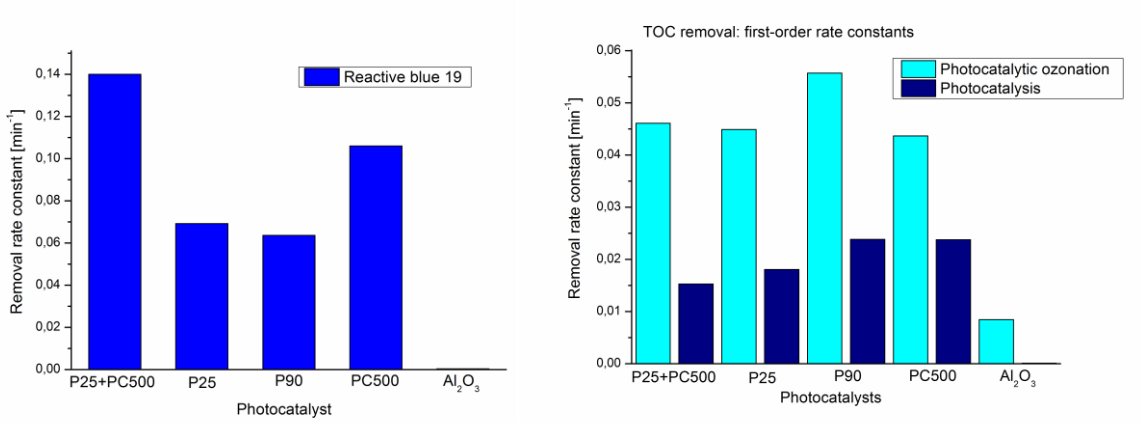

Figure 56. First order initial degradation rate constants of RB 19 photocatalytic degradation (left) and corresponding TOC during photocatalytic experiments in presence of four different commercial TiO_2 immobilized on Al_2O_3 monolith (right). Experiment performed with Al_2O_3 monolith represents a blank experiment.

On the first sight the PC/PH-OZ degradation data of blue dye show that, photocatalytic reactions of RB 19 are much more related to photocatalysts surface, because the enhancement factors are higher for photocatalytic process. For PH-OZ process, on the other hand, the photocatalytic surface area is of equal importance, but since this is limited and reactions of PH-OZ process can occur also in solution bulk (Section 2.4), it is most probably reached the limit of efficiency in present reactor. Therefore it can be also claimed, that differences in ozone photocatalytic decomposition efficacy doesn't affect the PH-OZ noticeably.

5.7.2.5 LAS + PBIS

The tests using LAS+PBIS solution show that in general, these two pollutants are again degraded faster when PH-OZ process is applied (**Figure 57**). The differences between photocatalysts are small and do not correlate to ozone cleavage ability. Unlike in the case of parent compounds degradation, the TOC removal constants (**Figure 58**) are not much different for PC and PH-OZ processes, except in case of P90 which shows almost 45% increase. Contrary is photocatalysis in case of P25 even more efficient. Anyhow, the important fact is, that PH-OZ TOC degradation constants are for all catalysts comparable. This fact is showing that the influence of TiO_2 physicochemical properties is decreased when using immobilized photocatalyst in combination with ozone and that the limit of these commercial photocatalysts in compact reactor is probably almost achieved. Photocatalyst mixture of P25 and PC500 gave the shortest TOC half life, which was 36.5 min.

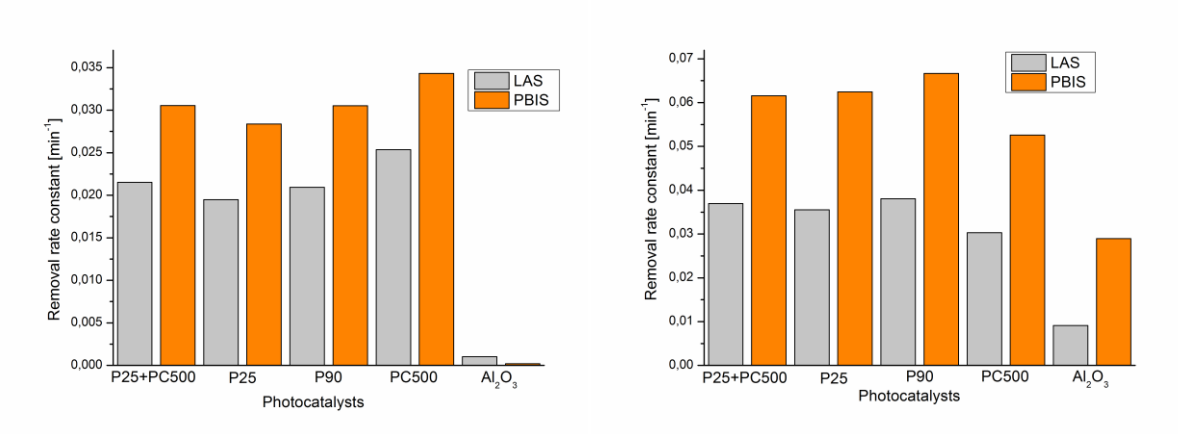

Figure 57. Photocatalytic (left) and PH-OZ removal (right) constants of LAS and PBIS simultaneously present in water, achieved with different immobilized photocatalysts. Experiment performed with Al_2O_3 monolith represents a blank experiment.

When comparing the PH-OZ processes conducted in compact to prototype reactor, the factor of increase in process pace is 9 for both pollutants and their TOC. Similarly as for RB 19 it can be concluded, that PH-OZ process effectiveness is limited due to limited surface. For PC experiments these factors are not constant. LAS is in comparison to prototype reactor degraded 8 times faster, while PBIS 11 and their TOC 10 times faster. These factors actually reflects the molecule stability and how it is distributed in water bulk. From this it can be concluded, that for LAS the surface area is less important than for PBIS, while the TOC factor is a compromise of both.

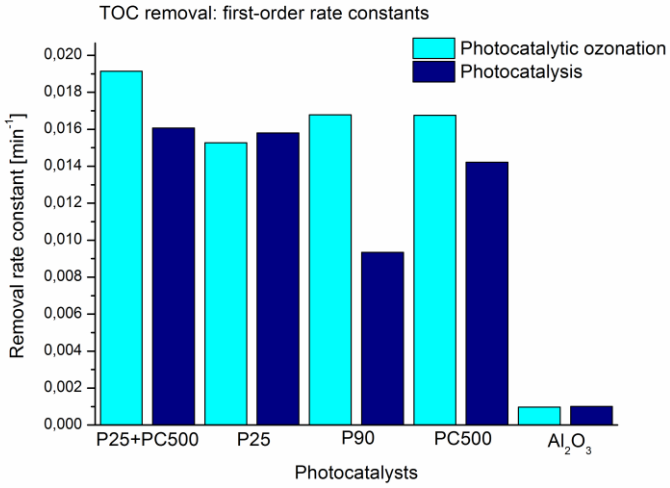

Figure 58. Photocatalytic ozonation removal constants of TOC corresponding to LAS+PBIS achieved with different immobilized photocatalysts. Experiment performed with Al_2O_3 monolith represents a blank experiment.

5.7.3 Synergism of photocatalytic ozonation process – immobilized TiO_2

With comparison of PH-OZ results to the sum of photolytic ozonation and photocatalytic results (**Figures 59**, **60**, **61**, **62**), the presence of synergistic effect was examined. In case of RB 19 first stage degradation this comparison couldn't be done due to fast PH-OZ and photolytic ozonation kinetics, which indicates that in this case there is no difference between these two processes and consequently no synergy. Experiments with surfactant solution on the other hand show mild synergy (**Figures 59**, **60**), with the exception of PC500. The synergy is in case of LAS a little higher, which is a consequence of much higher concentration and molecule stability against

ozone, which is not true for PBIS. In both cases the synergy factors are not so different, this means that the reaction mechanism is similar for both pollutants.

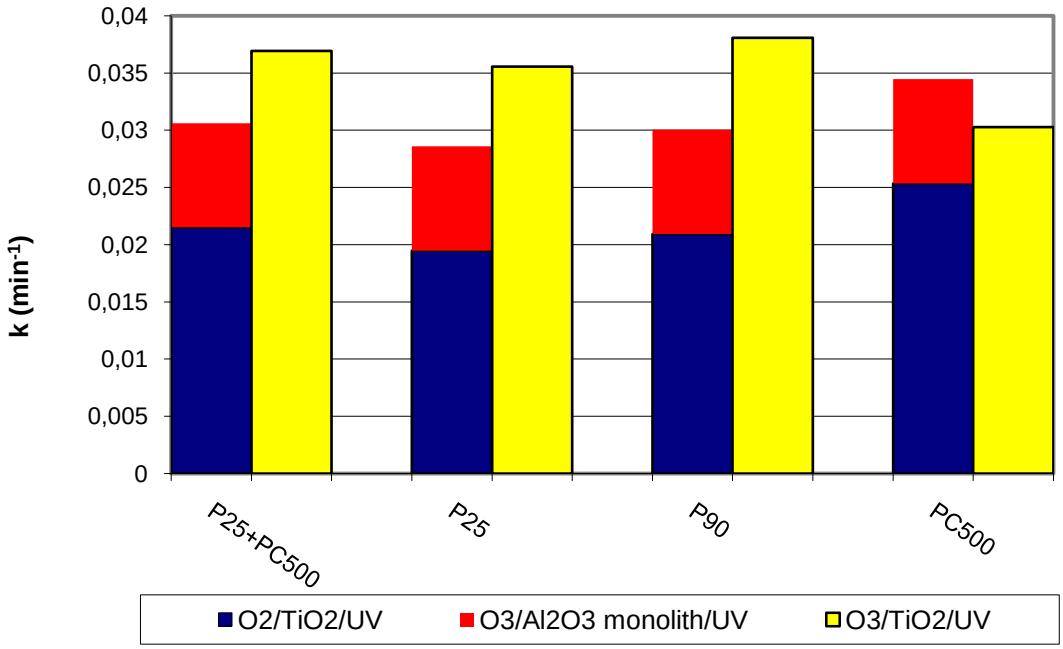

Figure 59. Comparison of initial degradation rates of LAS photocatalytic ozonation ($O_3/TiO_2/UV$) to the sum of ozonation ($O_3/Al_2O_3/UV$) and photocatalysis ($O_2/TiO_2/UV$).

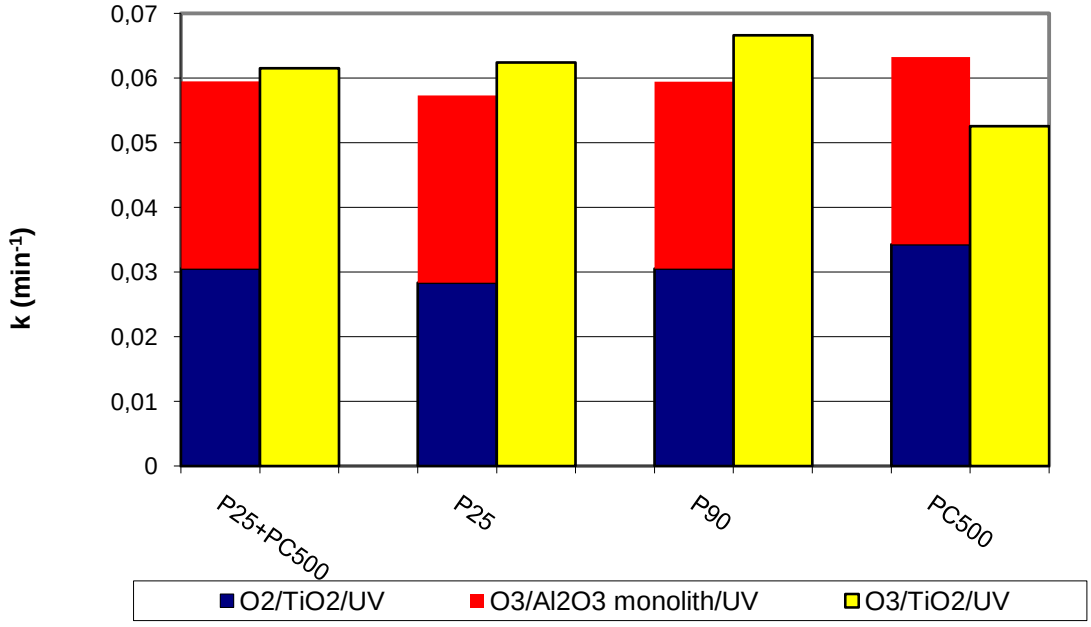

Figure 60. Comparison of initial degradation rates of PBIS photocatalytic ozonation ($O_3/TiO_2/UV$) to the sum of ozonation ($O_3/Al_2O_3/UV$) and photocatalysis ($O_2/TiO_2/UV$).

Synergistic effect of RB 19 mineralization is more obvious (**Figure 61**) and PH-OZ is in case of P25+PC500 even twice more efficient in comparison to the sum of PC and photolytic ozonation. The reasons for this fact are easy degradation of RB 19 decomposition products and their adsorption to TiO_2 surface, which is very important factor in PH-OZ (Section 0). On the other hand surfactants parent molecules and especially degradation products are more resistant, much less adsorbed and consequently decompose slower, which negatively influences the mineralization

step velocity (**Figure 62**). The reaction coefficients for PH-OZ mineralization achieved with photocatalysts are comparable for each pollutant separately. Small differences are mainly due to differences in monolith shape and geometrical surface area, irradiation distribution and other TiO_2 layers properties. This indicates, that the limit of degradation capability of this reactor is probably early achieved because of small surface in comparison to slurry reactors and consequently higher mass transfer limitations.

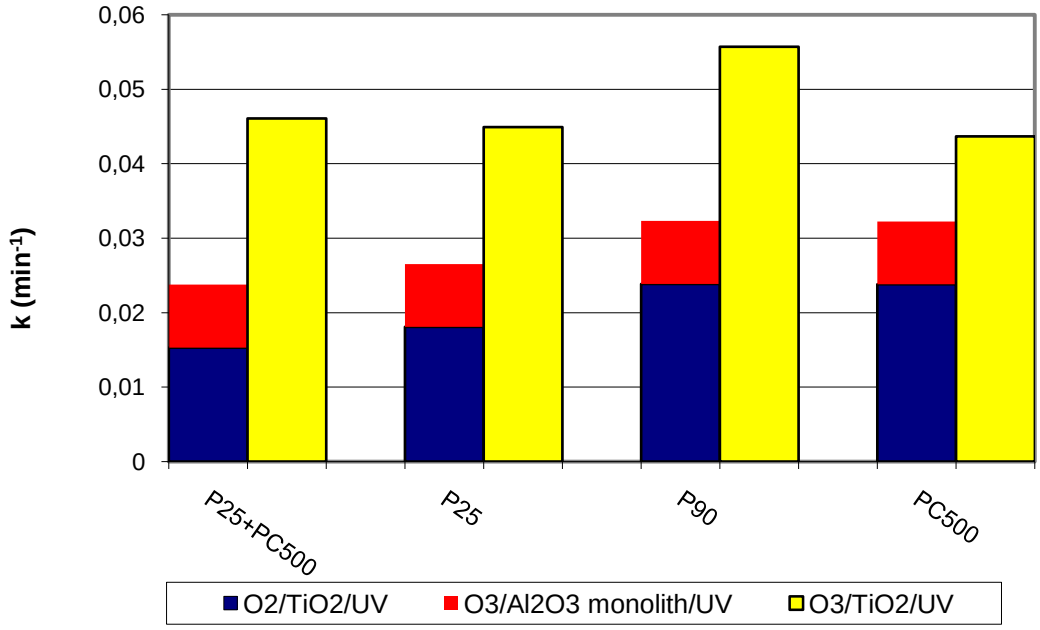

Figure 61. Comparison of initial degradation rates of TOC (RB 19) photocatalytic ozonation ($O_3/TiO_2/UV$) to the sum of ozonation ($O_3/Al_2O_3/UV$) and photocatalysis ($O_2/TiO_2/UV$).

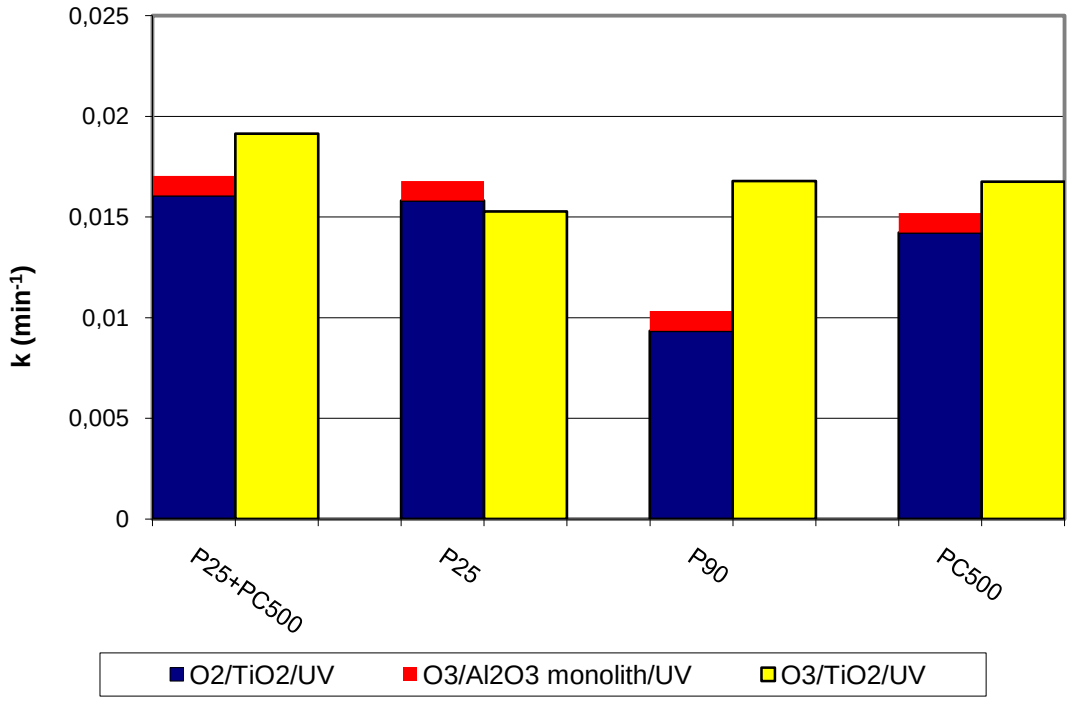

Figure 62. Comparison of initial degradation rates of TOC (LAS+PBIS) photocatalytic ozonation ($O_3/TiO_2/UV$) to the sum of ozonation ($O_3/Al_2O_3/UV$) and photocatalysis ($O_2/TiO_2/UV$).

One of the main tasks of present work was to clarify, if PH-OZ process is really worth to use in case of dye and surfactants mineralization. It is obvious that mineralization process is slower or at the best of the same velocity as primary molecule degradation and therefore it represents bottleneck of organics removal. PC mineralization coefficients of RB 19 are comparable or even higher to those of surfactants achieved with PH-OZ or PC process. From practical point of view, this means, that instead using ozone it would be better to increase photocatalyst geometrical surface to volume of treated water. This would at the end result in less complex, more environmentally and user friendly reactor system.

5.7.4 Simulated waste water

Simulated waste water was treated by photocatalysis or PH-OZ process using P90 as immobilized photocatalyst. P90 was selected because of good mechanical resistance and its cleaning performance in combination with ozone shown in previous experiments.

Experiment profile (**Figure 63**) is similar to those already presented (Section 5.7.2.3). The main distinctions are higher pH, which is due to different anions present in tap water commonly CO_3^{2-} or HCO_3^- and lower concentration of dissolved ozone, which is most probably due to its reaction with organic matter already present in water. Another fact that can be noticed is quite long phase of decreased ozone concentration, which is ascribed to high total amount of RB 19 and phenol that are less stable against ozone and are in this phase efficiently removed by ozonation and PH-OZ processes. Starting concentration of TOC in both experiments was in the range between 65 – 71 mg/L. This value includes 47 mg/L of TOC represented by model pollutants and 23 – 26 mg/L of background TOC already present in tap water. The lower starting TOC concentration (65 mg/L) in PH-OZ process is a consequence of purging the reactor system with ozone prior adding the pollutants solution. In this case some of background TOC was already removed just by ozonation.

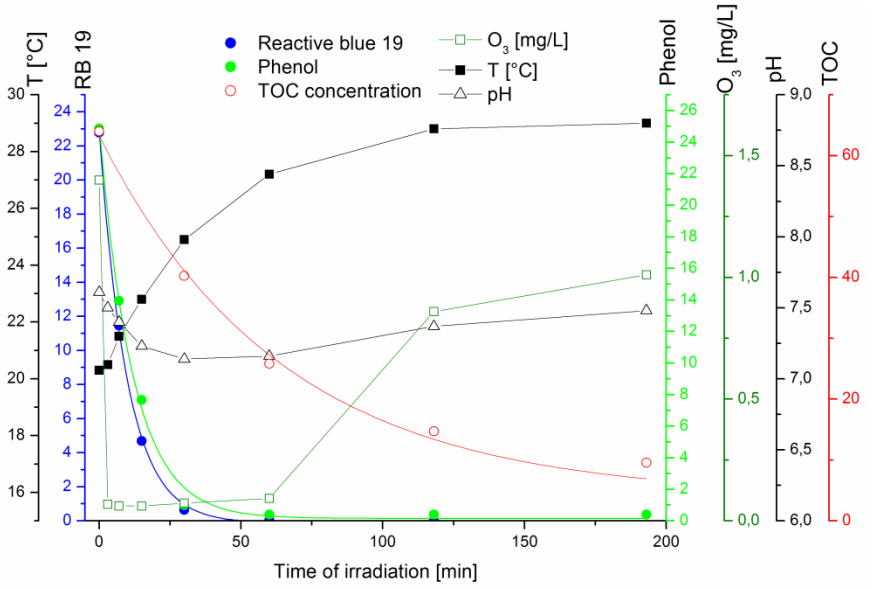

Figure 63. Experiment of photocatalytic ozonation (O_3/TiO_2/UVA) of pollutant mixture (RB19, LAS, PBIS and phenol) using P90 TiO_2 immobilized on Al_2O_3 monolith. The graph presents all variables monitored during the degradation experiments.

Removal rate constants (**Figure 64**) obtained by fitting a first-order degradation function show that when mixture of pollutants was treated, their removal constants are lower in comparison to those obtained in solutions polluted just by one organic compound. This was expected, since (I) pollutants compete for reactive species and sites on or near photocatalysts surface, (II) different chemical stability of model pollutants and (III) wide selection of radicals present react differently with each of four pollutants. Removal of LAS and PBIS was not followed since their main absorption peaks overlap with phenol and Reactive blue 19 in UV region.

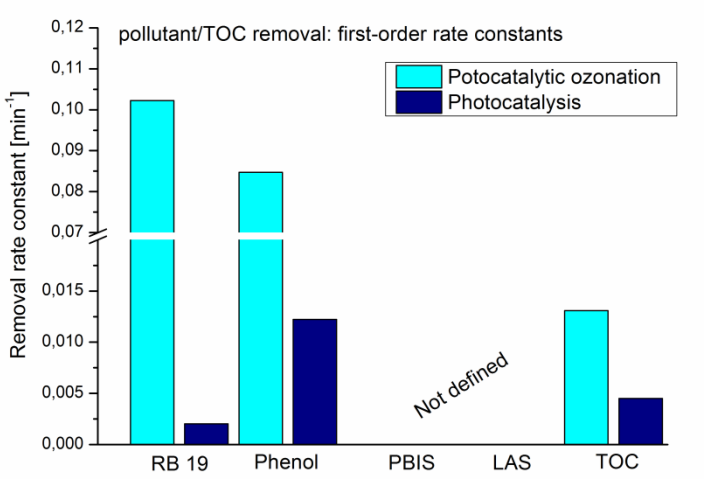

Figure 64. Removal rate constants of pollutants/TOC obtained in compact reactor using P90 as immobilized photocatalyst in processes of photocatalysis or photocatalytic ozonation treatment of simulated waste water.

However, determination of removal rate constants of individual pollutant was not the goal of this experiment and greater attention was given to TOC reduction. This was in case of PH-OZ process significant. Just in 2 h 77% of TOC was removed, including TOC already present in tap water. The initial rate constant was lower in comparison to those achieved in experiments with LAS+PBIS, but was just 25% lower despite high TOC loading. In other words, half life was 53 min in comparison to 41 min achieved in case of LAS+PBIS degradation using P90. LAS and PBIS are more persistent and therefore, despite lower total TOC in comparison to total phenol and RB19 TOC, removed slower. On the other hand, experiment conducted by photocatalytic process alone shows much slower TOC reduction, approx. 52% in comparison to LAS+PBIS and points out the main weakness of photocatalysis, sensitivity to higher loads of pollutants. This result confirms that PH-OZ could be actually efficiently used for treatment of household grey waste water.

5.8 Conclusion

From the research of LAS+PBIS, phenol and RB 19 degradation in two reactors it can be concluded, that RB 19 and phenol are easily degradable due to several reasons: low stability in presence of ozone (RB 19), small and simpler molecule (phenol) and adsorption of their degradation products to TiO_2 surface. On the other hand LAS and PBIS are more resistant, so that PH-OZ process is actually not much more efficient in comparison to PC. The series of experiments in compact reactor was conducted at neutral-acidic pH, since it was reported by others and shown in prototype reactor, that alkaline pH negatively influences both PH-OZ and PC. With the regard to prototype reactor, photocatalyst geometrical surface to volume of treated solution was increased by 37 times, from 1.2 cm^2/mL to 44 cm^2/mL, which is big improvement. Nevertheless, the increase in photocatalytic efficiency was not linear. In case of PH-OZ this increase was from 9 to 11 times, while PC showed 10 to 15 times higher mineralization efficiency in comparison to prototype. These lower factors are consequence of lower irradiation intensity due to weaker UV lamps and non-homogeneously illuminated photocatalyst on nontransparent Al_2O_3 substrate. The reaction coefficients for PH-OZ mineralization of each pollutant achieved with photocatalysts are comparable. Small differences are mainly because of negligible impact of ozone decomposition ability of photocatalysts, differences in monolith shape and relatively small geometrical surface area in comparison to slurry reactors, irradiation distribution and other TiO_2 layers properties. Synergistic effect is much more expressed in mineralization reactions, but in case of LAS+PBIS this is still low. Actually is P25, when used in combination with UV and O_2, even more efficient. From practical point of view this means, that the appropriate AOP (PH-OZ or photocatalysis) should be chosen with respect to the most resistant pollutant. From the other side is PH-OZ much more flexible and efficient when the changes of pH occur and when the dyes should be removed, since they can block UV irradiation. Additionally is this advanced oxidation process very effective in case of "simulated waste water", which results in quite fast mineralization of moderately polluted water. All mentioned is in favor to PH-OZ process and shows its true

applicability. TOC half lives in compact reactor are despite higher concentrations of pollutants relatively short, 13 – 43 min and in case of mixed pollutants 53 min. These are very promising results, since the reactor was designed to treat small effluent volumes. With increase of reactor size (4 – 6x) and irradiation intensity (2 – 3x) the cleaning capacity would be significantly improved.

6 Conclusions of the thesis

The main findings of the thesis can be summarized in set of areas concerning: (I) photocatalytic ozonation (PH-OZ) process, (II) immobilization of photocatalyst to different substrates, (III) reactor development and (IV) cleaning performance of PH-OZ conducted in compact reactor.

Photocatalytic ozonation process (PH-OZ) carried out in acidic environment using slurry reactor is (I) very efficient despite low UVA illumination intensity, (II) the experiments showed, that even in the case of PH-OZ process, the reactions near the TiO_2 surface are much faster than those in the solution bulk, since the $^{\bullet}OH$ radicals are highly reactive and consequently short lived species with low range of action (≤500 μm), so they consequently react with the nearest organic molecules, (III) the synergistic effect of PH-OZ process is much more emphasized in the solution bulk, which implies that ozone reacts just with outer surface of TiO_2 agglomerates, producing less reactive and long-lived radicals, which are transferred into solution bulk. After studying photocatalytic and PH-OZ processes in slurry reactor, it turned out that surface area (BET) of photocatalyst is much more important when degradation of adsorbed organic molecules is taking place in contrast to the species which are not well adsorbed.

Low-temperature sol-suspension procedure was successfully used to efficiently immobilize TiO_2 nanopowders to glass slides and foamed Al_2O_3 monoliths. Photocatalysts (P90, P25) that are easily dispersed to particle-like size or small agglomerates formed mechanically stable layers, which were used for the purpose of polluted water treatment.

The main concept of compact reactor was realized successfully: (I) by immobilizing photocatalysts to foamed Al_2O_3 monolith high geometric surface area of photocatalyst was achieved, without significantly influencing on the pressure drop of the system. (II) The problem of nontransparent foamed ceramic monolith was alleviated by placing the lamps in the center of monolith. (III) The cleaning capacity of developed compact reactor can be easily enhanced by increasing its dimensions thanks to its simple concept.

The activity-irradiance curves obtained by photocatalytic degradation of solid organic coating of terepthalic acid suggest that, compared to the rest of tested catalysts, P90 probably presents an improved electron-hole separation, which allows the whole process of photocatalysis to be more efficient at higher UVA irradiation intensities. However, it turned out that this effect was not observed for photocatalysis conducted in aqueous environment. From the research of aqueous LAS + PBIS, phenol and RB 19 degradation it can be concluded, that RB 19 and phenol are more easily degradable in presence of ozone. On the other hand LAS and PBIS are more resistant, so that PH-OZ process is actually not much more efficient in comparison to photocatalysis alone. It has been shown that synergistic effect of PH-OZ process is much more expressed in mineralization reactions, but in case of LAS+PBIS this was still low. From the other side, PH-OZ is much more flexible when the changes of pH occur, which gives better stability to this kind of AOP. Half lives of mineralization processes in compact reactor are, despite higher concentrations of pollutants, relatively short, 13 – 43 min. These are very promising results, since the compact reactor was designed to treat small effluent volumes. PH-OZ treatment of simulated waste water with moderate loading (65 mg/L) of organic pollutants (RB19, phenol, LAS and PBIS) in compact reactor showed that this process represents a realistic option for treatment of grey waste waters.

7 References

Agrios AG, Pichat P (2006) Recombination rate of photogenerated charges versus surface area: Opposing effects of TiO_2 sintering temperature on photocatalytic removal of phenol, anisole, and pyridine in water. Journal of Photochemistry and Photobiology A: Chemistry 180:130–135.

Agustina TE, Ang HM, Vareek VK (2005) A review of synergistic effect of photocatalysis and ozonation on waste water treatment. Journal of Photochemistry and Photobiology C: Photochemistry Reviews 6:264–273.

Ahmed S, Rasul MG, Brown R, Hashib MA (2011) Influence of parameters on the heterogeneous photocatalytic degradation of pesticides and phenolic contaminants in waste water: A short review. Journal of Environmental Management 92:311–330.

Alberici RM, Jardim WF (1994) Photocatalytic degradation of phenol and chlorinated phenols using Ag-TiO_2 in a slurry reactor. Water Research 28:1845–1849.

Almquist CB, Biswas P (2002) Role of Synthesis Method and Particle Size of Nanostructured TiO_2 on Its Photoactivity. Journal of Catalysis 212:145–156.

Andreozzi R, Caprio V, Insola A, et al. (2000) Photocatalytic oxidation of 4-nitrophenol in aqueous TiO_2 slurries: an experimental validation of literature kinetic models. Journal of Chemical Technology & Biotechnology 75:131–136.

Andreozzi R, Caprio V, Insola A, Marotta R (1999) Advanced oxidation processes (AOP) for water purification and recovery. Catalysis Today 53:51–59.

Anpo M, Shima T, Kodama S, Kubokawa Y (1987) Photocatalytic hydrogenation of propyne with water on small-particle titania: size quantization effects and reaction intermediates. The Journal of Physical Chemistry 91:4305–4310.

Armelao L, Barreca D, Bottaro G, et al. (2007) Photocatalytic and antibacterial activity of TiO_2 and Au/TiO_2 nanosystems. Nanotechnology 18:375709.

AS/NZS 2040.1:2005 AZ standard (2005) Performance of household electrical appliances-Clothes washing machine: Part 1-Methods for measuring performance, energy and water consumption. Australian/New Zealand standard AS/NZS 2040.1:2005

Banic N, Abramovic B, Krstic J, et al. (2011) Photodegradation of thiacloprid using Fe/TiO_2 as a heterogeneous photo-Fenton catalyst. Applied Catalysis B: Environmental 107:363–371.

Bekermann D, Gasparotto A, Barreca D, et al. (2012) Epitaxial-like Growth of Co_3O_4/ZnO Quasi-1D Nanocomposites. Crystal Growth & Design 12:5118–5124.

Beltran FJ, Aguinaco A, Garcia-Araya JF (2010) Kinetic modelling of TOC removal in the photocatalytic ozonation of diclofenac aqueous solutions. Applied Catalysis B: Environmental 100:289–298.

Beltran FJ, Aguinaco A, Garcia-Araya JF (2009) Mechanism and kinetics of sulfamethoxazole photocatalytic ozonation in water. Water Research 43:1359–1369.

Beltran FJ, Aguinaco A, Garcia-Araya JF, Oropesa A (2008) Ozone and photocatalytic processes to remove the antibiotic sulfamethoxazole from water. Water Research 42:3799–3808.

Beltran FJ, Garca-Araya JF, Alvarez PM (2000) Sodium Dodecylbenzenesulfonate Removal from Water and Waste water. 1. Kinetics of Decomposition by Ozonation. Industrial & Engineering Chemistry Research 39:2214–2220.

Beltran FJ, Rivas FJ, Gimeno O (2005) Comparison between photocatalytic ozonation and other oxidation processes for the removal of phenols from water. Journal of Chemical Technology & Biotechnology 80:973–984.

Beltran FJ, Rivas FJ, Montero-de-Espinosa R (2002) Catalytic ozonation of oxalic acid in an aqueous TiO_2 slurry reactor. Applied Catalysis B: Environmental 39:221–231.

Benotti MJ, Stanford BD, Wert EC, Snyder SA (2009) Evaluation of a photocatalytic reactor membrane pilot system for the removal of pharmaceuticals and endocrine disrupting compounds from water. Water Research 43:1513–1522.

Bradley B, Daigger G, Rubin R, Tchobanoglous G (2002) Evaluation of onsite waste water treatment technologies using sustainable development criteria. Clean Technologies and Environmental Policy 4:87–99.

Brosillon S, Lhomme L, Vallet C, et al. (2008) Gas phase photocatalysis and liquid phase photocatalysis: Interdependence and influence of substrate concentration and photon flow on degradation reaction kinetics. Applied Catalysis B: Environmental 78:232–241.

Brunauer S, Emmett PH, Teller E (1938) Adsorption of Gases in Multimolecular Layers. Journal of the American Chemical Society 60:309–319.

Busca G, Berardinelli S, Resini C, Arrighi L (2008) Technologies for the removal of phenol from fluid streams: A short review of recent developments. Journal of Hazardous Materials 160:265–288.

Butters BE, Powell AL (1995) Method and system for photocatalytic decontamination. US Patent No. 5.462.674

Byrne JA, Eggins BR, Brown NMD, et al. (1998) Immobilisation of TiO_2 powder for the treatment of polluted water. Applied Catalysis B: Environmental 17:25–36.

Camacho-Munoz D, Martin J, Santos JL, et al. (2014) Occurrence of surfactants in waste water: Hourly and seasonal variations in urban and industrial waste waters from Seville (Southern Spain). Science of The Total Environment 468 - 469:977–984.

Cerna M, Vesey M, Dzik P, et al. (2013) Fabrication, characterization and photocatalytic activity of TiO_2 layers prepared by inkjet printing of stabilized nanocrystalline suspensions. Applied Catalysis B: Environmental 138 - 139:84–94.

Cernigoj U (2007) Photodegradation of organic pollutants in aqueous solutions catalyzed by immobilized titanium dioxide: novel routes towards higher efficiency. Dissertation, University of Nova Gorica

Cernigoj U, Kete M, Štangar UL (2010a) Development of a fluorescence-based method for evaluation of self-cleaning properties of photocatalytic layers. Catalysis Today 151:46–52.

Cernigoj U, Štangar UL, Jirkovsky J (2010b) Effect of dissolved ozone or ferric ions on photodegradation of thiacloprid in presence of different TiO_2 catalysts. Journal of Hazardous Materials 177:399–406.

Cernigoj U, Štangar UL, Trebše P (2007a) Degradation of neonicotinoid insecticides by different advanced oxidation processes and studying the effect of ozone on TiO_2 photocatalysis. Applied Catalysis B: Environmental 75:229–238.

Cernigoj U, Štangar UL, Trebše P (2007b) Evaluation of a novel Carberry type photoreactor for the degradation of organic pollutants in water. Journal of Photochemistry and Photobiology A: Chemistry 188:169–176.

Chen D, Ray AK (1999) Photocatalytic kinetics of phenol and its derivatives over UV irradiated TiO_2. Applied Catalysis B: Environmental 23:143–157.

Chen D, Ray AK (1998) Photodegradation kinetics of 4-nitrophenol in TiO_2 suspension. Water Research 32:3223–3234.

Chen TY, Kao CM, Hong A, et al. (2009) Application of ozone on the decolorization of reactive dyes - Orange-13 and Blue-19. Desalination 249:1238–1242.

Chen Y, Dionysiou DD (2006) TiO_2 photocatalytic films on stainless steel: The role of Degussa P-25 in modified sol-gel methods. Applied Catalysis B: Environmental 62:255–264.

Chen Y, Dionysiou DD (2008) Bimodal mesoporous TiO_2-P25 composite thick films with high photocatalytic activity and improved structural integrity. Applied Catalysis B: Environmental 80:147–155.

Chen Y, Xie Y, Yang J, et al. (2014) Reaction mechanism and metal ion transformation in photocatalytic ozonation of phenol and oxalic acid with Ag+/TiO_2. Journal of Environmental Sciences 26:662–672.

Chong MN, Jin B, Chow CWK, Saint C (2010) Recent developments in photocatalytic water treatment technology: A review. Water Research 44:2997–3027.

Christova-Boal D, Eden RE, McFarlane S (1996) An investigation into greywater reuse for urban residential properties. Desalination 106:391–397.

Coleman HM, Marquis CP, Scott JA, et al. (2005) Bactericidal effects of titanium dioxide-based photocatalysts. Chemical Engineering Journal 113:55–63.

Colombo A, Cappelletti G, Ardizzone S, et al. (2012) Bisphenol A endocrine disruptor complete degradation using TiO_2 photocatalysis with ozone. Environmental Chemistry Letters 10:55–60.

Czili H, Horvath A (2009) Photodegradation of chloroacetic acids over bare and silver-deposited TiO_2: Identification of species attacking model compounds, a mechanistic approach. Applied Catalysis B: Environmental 89:342–348.

Doll TE, Frimmel FH (2005) Cross-flow microfiltration with periodical back-washing for photocatalytic degradation of pharmaceutical and diagnostic residues-evaluation of the long-term stability of the photocatalytic activity of TiO_2. Water Research 39:847–854.

Dominguez JR, Beltran J, Rodriguez O (2005) Vis and UV photocatalytic detoxification methods using TiO_2, TiO_2/H_2O_2, TiO_2/O_3, $TiO_2/S_2O_8^{2-}$, O_3, H_2O_2, $S_2O_8^{2-}$, Fe^{3+}/H_2O_2 and $Fe^{3+}/H_2O_2/C_2O_4^{2-}$ for dyes treatment. Catalysis Today 101:389–395.

Dostanic J, Grbic B, Radic N, et al. (2013) Preparation and photocatalyic properties of TiO_2-P25 film prepared by spray pyrolysis method. Applied Surface Science 274:321–327.

Doucet N, Bocquillon F, Zahraa O, Bouchy M (2006) Kinetics of photocatalytic {VOCs} abatement in a standardized reactor. Chemosphere 65:1188–1196.

Duirk SE, Valentine RL (2006) Modeling dichloroacetic acid formation from the reaction of monochloramine with natural organic matter. Water Research 40:2667–2674.

Al-Ekabi H, Serpone N, Pelizzeti E, et al. (1989) Kinetic studies in heterogeneous photocatalysis. 2. TiO_2 mediated degradation of 4-chlorophenol alone and in a three component mixture of 4-chlorophenol, 2-4-dichlorophenol and 2-4-5-trichlorophenol in air equilibrated aqueous media. Langmuir 5:250–255.

Enriquez R, Agrios AG, Pichat P (2007) Probing multiple effects of TiO_2 sintering temperature on photocatalytic activity in water by use of a series of organic pollutant molecules. Catalysis Today 120:196–202.

Enriquez R, Beaugiraud B, Pichat P (2004) Mechanistic implications of the effect of TiO_2 accessibility in TiO_2-SiO_2 coatings upon chlorinated organics photocatalytic removal in water. Water Science and Technology 49 (4):147–152.

Eriksson E, Auffarth K, Henze M, Ledin A (2002) Characteristics of grey waste water. Urban Water 4:85–104.

Esplugas S, Gimenez J, Contreras S, et al. (2002) Comparison of different advanced oxidation processes for phenol degradation . Water Research 36:1034–1042.

Etchepare R, Hoek JP van der (2015) Health risk assessment of organic micropollutants in greywater for potable reuse. Water Research 72 (1):86–98

European Commission Mediterranean waste water reuse working group (2007) Mediterranean Waste water Reuse Report, http://ec.europa.eu/environment/water/blueprint/pdf/med_final_report.pdf.

Fekete L, Kusova K, Petrak V, Kratochvilova I (2012) AFM topographies of densely packed nanoparticles: a quick way to determine the lateral size distribution by autocorrelation function analysis. Journal of Nanoparticle Research 14:1–10.

Fernandez-Ibanez P, Blanco J, Malato S, Nieves FJ d. las (2003) Application of the colloidal stability of TiO_2 particles for recovery and reuse in solar photocatalysis. Water Research 37:3180–3188.

Fitzsimmons PN, Hoffman AD, Lien GJ, et al. (2009) Kinetics and effects of dichloroacetic acid in rainbow trout. Aquatic Toxicology 94:186–194.

Fogler HS (1999) Elements of Chemical Reaction Engineering: Chapter 10: Catalysis and Catalytic Reactors. Prentice-Hall PTR Inc. 581–685.

Fountoulakis MS, Terzakis S, Kalogerakis N, Manios T (2009) Removal of polycyclic aromatic hydrocarbons and linear alkylbenzene sulfonates from domestic waste water in pilot constructed wetlands and a gravel filter. Ecological Engineering 35:1702–1709.

Friedler E (2004) Quality of Individual Domestic Greywater Streams and its Implication for On-Site Treatment and Reuse Possibilities. Environmental Technology 25:997–1008.

Friedler E, Kovalio R, Galil N (2005) On-site greywater treatment and reuse in multi-storey buildings. Water Science & Technology 51:187–194.

Fujishima A, Zhang X, Tryk DA (2008) TiO_2 photocatalysis and related surface phenomena. Surface Science Reports 63:515–582.

Gaya UI, Abdullah AH (2008) Heterogeneous photocatalytic degradation of organic contaminants over titanium dioxide: A review of fundamentals, progress and problems. Journal of Photochemistry and Photobiology C: Photochemistry Reviews 9:1–12.

Gerven TV, Mul G, Moulijn J, Stankiewicz A (2007) A review of intensification of photocatalytic processes. Chemical Engineering and Processing: Process Intensification 46:781–789.

Gimeno O, Rivas FJ, Beltran FJ, Carbajo M (2007) Photocatalytic Ozonation of Winery Waste waters. Journal of Agricultural and Food Chemistry 55:9944–9950.

Glaze WH, Kang J-W, Chapin DH (1987) The Chemistry of Water Treatment Processes Involving Ozone, Hydrogen Peroxide and Ultraviolet Radiation. Ozone: Science & Engineering 9:335–352.

Guimaraes JR, Maniero MG, Araujo RN de (2012) A comparative study on the degradation of RB-19 dye in an aqueous medium by advanced oxidation processes. Journal of Environmental Management 110:33–39.

Gumy D, Giraldo SA, Rengifo J, Pulgarin C (2008) Effect of suspended TiO_2 physicochemical characteristics on benzene derivatives photocatalytic degradation. Applied Catalysis B: Environmental 78:19–29.

Habibi MH, Hassanzadeh A, Mahdavi S (2005) The effect of operational parameters on the photocatalytic degradation of three textile azo dyes in aqueous TiO_2 suspensions . Journal of Photochemistry and Photobiology A: Chemistry 172:89–96.

Hadjltaief HB, Galvez ME, Zina MB, Costa PD (2014) TiO_2/clay as a heterogeneous catalyst in photocatalytic/photochemical oxidation of anionic reactive blue 19. Arabian Journal of Chemistry. In Press–Corected Proof. doi:10.1016/j.arabjc.2014.11.006

Hanson ML, Sibley PK, Mabury SA, et al. (2003) Field level evaluation and risk assessment of the toxicity of dichloroacetic acid to the aquatic macrophytes Lemna gibba, Myriophyllum spicatum, and Myriophyllum sibiricum. Ecotoxicology and Environmental Safety 55:46–63.

Hathway T, Jenks WS (2008) Effects of sintering of TiO_2 particles on the mechanisms of photocatalytic degradation of organic molecules in water. Journal of Photochemistry and Photobiology A: Chemistry 200:216–224.

He Z, Lin L, Song S, et al. (2008) Mineralization of C.I. Reactive Blue 19 by ozonation combined with sonolysis: Performance optimization and degradation mechanism. Separation and Purification Technology 62:376–381.

Hernandez-Alonso MD, Coronado JM, Maira AJ, et al. (2002) Ozone enhanced activity of aqueous titanium dioxide suspensions for photocatalytic oxidation of free cyanide ions. Applied Catalysis B: Environmental 39:257–267.

Hernandez-Leal L, Temmink H, Zeeman G, Buisman CJN (2011) Removal of micropollutants from aerobically treated grey water via ozone and activated carbon. Water Research 45:2887–2896.

Herrmann J-M (1999) Heterogeneous photocatalysis: fundamentals and applications to the removal of various types of aqueous pollutants. Catalysis Today 53:115–129.

Herrmann J-M (2010) Photocatalysis fundamentals revisited to avoid several misconceptions. Applied Catalysis B: Environmental 99:461–468.

Hofstadler K, Bauer R, Novalic S, Heisler G (1994) New Reactor Design for Photocatalytic Waste water Treatment with TiO_2 Immobilized on Fused-Silica Glass Fibers: Photomineralization of 4-Chlorophenol. Environmental Science & Technology 28:670–674.

Hoigne J (1998) Chemistry of aqueous ozone and transformation of pollutants by ozonation and advanced oxidation processes. In: The handbook of environmental chemistry 5, Part C. 84–141.

Horn TB, Zerwes FV, Kist LT, Machado EL (2014) Constructed wetland and photocatalytic ozonation for university sewage treatment. Ecological Engineering 63:134–141.

Imamura S, Ikebata M, Ito T, Ogita T (1991) Decomposition of ozone on a silver catalyst. Industrial & Engineering Chemistry Research 30:217–221.

Imoberdorf GE, Vella G, Sclafani A, et al. (2010) Radiation model of a TiO_2-coated, quartz wool, packed-bed photocatalytic reactor. AIChE Journal 56:1030–1044.

Jeschke P, Moriya K, Lantzsch R, al. et (2001) Thiacloprid (Bay YRC 2894)-A new member of the chloronicotinyl insecticide (CNI) family. Pflanzenschutz Nachrichten Bayer 54:147–160.

Jing Y, Li L, Zhang Q, et al. (2011) Photocatalytic ozonation of dimethyl phthalate with TiO_2 prepared by a hydrothermal method. Journal of Hazardous Materials 189:40–47.

Kesmez O, Camurlu HE, Burunkaya E, Arpac E (2009) Sol-gel preparation and characterization of anti-reflective and self-cleaning SiO_2-TiO_2 double-layer nanometric films. Solar Energy Materials and Solar Cells 93:1833–1839.

Kete M, Pavlica E, Fresno F, et al. (2014) Highly active photocatalytic coatings prepared by a low-temperature method. Environmental Science and Pollution Research 21:11238–11249.

Kim J, Kim J, Lee M (2010) Laser-induced enhancement of the surface hardness of nanoparticulate TiO_2 self-cleaning layer. Surface and Coatings Technology 205:372–376.

Klug HP, Alexander LE (1974) X-ray diffraction procedures. 2nd Ed. John Wiley & Sons Inc. p. 687.

Kopf P, Gilbert E, Eberle SH (2000) TiO_2 photocatalytic oxidation of monochloroacetic acid and pyridine: influence of ozone. Journal of Photochemistry and Photobiology A: Chemistry 136:163–168.

Krohn J (2001) Behaviour of thiacloprid in the environment. Pflanzenschutz Nachrichten Bayer 54:281–290.

Krysa J, Keppert M, Waldner G, Jirkovsky J (2005) Immobilized particulate TiO_2 photocatalysts for degradation of organic pollutants: Effect of layer thickness. Electrochimica Acta 50:5255–5260.

Legrini O, Oliveros E, Braun AM (1993) Photochemical processes for water treatment. Chemical Reviews 93:671–698.

Lin H, Huang CP, Li W, et al. (2006) Size dependency of nanocrystalline TiO_2 on its optical property and photocatalytic reactivity exemplified by 2-chlorophenol. Applied Catalysis B: Environmental 68:1–11.

Liu J, Wang R, Yang J (2005) Metabolism and Driving Forces of Chinese Urban Household Consumption. Population and Environment 26:325–341.

Liu Y, Hua L, Li S (2010) Photocatalytic degradation of Reactive Brilliant Blue KN-R by TiO_2/UV process. Desalination 258:48–53.

Lopez L, Daoud WA, Dutta D, et al. (2013) Effect of substrate on surface morphology and photocatalysis of large-scale TiO_2 films. Applied Surface Science 265:162–168.

Lu J, Zhang T, Ma J, Chen Z (2009) Evaluation of disinfection byproducts formation during chlorination and chloramination of dissolved natural organic matter fractions isolated from a filtered river water. Journal of Hazardous Materials 162:140–145.

Lu M-C, Roam G-D, Chen J-N, Huang C-P (1996) Adsorption characteristics of dichlorvos onto hydrous titanium dioxide surface . Water Research 30:1670–1676.

Lucas MS, Peres JA, Lan BY, Puma GL (2009) Ozonation kinetics of winery waste water in a pilot-scale bubble column reactor. Water Research 43:1523–1532.

Mainali B, Ngo HH, Guo W, et al. (2011) Feasibility assessment of recycled water use for washing machines in Australia through SWOT analysis. Resources, Conservation and Recycling 56:87–91.

Maira AJ, Yeung KL, Lee CY, et al. (2000) Size Effects in Gas-Phase Photo-oxidation of Trichloroethylene Using Nanometer-Sized TiO_2 Catalysts. Journal of Catalysis 192:185–196.

Malato S, Fernandez-Ibanez P, Maldonado MI, et al. (2009) Decontamination and disinfection of water by solar photocatalysis: Recent overview and trends. Catalysis Today 147:1–59.

Mallak M, Bockmeyer M, Lobmann P (2007) Liquid phase deposition of TiO_2 on glass: Systematic comparison to films prepared by sol-gel processing. Thin Solid Films 515:8072–8077.

Manousaki E, Psillakis E, Kalogerakis N, Mantzavinos D (2004) Degradation of sodium dodecylbenzene sulfonate in water by ultrasonic irradiation. Water Research 38:3751–3759.

Marques SM, Tavares CJ, Oliveira LF, Oliveira-Campos AMF (2010) Photocatalytic degradation of C.I. Reactive Blue 19 with nitrogen-doped TiO_2 catalysts thin films under UV/visible light. Journal of Molecular Structure 983:147–152.

Matos C, Sampaio A, Duarte AA, Bentes I (2011) Characterization of greywater by appliance: pattern of discharge along the day. IWRA

Mehrjouei M, Muller S, Moller D (2014) Decomposition kinetics of MTBE, ETBE and, TAEE in water and waste water using catalytic and photocatalytic ozonation. Journal of Molecular Catalysis A: Chemical 386:61–68.

Minero C, Vione D (2006) A quantitative evalution of the photocatalytic performance of TiO_2 slurries. Applied Catalysis B: Environmental 67:257–269.

Miranda-Garcia N, Maldonado MI, Coronado JM, Malato S (2010) Degradation study of 15 emerging contaminants at low concentration by immobilized TiO_2 in a pilot plant. Catalysis Today 151:107–113.

Miranda-Garcia N, Suarez S, Sanchez B, et al. (2011) Photocatalytic degradation of emerging contaminants in municipal waste water treatment plant effluents using immobilized TiO_2 in a solar pilot plant. Applied Catalysis B: Environmental 103:294–301.

Molinari R, Pirillo F, Falco M, et al. (2004) Photocatalytic degradation of dyes by using a membrane reactor. Chemical Engineering and Processing: Process Intensification 43:1103–1114.

Mukherjee PS, Ray AK (1999) Major Challenges in the Design of a Large-Scale Photocatalytic Reactor for Water Treatment. Chemical Engineering & Technology 22:253–260.

Murov S.L. HGL Carmichael I. (1993) Handbook of Photochemistry,second ed. Marcel Dekker Inc., New York, 302–304.

Murphy AB (2007) Band-gap determination from diffuse reflectance measurements of semiconductor films, and application to photoelectrochemical water-splitting . Solar Energy Materials and Solar Cells 91:1326–1337.

Nagaveni K, Sivalingam G, Hegde M., Madras G (2004a) Solar photocatalytic degradation of dyes: high activity of combustion synthesized nano TiO_2. Applied Catalysis B: Environmental 48:83–93.

Nagaveni K, Sivalingam G, Hegde MS, Madras G (2004b) Photocatalytic Degradation of Organic Compounds over Combustion-Synthesized Nano-TiO_2. Environmental Science & Technology 38:1600–1604.

Nair RG, Paul S, Samdarshi SK (2011) High UV/visible light activity of mixed phase titania: A generic mechanism. Solar Energy Materials and Solar Cells 95:1901–1907.

Nasuhoglu D, Rodayan A, Berk D, Yargeau V (2012) Removal of the antibiotic levofloxacin (LEVO) in water by ozonation and TiO_2 photocatalysis. Chemical Engineering Journal 189-190:41–48.

Nawi MA, Zain SM (2012) Enhancing the surface properties of the immobilized Degussa P-25 TiO_2 for the efficient photocatalytic removal of methylene blue from aqueous solution. Applied Surface Science 258:6148–6157.

Nelson RJ, Flakker CL, Muggli DS (2007) Photocatalytic oxidation of methanol using titania-based fluidized beds. Applied Catalysis B: Environmental 69:189–195.

Neti NR, Parmar GR, Bakardjieva S, Subrt J (2010) Thick film titania on glass supports for vapour phase photocatalytic degradation of toluene, acetone, and ethanol. Chemical Engineering Journal 163:219–229.

Neyens E, Baeyens J (2003) A review of classic Fenton's peroxidation as an advanced oxidation technique. Journal of Hazardous Materials 98:33–50.

Novotna P, Zita J, Krysa J, et al. (2008) Two-component transparent TiO_2/SiO_2 and TiO_2/PDMS films as efficient photocatalysts for environmental cleaning. Applied Catalysis B: Environmental 79:179–185.

Obana H, Okihashi M, Akutsu K, et al. (2003) Determination of Neonicotinoid Pesticide Residues in Vegetables and Fruits with Solid Phase Extraction and Liquid Chromatography Mass Spectrometry. Journal of Agricultural and Food Chemistry 51:2501–2505.

Ochuma IJ, Osibo OO, Fishwick RP, et al. (2007) Three-phase photocatalysis using suspended titania and titania supported on a reticulated foam monolith for water purification. Catalysis Today 128:100–107.

Ohtani B (2010) Photocatalysis A to Z - What we know and what we do not know in a scientific sense. Journal of Photochemistry and Photobiology C: Photochemistry Reviews 11:157–178.

Ohtani B (2008) Preparing Articles on Photocatalysis - Beyond the Illusions, Misconceptions, and Speculation. Chemistry Letters 37:216–229.

Ohtani B, Zhang S-W, Nishimoto S, Kagiya T (1992) Catalytic and photocatalytic decomposition of ozone at room temperature over titanium(IV) oxide. J Chem Soc, Faraday Trans 88:1049–1053.

Oppenlander T (2007) Photochemical Purification of Water and Air: Advanced Oxidation Processes (AOPs): Principles, Reaction Mechanisms, Reactor Concepts. Photochemical Purification of Water and Air. Wiley-VCH Verlag GmbH & Co. KGaA, pp 5–17

Oyama T, Otsu T, Hidano Y, et al. (2011) Enhanced remediation of simulated waste waters contaminated with 2-chlorophenol and other aquatic pollutants by TiO_2-photoassisted ozonation in a sunlight-driven pilot-plant scale photoreactor. Solar Energy 85:938–944.

Padmanabhan PVA, Sreekumar KP, Thiyagarajan TK, et al. (2006) Nano-crystalline titanium dioxide formed by reactive plasma synthesis. Vacuum 80:1252–1255.

Panda KK, Mathews AP (2014) Ozone oxidation kinetics of Reactive Blue 19 anthraquinone dye in a tubular in situ ozone generator and reactor: Modeling and sensitivity analyses. Chemical Engineering Journal 255:553–567.

Paola AD, Bellardita M, Palmisano L, et al. (2014) Influence of crystallinity and OH surface density on the photocatalytic activity of TiO_2 powders. Journal of Photochemistry and Photobiology A: Chemistry 273:59–67.

Peill NJ, Hoffmann MR (1998) Mathematical Model of a Photocatalytic Fiber-Optic Cable Reactor for Heterogeneous Photocatalysis. Environmental Science & Technology 32:398–404.

Pelaez M, Nolan NT, Pillai SC, et al. (2012) A review on the visible light active titanium dioxide photocatalysts for environmental applications. Applied Catalysis B: Environmental 125:331–349.

Peng D, Joana C, Jacob MA, Guido M (2008) A novel photocatalytic monolith reactor for multiphase heterogeneous photocatalysis. Applied Catalysis A: General 334:119–128.

Pera-Titus M, Garcia-Molina V, Banos MA, et al. (2004) Degradation of chlorophenols by means of advanced oxidation processes: a general review. Applied Catalysis B: Environmental 47:219–256.

Petrenko VI, Avdeev MV, Garamus VM, et al. (2010) Micelle formation in aqueous solutions of dodecylbenzene sulfonic acid studied by small-angle neutron scattering. Colloids and Surfaces A: Physicochemical and Engineering Aspects 369:160–164.

Pichat P, Cermenati L, Albini A, et al. (2000) Degradation processes of organic compounds over UV-irradiated TiO_2 - Effect of ozone. Research on Chemical Intermediates 26:161–170.

Plesch G, Gorbar M, Vogt UF, et al. (2009) Reticulated macroporous ceramic foam supported TiO_2 for photocatalytic applications. Materials Letters 63:461–463.

Plesch G, Vargova M, Vogt UF, et al. (2012) Zr doped anatase supported reticulated ceramic foams for photocatalytic water purification. Materials Research Bulletin 47:1680–1686.

Qiu W, Zheng Y (2007) A comprehensive assessment of supported titania photocatalysts in a fluidized bed photoreactor: Photocatalytic activity and adherence stability. Applied Catalysis B: Environmental 71:151–162.

Radcliffe JC (2006) Future directions for water recycling in Australia. Desalination 187:77–87.

Raupp GB, Alexiadis A, Hossain MM, Changrani R (2001) First-principles modeling, scaling laws and design of structured photocatalytic oxidation reactors for air purification. Catalysis Today 69:41–49.

Ray AK (2009) Photocatalytic Reactor Configurations for Water Purification: Experimentation and Modeling. In: Lasa HI de, Rosales BS (eds) Advances in Chemical Engineering Photocatalytic Technologies. Academic Press, pp 145–184

Ray AK, Beenackers AAC. (1998a) Development of a new photocatalytic reactor for water purification. Catalysis Today 40:73–83.

Ray AK, Beenackers AACM (1997) Novel swirl-flow reactor for kinetic studies of semiconductor photocatalysis. AIChE Journal 43:2571–2578.

Ray AK, Beenackers AACM (1998b) Novel photocatalytic reactor for water purification. AIChE Journal 44:477–483.

Richardson JT, Peng Y, Remue D (2000) Properties of ceramic foam catalyst supports: pressure drop. Applied Catalysis A: General 204:19–32.

Richardson SD (2008) Environmental mass spectrometry: Emerging contaminants and current issues. Analytical Chemistry 80:4373–4402.

Richardson SD, Plewa MJ, Wagner ED, et al. (2007) Occurrence, genotoxicity, and carcinogenicity of regulated and emerging disinfection by-products in drinking water: A review and roadmap for research. Mutation Research/Reviews in Mutation Research 636:178–242.

Rivas FJ, Beltran FJ, Encinas A (2012) Removal of emergent contaminants: Integration of ozone and photocatalysis. Journal of Environmental Management 100:10–15.

Rivera-Utrilla J, Sanchez-Polo M, Mandez-Diaz JD, et al. (2008) Behavior of two different constituents of natural organic matter in the removal of sodium dodecylbenzenesulfonate by O_3 and O_3-based advanced oxidation processes. Journal of Colloid and Interface Science 325:432–439.

Robertson M, Henderson RB (1990) Fluid Purification. USA Patent 4892712

Rodriguez EM, Fernandez G, Alvarez PM, Beltran FJ (2012) TiO_2 and Fe(III) photocatalytic ozonation processes of a mixture of emergent contaminants of water. Water Research 46:152–166.

Rosal R, Rodriguez A, Zerhouni M (2006) Enhancement of gas-liquid mass transfer during the unsteady-state catalytic decomposition of ozone in water. Applied Catalysis A: General 305:169–175.

Rosal R, Rodriguez. A, Gonzalo MS, Garcia-Calvo E (2008) Catalytic ozonation of naproxen and carbamazepine on titanium dioxide. Applied Catalysis B: Environmental 84:48–57.

Roupp GB, Nico JA, Annangi S, et al. (1997) Two-flux radiation-field model for an annular packed-bed photocatalytic oxidation reactor. AIChE Journal 43:792–801.

Ryu J, Choi W (2008) Substrate-Specific Photocatalytic Activities of TiO_2 and Multiactivity Test for Water Treatment Application. Environmental Science & Technology 42:294–300.

Salaices M, Serrano B, Lasa HI de (2001) Photocatalytic Conversion of Organic Pollutants Extinction Coefficients and Quantum Efficiencies. Industrial & Engineering Chemistry Research 40:5455–5464.

Sampaio MJ, Silva CG, Silva AMT, et al. (2013) Photocatalytic activity of TiO_2-coated glass raschig rings on the degradation of phenolic derivatives under simulated solar light irradiation. Chemical Engineering Journal 224:32–38.

Sano N, Yamamoto T, Yamamoto D, et al. (2007) Degradation of aqueous phenol by simultaneous use of ozone with silica-gel and zeolite. Chemical Engineering and Processing: Process Intensification 46:513–519.

Say J. HP Bonnecaze R. Heller A. Sitkiewitz S. Heller E. (1990) Apparatus for photocatalytic fluid purification. US Patent No. 5.790.934.

Sczechowski JG, Koval CA, Noble RD (1995) A Taylor vortex reactor for heterogeneous photocatalysis. Chemical Engineering Science 50:3163–3173.

Seccia S, Fidente P, Barbini DA, Morrica P (2005) Multiresidue determination of nicotinoid insecticide residues in drinking water by liquid chromatography with electrospray ionization mass spectrometry. Analytica Chimica Acta 553:21–26.

Shan AY, Ghazi TIM, Rashid SA (2010) Immobilisation of titanium dioxide onto supporting materials in heterogeneous photocatalysis: A review. Applied Catalysis A: General 389:1–8.

Shin D, Jang M, Cui M, et al. (2013) Enhanced removal of dichloroacetonitrile from drinking water by the combination of solar-photocatalysis and ozonation. Chemosphere 93:2901–2908.

Siddiquey IA, Furusawa T, Sato M, et al. (2008) Control of the photocatalytic activity of TiO_2 nanoparticles by silica coating with polydiethoxysiloxane. Dyes and Pigments 76:754–759.

Song S, Liu Z, He Z, et al. (2010) Impacts of Morphology and Crystallite Phases of Titanium Oxide on the Catalytic Ozonation of Phenol. Environmental Science & Technology 44:3913–3918.

Sopajaree K, Qasim SA, Basak S, Rajeshwar K (1999) An integrated flow reactor-membrane filtration system for heterogeneous photocatalysis. Part I: Experiments and modelling of a batch-recirculated photoreactor. Journal of Applied Electrochemistry 29:533–539.

Souzanchi S, Vahabzadeh F, Fazel S, Hosseini SN (2013) Performance of an Annular Sieve-Plate Column photoreactor using immobilized TiO_2 on stainless steel support for phenol degradation. Chemical Engineering Journal 223:268–276.

Suarez S, Carballa M, Omil F, Lema JM (2008) How are pharmaceutical and personal care products (PPCPs) removed from urban waste waters. Reviews in Environmental Science and Biotechnology 7:125–138.

Sumita T, Yamaki T, Yamamoto S, Miyashita A (2002) Photo-induced surface charge separation of highly oriented TiO_2 anatase and rutile thin films. Applied Surface Science 200:21–26.

Šuligoj A, Cernigoj U, Štangar LU (2010) Preparation procedure of durable titania coatings on metal supports for photocatalytic cleaning applications. Patent number SI 23585 A:The Slovenian Intellectual Property Office, Ljubljana.

Tasbihi M, Kete M, Raichur. AM, et al. (2012) Photocatalytic degradation of gaseous toluene by using immobilized titania/silica on aluminum sheets. Environmental Science and Pollution Research 19:3735–3742.

Tomova D, Iliev V, Rakovsky S, et al. (2012) Photocatalytic oxidation of 2,4,6-trinitrotoluene in the presence of ozone under irradiation with UV and visible light. Journal of Photochemistry and Photobiology A: Chemistry 231:1–8.

Turhan K, Uzman S (2008) Removal of phenol from water using ozone. Desalination 229:257–263.

Twigg MV, Richardson JT (2007) Fundamentals and Applications of Structured Ceramic Foam Catalysts. Industrial & Engineering Chemistry Research 46:4166–4177.

Vargova M, Plesch G, Vogt UF, et al. (2011) TiO_2 thick films supported on reticulated macroporous Al2O3 foams and their photoactivity in phenol mineralization. Applied Surface Science 257:4678–4684.

Vinodgopal K, Kamat PV (1992) Photochemistry on surfaces: photodegradation of 1,3-diphenylisobenzofuran over metal oxide particles. The Journal of Physical Chemistry 96:5053–5059.

Vione D, Minero C, Maurino V, et al. (2005) Degradation of phenol and benzoic acid in the presence of a TiO_2-based heterogeneous photocatalyst. Applied Catalysis B: Environmental 58:79–88.

Vymazal J (2009) The use constructed wetlands with horizontal sub-surface flow for various types of waste water. Ecological Engineering 35:1–17.

Wang S, Shiraishi F, Nakano K (2002) A synergistic effect of photocatalysis and ozonation on decomposition of formic acid in an aqueous solution. Chemical Engineering Journal 87:261–271.

Wang X, Han F, Wang X, Li Y (2014) Effect of aluminum foam support and polyethylene glycol on surface morphology and photocatalytic behavior of TiO_2 films. Materials Chemistry and Physics 145:68–74.

Willis RM, Stewart RA, Giurco DP, et al. (2011) End use water consumption in households: impact of socio-demographic factors and efficient devices. Journal of Cleaner Production 60:107–115

Wintgens T, Melin T, Salehi F, Hochstrat R (2008) Emerging contaminants and treatment options in water recycling for indirect potable use. Water Science and Technologie 57:99–107.

Yang GCC, Li C-J (2007) Electrofiltration of silica nanoparticle-containing waste water using tubular ceramic membranes. Separation and Purification Technology 58:159–165.

Yang H, Cheng H (2007) Controlling nitrite level in drinking water by chlorination and chloramination. Separation and Purification Technology 56:392–396.

Yang Y, Ma J, Qin Q, Zhai X (2007) Degradation of nitrobenzene by nano-TiO_2 catalyzed ozonation. Journal of Molecular Catalysis A: Chemical 267:41–48.

Yildirim AO, Gul S, Eren O, Kusvuran E (2011) A Comparative Study of Ozonation, Homogeneous Catalytic Ozonation, and Photocatalytic Ozonation for C.I. Reactive Red 194 Azo Dye Degradation. CLEAN - Soil, Air, Water 39:795–805.

Zhai X, Chen Z, Zhao S, et al. (2010) Enhanced ozonation of dichloroacetic acid in aqueous solution using nanometer ZnO powders. Journal of Environmental Sciences 22:1527–1533.

Zhang X, Du AJ, Lee P, et al. (2008) TiO_2 nanowire membrane for concurrent filtration and photocatalytic oxidation of humic acid in water. Journal of Membrane Science 313:44–51.

Zhao L, Sun Z, Ma J (2009) Novel Relationship between Hydroxyl Radical Initiation and Surface Group of Ceramic Honeycomb Supported Metals for the Catalytic Ozonation of Nitrobenzene in Aqueous Solution. Environmental Science & Technology 43:4157–4163.

Zhao Y, Zhong J, Li H, et al. (2002) Fouling and regeneration of ceramic microfiltration membranes in processing acid waste water containing fine TiO_2 particles. Journal of Membrane Science 208:331–341.

Zsilak Z, Szabo-Bardos E, Fonagy O, et al. (2014) Degradation of benzenesulfonate by heterogeneous photocatalysis combined with ozonation. Catalysis Today 230:55–60.